A Micro-Analytical System for Complex Vapor Mixtures– Development and Application to Indoor Air Contaminants

by

Sun Kyu Kim

A dissertation submitted in partial fulfillment
of the requirements for the degree of
Doctor of Philosophy
(Environmental Health Sciences)
in The University of Michigan
2012

Doctoral Committee:

Professor Edward T. Zellers, Chair
Professor Robert T. Kennedy
Professor Stuart Batterman
Associate Professor Katsuo Kurabayashi

DEDICATION

To My Family, Miyoung, Jiho, and Junho

ACKNOWLEDGMENTS

First I would like to thank my advisor Prof. Edward T. Zellers for his guidance and support. It was a wonderful chance to work with him. Working with him, I have learned many valuable lessons, including scientific thinking, communication and writing skills, and so on, which must be treasure for my future career. Interdisciplinary work he is involved in provided me unique opportunities how to collaborate with other researchers.

The next I would like to thank is my dissertation committee members, Dr. Robert Kennedy, Dr. Stuart Batterman, and Dr. Katsuo Kurabayashi. They have provided wonderful insights into my research and also helped me to breakthrough all the hard milestones to reach this point.

I would also like to thank all the WIMS members. Katharine Beach, Robert Gordenker, and Brendan Casey, they deserve acknowledgement for all their help, fabrication, wirebonding, and other necessary assistance.

Without members of the Zellers group, it would not be possible I could finish this dissertation. I have learned a great deal from all of them and have enjoyed working with them. I thank Qiongyan Zhong (Judy), Chunguang Jin (Jerry), who trained me very well, and also all former Zellers group members.

It was a luck to meet David Burris during my research. I would like to specially thank David Burris for his great help and patience. He helped me enormously to complete this dissertation.

I would like to thank my father, brother (Sun-Wook) and in-laws for their infinite support. Mom, I really wanted to give it to you, but it is not possible now. However, this is for you, RIP.

Last, thank you to my wife, Miyoung and my children (Jiho and Junho). She has been devoted for me to focus on my research. Jiho and Junho, you are the reason why I survive. Thank you for being my children.

It was lucky to have stable funding sources provided by DoD ESTCP Grant ER-200702 through a subcontract with IST, Inc., and by the Engineering Research Centers Program of the National Science Foundation under Award Number ERC-9986866.

Thank you.

TABLE OF CONTENTS

DEDICATION ..... **ii**

ACKNOWLEDGMENTS ..... **iii**

LIST OF FIGURES ..... **x**

LIST OF TABLES ..... **xiii**

LIST OF APPENDICES ..... **xv**

CHAPTER

I. Introduction……..... **1**

1.1 Dissertation Overview…..... 1

1.2 Background and Significance..... 3

1.2.1 Volatile Organic Compounds and Vapor Intrusion ..…..…….. 3

1.2.2 TCEVI, Regulations, and Monitoring Methods…… 5

1.2.3 Portable Direct-Reading Instruments…...…….…… 8

1.2.4 Micro-Analytical Systems for VOCs……..… 10

1.2.5 Meso- and Micro-scale GC at the University of Michigan….. 12

1.2.6 Microscale Chemiresistor Employing Gold Nanoparticles….. 13

1.2.7 Chemometics for μGC with a CR sensor array…… 15

1.3 References 19

II. Prototype Field-Portable GC with Nanoparticle-Coated Chemiresistor Array Detector for Sub-ppb Determinations of TCE Encountered in Homes Contaminated by Vapor Intrusion..... 31

2.1 Introduction…….. ……..... 31

2.2 Prototype Description and Experimental Methods……..... 34

2.2.1 Instrument Description and Operation……..……...….... 34

2.2.2 Selection of Interferences and Test Atmosphere Generation.. 38

2.2.3 Instrument Calibration and Laboratory Samples...…….. 39

2.3 Results and Discussion …….....40

2.3.1 Calibration and Detection Limits..…..……..……...….... 40

2.3.2 Separation and Response Patterns…… 41

2.3.3 Laboratory Sample Test……..……. 42

2.4 Conclusions ….....……. 43

2.5 References ….....……. 44

III. Microfabricated Gas Chromatograph for the Selective Determination of Trichloroethylene Vapor at Sub-Parts-Per-Billion Concentrations in Complex Mixtures.....54

3.1 Introduction…….. ……..... 54

3.1.1 Analytical Subsystem Design and Operating Conditions…… 57

3.2 Experimental Methods……. …….. 59

3.2.1 Materials……..……...……...….... 59

3.2.2 PCF Module Components...…… 60

3.2.3 Microcolumns…….. 62

3.2.4 Chemiresistor (CR) Array…… 62

3.2.5 Device Mounting and System Integration…… 63

3.2.6 Device Control and System Operation……. 64

3.2.7 Test-Atmosphere Generation……65

3.3 Results and Discussion……..…… 66

3.3.1 System Integration……... 66

3.3.2 Chromatographic Resolution and Array Response Patterns …67

3.3.3 Calibration, Detection Limits, and Accuracy……69

3.3.4 Stability…….71

3.3.5 Complex Mixture Analysis…….. 72

3.4 Conclusions…… 73

3.5 References…….. 74

IV. Microfabricated Gas Chromatograph for On-Site Determination of Trichloroethylene in Indoor Air Arising from Vapor Intrusion Part I: Field Evaluation 87

4.1 Introduction…….....87

4.2 Instrumentation and Methodology……...90

4.2.1 μGC Prototype Description and Operation ……90

4.2.2 Control, Data Acquisition, and Data Processing ……..…. 92

4.2.3 Field Calibration and Reference Method……93

4.2.4 Field Demonstration Site ……..…. 94

4.3 Results and Discussion ……..…… 95

4.3.1 Field Calibration and Detection Limits……. 95

4.3.2 TCE Standardization and Inter-Prototype Comparisons…….. 96

4.3.3 Accuracy of μGC TCE Determinations…… 99

4.4 Conclusions……103

4.5 References …….. 104

V. Microfabricated Gas Chromatograph for On-Site Determination of Trichloroethylene in Indoor Air Arising from Vapor Intrusion Part II: Spatial/Temporal Monitoring 119

5.1 Introduction……..... 119

5.2 Experimental Methods…….…….... 121

5.2.1 Prototype Features and Functions ……121

5.2.2 Field Demonstration Sites …….……..123

5.2.3 Reference measurements ……..…….. 124

5.2.4 Temporal Variations …….……...124

5.2.5 Spatial Variations…….125

5.3 Results and Discussion …….…….. 126

5.3.1 Temporal Monitoring…….…… 126

5.3.2 Spatial Monitoring …….. 131

5.4 Conclusions……132

5.5 References ….……134

VI. Multivariate Curve Resolution of Co-Eluting Peaks Measured with Microsensor Array Detectors in Micro- and Meso-Scale Gas Chromatographs..... 142

6.1 Introduction……..... 142

6.2 Experimental Methods…….…….... 145

6.2.1 Materials……..…… 145

6.2.2 Instrument Description, Experimental Setup and Vapor Selection

…….…… 146

6.2.3 Calibration and Data Set Generation …….. 148

6.2.4 Multivariate Curve Resolution (EFA-ALS)…… 149

6.2.5 Fidelity, Confusion and Recognition of Recovered Pattern… 150

6.2.6 Software and Calculations …….. 151

6.3 Results and Discussion …….…….. 151

6.3.1 Calibration, Response pattern and Parameter Adjustment….. 151

6.3.2 Number of Components in the Composite Peak……. 153

6.3.3 Fidelity, Confusion, and Pattern Recognition……. 153

6.3.4 Influence of Chromatographic Resolution and Relative Response Ratio……. 156

6.4 Conclusions……157

6.5 References ……..…….. 159

VII. Summary and Conclusions……..... 169

APPENDICES 177

LIST OF FIGURES

Figure

1-1. Generalized schematic of the pathway for subsurface VI into indoor air……. 27

1-2. Meso-scale portable GC…….....… 28

1-3 Concept diagram of WIMS^2 μGC…….. 29

1-4. Deconvolution of overlapped peaks 30

2-1. Block diagram of instrument and flow direction at each operation mode ……46

2-2. Calibration result of the CR sensor array with TCE samples ranging from 0.51 ppb to 54 ppb…… 47

2-3. Chromatogram traces of TCE and 10 common VOCs found in indoor air at homes near an air force base …… 48

2-4. Comparison results of the GC performance versus US EPA Method TO-15…….. 49

2-5. Sub-ppb level (0.4 ppb) TCE determination with the GC……. 50

3-1. Fluidic diagram of the μGC prototype and photographs of the major components.. 78

3-2. Representative (experimental) heating profile for the μF during desorption/ injection ……... 79

3-3. (a) 3-min chromatograms from the four CR microsensors and a downstream FID generated from the analysis of a 20-L air sample spiked with TCE and 11 VOC interferences by the μGC prototype. (b) Normalized CR array response patterns for TCE and proximate interferences ……. 80

3-4. Calibration curves generated from sampling different volumes of test atmospheres of TCE in air…….. 81

3-5. Chromatograms from the four CR microsensors generated from the analysis of a 20-L air sample spiked with TCE and 45 interferences……. 82

4-1. Prototype μGC system and components ……..107

4-2. Field calibration curves for a) Proto 1 and b) Proto 2……. 108

4-3. Results of periodic analysis (standardization check) of the TCE tank standard (2-L sample; 9.6 ppb TCE) showing stability of responses and relative response patterns over the 3-week study (RSD = 17%)……..… 109

4-4. Inter-prototype comparison of TCE concentrations for 23 side-by-side air samples…….110

4-5. (a) Representative chromatograms from the MPN-coated CR array for a measurement obtained from Proto-1 having a TCE concentration of 12 ppb; (b) Normalized response patterns (bar charts) for TCE and the selected (unknown) VOCs designated in (a)…….. 111

4-6. Chromatograms obtained from Proto 2 for an indoor air sample containing TCE..112

4-7. Extracted subsections of several chromatograms from the OPH sensor of Proto 1 113

4-8.Correlation of the pooled measurements from the μGC prototypes with the corresponding canister samples analyzed by GC-MS…….114

4-9.Comparison of TCE measurements from the prototypes and from the reference method (TO-15) for matched samples…….115

5-1. Photographs of (a) PCB-mounted microfabricated components of the prototype μGC (iPhone is shown for scale); (b) laptop and prototype in the kitchen of House 1; (c) crawl

space and hallway in the basement of House 1, with the Hapsite GC-MS and pressure sensor readout unit (prototypes are situated on the table in the room to the left); and (d) prototype and Summa canister during measurement of spatial TCE distribution in House 1……137

5-2. Temporal variations in the TCE concentration (left-hand ordinate) determined by Proto 1 (open triangles), Proto 2 (filled triangles), canister/TO-15 (open circles), and Hapsite GC-MS (filled circles)……138

5-3. Results of 48 hr of continuous, automated (unattended) TCE concentration measurements (left-hand ordinate) with Proto 1 (open triangles, crawl space) and Proto 2 (filled triangles, hallway)…….139

5-4. Floor plan of House 1 showing the spatial distribution of TCE vapor concentrations……..140

5-5. Spatial distributions of TCE in House 2 in which a non-VI source of TCE was placed…….. 141

6-1. Schematic diagrams of a) portable and b) micro-scale GCs……161

6-2. Example chromatograms of pure and binary mixture with various a) *R* with *RRR*=1:1 and b) *RRR* with *R*=0.5……162

6-3. CR array response patterns to selected vapors, a) TCE (trichloroethylene) and HEP (n-heptane) with ρ = 0.80, and b) CHX (cyclohexane) and BOH (n-butanol) with ρ = 0.20…….. 163

6-4. Example of EFA-ALS analysis (*S/N ratio*=10, *R*=0.5, *RRR*=1:1) …..…… 164

6-5. Influence of variables on the quality of recovery…… 165

LIST OF TABLES

Table

2-1. Target compound and interferences detected in homes near an Air Force base…....51

2-2. Relative response patterns, response ratio, and correlation coefficient of TCE and other vapors from the GC analysis of an 11-vapor mixture including TCE and 10 other interferences…….. 52

2-3. Result of laboratory sample test with meso-GC, including blind sample, duplicate samples…….. 53

3-1. List of 46 test compounds and their vapor pressures (p_v)…….. 83

3-2. Confusion matrix for single-vapor discrimination…….84

3-3. Limits of detection for TCE from each sensor in the array for two assumed sample volumes……. 85

3-4. Short- and medium-term stability of retention times and sensor responses……. 86

4-1. Limit of Detection (LOD, ppb) for TCE with both prototypes for assumed sample volumes of 4 L (20 L)…… 116

4-2. Comparison of TCE measurements obtained concurrently from the μGC prototypes and from canister samples analyzed by GC-MS (reference method)…… 117

4-3. Concentrations of TCE and co-eluting interferences from reference samples subjected to expanded GC-MS analysis (TO-15), and the corresponding TCE concentrations from the μGC prototypes (matched samples)…… 118

6-1. Chemical properties of selected vapors……166

6-2. Conditions for binary mixture data generation and number of components determined by EFA analysis. ……..167

6-3. MCR analysis results for binary mixtures having different pattern similarities under various conditions of S/N ratio, resolution, and relative response ratio..……...168

LIST OF APPENDICES

Appendix

I. Supporting Information for Chapter 3…….……177

II. Supporting Information for Chapter 6…… 182

CHAPTER 1

Introduction

1.1 Dissertation Overview

Indoor air contamination by vapor intrusion (VI) from soil contaminated with toxic chemicals has become a great concern as a public health issue.[1] On-site quantitative monitoring of those chemicals is in demand for policy making, establishing counterplans and so on related to the problem of indoor air contamination by VI. In the response to the need, this dissertation describes a series of projects related to the development and application of a field-deployable microfabricated gas chromatograph (μGC) for VI monitoring. One of prevalent chemicals of concern (COC) related to VI is trichloroethylene (TCE). Thus, this dissertation focuses on design, assembly and demonstration of the application of the μGC, named SPIRON in this study, to determine the low- and sub-parts-per-billion (ppb) concentrations of TCE vapors in complex mixtures. The research has direct relevance to environmental health sciences, specifically exposure assessment via indoor air quality monitoring. It is the culmination of the past ten years of research in Professor Zellers' group directed at developing miniaturized GCs, such as meso-scale (portable)[2-5] and micro-scale GCs[6-13] for the determination of volatile organic compounds (VOC) and semi-VOCs (SVOC) in air. This includes development of preconcentrator,[14-19] separation column,[20,21] and sensor array detectors[2-5, 22-33] as well as

integration of these components into functional prototypes.[6-13]

The SPIRON μGC has been designed on the basis of previous WIMS μGC prototypes, [6] but it incorporates several design and operational modifications to optimize it for the unique aspects of determining the VOC components in indoor air, specifically for TCE determination. The μGC consists of preconcentration, chromatographic separation, and microsensor array detection modules. Targets in complex vapor mixtures are selectively preconcentrated, spatially resolved along the separation column, and detected by a sensor array that uses nanoparticles as interface layers.

Chapter 1 provides the background and significance of the research, as well as an overview of an extant meso-GC developed prior to this research. Chapter 2 describes the adaptation of the meso-GC to the determination of TCE vapors at sub-ppb concentrations in the presence of interferences encountered in homes affected by vapor intrusion (VI) from TCE-contaminated soil. Results from this work were used to guide the design, assembly, and laboratory characterization of the SPIRON μGC prototype. Chapter 3 describes design and development of the SPIRON prototype, and its laboratory characterization performed prior to the field demonstration. This chapter has been published with minor modifications in the journal *Analytical Chemistry*.[33] Following this laboratory validation, two μGC prototypes were taken to the field for demonstration in homes suffering from vapor intrusion by TCE in Utah. Chapters 4 and 5 present results of the field evaluation and application of the μGC prototypes, respectively. These chapters have been submitted together as a series to the journal *Environmental Science & Technology* for publication. Chapter 6 explores the application of a known multivariate curve resolution (MCR) technique, which was developed for resolving partially

overlapping peaks obtained from a microsensor array GC detector,[28] to experimental data generated from such an array with the meso-scale and μGC prototypes described mentioned in preceding. Chapter 7 summarizes the key findings and major contribution of this dissertation research and suggests future studies.

1.2 Background and Significance

1.2.1 Volatile Organic Compounds and Vapor Intrusion

Volatile organic compounds (VOC) are defined by authorities such as the US Environmental Protection Agency (EPA), the European Parliament, and World Health Organization (WHO).[34-36] By US EPA definition, VOCs are any compound of carbon, excluding carbon monoxide, carbon dioxide, carbonic acid, metallic carbides or carbonates, and ammonium carbonate, that participates in atmospheric photochemical reactions, other than compounds which have been determined to have negligible photochemical reactivity.[34] European law defines VOC as any organic compound having an initial boiling point less than or equal to 250°C measured at a standard atmospheric pressure of 101.3 kPa.[35] WHO defines VOC similarly as organic compounds includes all organic compounds (substances made up of predominantly carbon and hydrogen) with boiling temperatures below 250-260°C, excluding pesticides.[36]

VOCs, arising from solids or liquids with finite vapor pressures under ambient conditions, are ubiquitous. VOC exposures are of concern in the general environment, where concentrations are typically low (i.e., < 100 ppb)[37-39] and in the occupational environment, where concentrations can be quite high (i.e., > 100 ppm). [40,41] The dominant route of human VOC exposure is by inhalation of contaminated air. Ingestion

through contact with VOC-enriched airborne particles or absorption through skin may be other potential exposure routes. The risk of health effects from VOC exposure depends on the toxicity, concentration (or dose), duration, and frequency of the exposure. Many VOCs exhibit adverse acute or chronic health effects in humans. Acutely toxic VOCs can be a cause of conjunctival irritation, nose and throat discomfort, headache, allergic skin reaction, dyspnea, declines in serum cholinesterase levels, nausea, emesis, epistaxis, fatigue, dizziness,[42,43] while chronically toxic VOCs may cause cancer or damage to the liver, kidney, or central nervous system (CNS).[44] Regardless, the ability to measure exposures continuously is desirable in order to accurately characterize and/or control risks of adverse health effects.

Concentrations of many VOCs are known to be consistently two to five (up to ten) times higher on average indoors than outdoors.[43, 45] The major sources of indoor VOCs are: 1) emissions from building materials; 2) infiltration from outdoor air; 3) human activities; 4) microorganisms; and 5) reaction products of existing VOCs. Although the role of VOCs in indoor health problems is recognized, no indoor air quality standard for VOCs has been set in non-industrial settings.[43] In addition to the major sources, vapor intrusion (VI) has been identified as a potential mechanism for human exposure to VOCs. VI is a term used to describe the migration of volatile chemicals from contaminated groundwater or soil into an overlying building. Volatile chemicals can include VOCs, semi-VOCs, and some inorganic analytes, such as elemental mercury, radon, and hydrogen sulfide.[46] The pathways for VI contamination of indoor air (shown in Figure 1-1) typically involve permeation or penetration through sub-surface walls, and they are considered separate from indoor air contamination arising from sources within the

building or from infiltration of ambient air contaminants.[1]

According to the EPA report, [46] the vapors may accumulate in occupied buildings to the extent that may cause near-term safety hazards (e.g., explosion), acute health effects, or aesthetic problems (e.g., odors). However, the chemical concentration levels are typically low and may not be present at detectable concentrations. In buildings with such low concentrations, whether the chemicals may cause an unacceptable risk of chronic health effects due to long-term exposure to these low levels is the main concern. To evaluate the potential chronic risk from vapor intrusion, it is important to monitor the extent of VI accurately, but it is often complicated because of potential presence of some of the same chemicals from emission sources in the building (e.g., household solvents, gasoline, cleaners) that may cause a significant human health risk separately or in combination with vapor intrusion.

1.2.2 TCE VI, Regulations, and Monitoring Methods

VI is an emerging problem, the extent of which has only recently been recognized by Department of Defense (DoD), regulators, private industry and others. There are more than 10 DoD facilities currently known to have VI concerns, including Hill Air Force Base (AFB), located in Utah (the site of our planned field study). Trichloroethylene (TCE) is the most common contaminant of concern at VI-impacted DoD sites above shallow groundwater plumes.[47] It was used as a solvent for cleaning of metal parts and was released into the environment, either accidentally through leaks and spills or deliberately through dumping, during 1960's and 1970's.[48-50] The problem is that TCE can migrate through the soil and reach the underlying groundwater because of its moderate solubility,

persistence in the environment, and relatively high Henry's Law constant ($H = 2.0\times10^{-2}$ atm·m^3/mol at 20 °C),[51] and then can move a substantial distance from the original discharge point.[52] Due to its relatively high vapor pressure (69 Torr at 25 °C), it volatilizes into the overlying soil and can migrate through the soil. VI of TCE into residences has been documented to occur by this pathway.[50] The Agency for Toxic Substances and Disease Registry (ATSDR) reported that TCE mainly affects the CNS, with symptoms including sleepiness, fatigue, headache, confusion, and euphoria.[51] Chronic effects on the liver, kidneys, gastrointestinal system, and skin have also been noted, as well as the association with several types of cancers in humans, especially in the kidney, liver, cervix, and lymphatic system.[51] Based on these factors, the U. S. Air Force has implemented an environmental management program for hundreds of sites across the country, including both active and closed bases.[52]

Risk-based limits for indoor air concentrations of TCE (and other concerning compounds) arising from VI are in the low- or sub-parts-per-billion (ppb) range.[1, 53] No standards have been set for VOCs in non-industrial settings. Indoor air quality criteria for TCE vary among regulatory jurisdictions. The U.S. EPA 2002 Draft Subsurface VI Guidance Document sets a generic screening level of 0.41 ppb (at 10^{-4} cancer risk), [1] whereas the EPA Regional Screening Level for TCE in residential indoor air for Regions 3, 6, and 9 is 0.22 ppb.[54] In the vicinity of Hill Air Force Base (AFB), where the field testing described in this study was performed, the TCE mitigation action level (MAL) has been recently reset from 0.4 ppb to 2.3 ppb for residential buildings.[55] A recent EPA review of the 2002 Draft Subsurface VI Guidance Document suggests an increased reliance on indoor air concentrations in future VI evaluations.[55]

To assess VI, there are several sampling options such as groundwater sampling, bulk soil sampling, soil gas sampling, passive soil gas survey, sub-slab sampling of vapors beneath buildings, and indoor air sampling.[46] Among those, indoor air sampling should be performed to aid in the assessment of VI, because it is most relevant to the health problems of residents. U. S. EPA Method TO-15,[57] which uses Summa canisters for sample collection followed by GC-FID or GC-MS analysis, has become the standard method to quantify low-level indoor VOCs suspected of arising from VI. EPA Method TO-17,[58] involving capture on adsorbent-packed tubes followed by GC-FID/MS analysis, is also used, but with lower frequency.[59]

However, the usual shortcomings associated with time-integrated sampling and subsequent laboratory analyses can be cited as factors that limit the quantity and quality of data available to guide VI investigations and interventions. The current standard 24-hour collection period used for TO-15 does not capture temporal variations in exposure to the residents. Also, the unavoidable delay between sampling and laboratory analysis precludes timely response or remediation efforts. Furthermore, background VOCs in indoor air, associated with household products or human activities, can make it difficult to differentiate such sources of TCE from that generated by VI. This, in turn, has an impact on the nature of mitigation efforts implemented. Thus, there are several drivers for developing portable or permanently installed on-site analytical systems (i.e. direct reading instruments) that can accurately determine TCE (or other VOCs of interest) at the low- or sub-ppb concentrations prevalent in most VI-impacted residences in the presence of other background VOCs.

1.2.3 Portable Direct-Reading Instruments

There are relatively few field portable instruments currently available that can provide determinations of multiple VOCs. As mentioned in the previous section, it is required to determine VOCs at sub- or low-ppb level concentrations for indoor air quality investigations, but no instrument can do so, except portable GC-mass spectrometer (MS).[60,61] However, such an instrument requires high capital cost, maintenance requirements, and need for on-board carrier gas limit the use of such instruments for routine or extended on-site monitoring. Instruments capable of multi-VOC determinations that have been adapted for field use include infrared (IR) spectrometers (including conventional IR,[62,63] Fourier Transform IR (FTIR),[64, 65] and quantum cascade laser (QCL) IR[66]), portable MS,[67-69] and portable GCs with various detectors including MS,[70-72] flame ionization detector (FID),[73,74] thermal conductivity detector (TCD),[75] photoionization detector (PID),[76,77] ion mobility spectrometer (IMS),[78,79] helium ionization detector (HID),[80] electron capture detector (ECD),[77,81,82] and gas sensors.[83]

Some of the portable instruments have been commercialized. The MIRAN SapphlRe (~11 kg, Thermo scientific, Waltham, MA) is a conventional IR that can detect over 100 different single gases or vapors and VOC mixtures of up to 3-5 compounds with ppm level LODs and ~10 W power consumption.[63] A portable FTIR instrument, the Gasmet^{TM} DX 4030 (~ 14 kg, Gasmet Technologies, Helsinki, Finland) can detect 10 target compounds and five interferences simultaneously with ppm-ppb level LODs and 300W power consumption.[65] Portable GCs, such as the Photovac Voyager (~7 kg, Geotechnical Services, Tustin, CA), employing PID/ECD can detect VOCs with LODs of 5-50 ppb level, varying depending on compounds.[81] The Agilent 3000 Micro-

GC, a portable GC with a micro-TCD, can detect simple VOC mixtures at the ~1 ppm levels but does not identify the compounds because of the use of a single, universal detector.[75] The "man-portable" Hapsite GC-MS (~ 18 kg, Inficon, East Syracuse, NY), can detect VOCs at low- to sub-ppb levels with a Quadrupole MS,[72] but it is very expensive (> $100,000) and consumes a large amount of power which limits operation from batteries. Thus, most portable instruments cannot achieve ppb-level detection limits without separate preconcentration prior to sample injection. Although quite sensitive, LODs for portable MS and portable GC-MS instruments are not low enough to determine VOCs at levels prevalent in VI-impacted homes, and most of them are not small enough to be used for routine or large scale on-site measurements of the components of complex VOC mixtures.

Among aformentioned currently available direct-reading instruments, only a few instruments would be capable of *in situ* determinations of TCE at such low concentrations in the presence of numerous possible co-contaminants. The portable GC-MS appears to be the most effective due to its combination of chromatographic separation and spectrometric detection.[72] However, the utility of GC-MS for continuous, long-term assessments of indoor air contamination in multiple locations is severely limited by its cost and operating complexity. Recently, Defiant Technologies (Albuquerque, NM) introduced their handheld micro GC, Canary-Three™, consisting of preconcentrator, microfabricated column, and surface acoustic wave (SAW) sensor as the detector,[83] which can determine target analytes from complex mixtures using a selective micro preconcentrator. Defiant Technologies is a startup company that takes advantage of microchemical detection technologies recently developed at Sandia National Laboratories.

It employs dual detectors for “intelligent sample collection” which is the instrument controls the sampling volume automatically based on the sample concentration. It can be performed using one detector as a screening purpose, while using the other for the actual sample detection coupled with the microfabricated column. This function allows the instrument prevents itself from being overwhelmed by high concentrations. It weighs ~2.4 lbs and consumes power of ~20W. The detection limit of this instrument is not reported. In 2010, the instrument was applied for the determination of TCE and tetrachloroethylene (PCE) in water and showed the detection limit of ~ 50 µg/L in water.[84] It is reported that the next target detection limit would be ~ 1 µg/L, with modifications on the column and detector, and that the sensitivity must be improved by a factor of 20. This system is still under developing at the proof-of-concept stage.

Thus, there still remains a need for portable instruments capable of determining trace levels of specific VOCs in complex mixtures, yet small, simple, and inexpensive enough to be used for routine monitoring.

1.2.4 Micro-Analytical Systems for VOCs

Numerous efforts have been mounted over the past 30 years to use silicon micromachining technology (also referred to as micro-electro-mechanical systems, MEMS) to build micro analytical systems for gas phase analytes (e.g., VOCs). Reports of micropumps,[85] micropreconcentrators,[14,15,19,86-89] microcolumns,[20,21,90-99], microsensor or microsensor-array detector[2-5,22-33,100,101] and integrated systems[6,8-11,13,83,104-108] have appeared. A few efforts have been published on miniaturized IR instruments (FTIR and Quantum Cascade Laser (QCL) array IR),[107-109] but with some significant limitations to

miniaturization, including that a smaller mirror reduces the resolution and sensitivity, that a long path length is required which limits the size of the instrument, and that significant power is required for temperature control of source and detector.

There has also been a significant amount of research on miniaturized MS, but they still have LODs of several hundred ppb, require large vacuum pumps, have limited mass resolution, and limited capabilities for differentiating VOC mixture components.[112,113] Due to the principle of MS, miniaturization of MS is challenging, because miniaturization may lower the sensitivity and reduce mass resolution/range which means lower selectivity/complexity.

As another route to meet the demand, there has also been a significant amount of work devoted to microfabricated GC (μGC) systems. Most of the research on μGC has focused on the individual components of such microsystems, including micropumps,[85] micropreconcentrators,[14-19,86-89] microcolumns,[20,21,90-99] and microsensor or microsensor-array detectors.[2-5,22-32,100] Several reports have described subsystems that combine a microcolumn with one other micro-scale component.[21,114,115] Yet, only a handful of studies have addressed complete μGC systems,[6,8-11,13,102-104] defined here as comprising a fluidically interconnected ensemble of at least the following three essential components, all of which are microfabricated: a preconcentrator or other injector, a separation column, and a detector. The small number of such reports attests to the challenges associated with microsystem integration. Some reports have shown the use of microsensor or microsensor array detection,[6,103-108,116] in to μGCs systems, including micromachined thermal conductivity detector (TCD),[114] single surface acoustic wave (SAW) sensor,[83,118] SAW sensor array,[18,119-121] and chemiresistor (CR) array.[2-5,22-33] Many of these efforts are

those of researchers at the University of Michigan Center for Wireless Integrated MicroSensing and Systems (WIMS^2).[122]

1.2.5 Meso- and Micro-scale GC at the University of Michigan

Progress towards development of meso-scale portable GCs with polymer-coated-SAW or nanoparticle-coated-CR array detectors has been made in Dr. Zellers' group over the past 10 years (Figure 1-2).[2-4,16] In such instrument key features include a miniature multi-stage adsorbent preconcentrator/injector (PCI), two series-coupled 4.5-m-long low-thermal-mass separation columns with pressure and temperature tunable retention control, and a detector comprising an integrated array of chemiresistor sensors coated with functionalized monolayer gold nanoparticle (MPN) as the sorption interface.[25] Scrubbed air is used as the carrier gas. The main advantages of using a microsensor array rather than using a conventional type detector is that multiple chromatograms can be obtained at once from the array, and they can be combined with retention time data to improve capability for identifying and quantifying vapors. In other words, response patterns could be obtained and treated as digital 'spectra' of eluting vapors.

Technologies obtained from the development of portable GC have been successfully adapted to the development of a μGC to determine VOC mixtures in WIMS^2.[2,6,11] These remain the only studies to demonstrate the quantitative analysis of a VOC mixture by a MEMS gas chromatograph employing micromachined preconcentrator, micromachined separation columns, and microsensor(-array) detection components. As presented in the diagram (Figure 1-3), the key components of the μGC

prototype are very similar to those in the meso-GC, including a micromachined preconcentrator/focuser (PCF), two 3-meter-long DRIE-Si/glass microcolumns with non-polar stationary phases coated on their internal walls, and a chemiresistor (CR) array that uses thiolate-monolayer-protected gold nanoparticle (MPNs) films as the interface layers. All the key components are fabricated using MEMS technology. Currently, in the WIMS^2 Center, there are multiple different μGC prototypes being developed for the determination of VOCs for several different applications, including indoor air quality monitoring; breath monitoring as a screening tool for detecting biomarkers of diseases in human breath; explosives detection; military surveillance such as for manless reconnaissance or for warfare agent detection; 2-dimensional μGC for more complex mixture analysis, etc.

Previous work[2,3,6] showed the possibility that the WIMS^2 μGC prototype could be developed for the determination of TCE vapors at such a low concentration level and that the existing meso-GC could be used as the platform to obtain knowledge to guide the new μGC design. Successful development of such μGC system would meet the purpose of this study which is to provide the portability of μGC to be deployed in the field and its capability to determine TCE in the presence of a wide range of complex VOC interferences.

1.2.6 Microscale Chemiresistor Employing Gold Nanoparticles

Sensors have been widely used for sensitive measurement of organic or inorganic analytes in liquid phase and for measurement of inorganic analytes in gaseous phase, such as H_2O, H_2, O_2, CO, CO_2, H_2S, NH_3, NO_2, Cl_2 and HCL.[123,124] Inorganic

semiconductor oxides, such as SnO_2, ZnO, In_2O_3, WO_3, and V_2O_5, have been the most commonly used sensing materials, because of their high redox reaction with gaseous analytes. As the reason, they have been commercialized for the detection of toxic or inflammable gases as industrial and domestic applications, including gas monitors, leak detectors, and alarm systems. However their inherent problem using redox reaction restricts their applications to the detection of gases that are redox reactive. There have been several studies on adapting those sensors to VOC determination,[125-128] but the detection limits are still not satisfying to apply for the determination of VOCs at ppb level.

Microfabricated sensors for the determinations of VOCs employing "sorption" mechanism (combination of vapor absorption and adsorption) have been studied extensively over the past decades.[24,129-134] This type of sensors has the ability to detect a wide range of vapors in the low- or sub-ppm concentration range without preconcentration.[25] Arrays of such sensors can produce information of partially selective responses to identify multiple individual vapors. Sorption based sensor can be made by depositing a thin layer of a vapor-sensitive material on a transducer. It measures the change of resistance of the sensing layer as the response to the sorption of analytes (VOCs). Polymers are often used as the interface, because of their rapid, reversible, and reproducible interactions with vapors. Several different transducers employing sorptive interface have been studied for VOC detection, including optical sensors that use change in absorption or fluorescence,[131] piezoelectric devices such as surface acoustic wave (SAW) sensors[18,83,118-121] and oscillators/resonators and thickness-sheer mode resonators (TSMRs) [130,133] that uses frequency changes. However, they are not appropriate to be

applied for micro-scale instrument due to the need for adequate light sources (optical sensors) or their mass-dependency (SAW and TSMR sensors).

Chemiresistor (CR) sensors using resistance changes in interfacial film to detect sorbed analytes have been studied.[22-33] CR sensors include pairs of electrodes, typically microfabricated, and have them deposited with chemically sensitive materials. Sorption of vapors generates a change in conductivity associated with the swelling of interfacial layers, resulting resistance changes of the interfacial material, which is used for the detection. Conductive polymers and carbon-doped polymers have been used as CR interfaces,[135] and nanostructured materials have also been used (discussed below).

New interfacial materials, gold-thiolate monolayer-protected nanoparticles (MPNs), have emerged with many potential applications including chemiresistor sensors. First sensors with these MPNs were reported in 1998 by Wohltjen and Snow using n-octanethiol (C8) MPNs for the analysis of toluene, perchloroethylene, 1-propanol, and water vapors.[136] Sensitivity and selectivity to vapors can be tailored for optimal performance by changing the composition of MPNs. A microfabricated array of chemiresistors coated with such MPNs has been employed as the detector in meso- and μGC, showing higher sensitivity as compared to other chemical sensors,[2-4,25,137,138] and simplified system-level and electrical requirements.

1.2.7 Chemometrics for μGC with a CR Array

Microsensor arrays that employ various types of sorptive interface layers have been widely studied.[2-5,22-33] The individual sensors in the array are partially selective, yet broadly responsive, to the vapors from a wide range of functional group classes. On the

basis of response patterns from a stand-alone array, individual vapors often can be resolved from each other by use of pattern recognition methods such as principle component analysis (PCA),[139-141] linear discriminant analysis (LDA),[142,143] or extended disjoint principal component regression (EDPCR).[2,3,24,26-28,32,121,144] However, an upstream chromatographic separation is still necessary to determine the components of mixtures of three or more VOCs with such an array because of inherent limitations on the degree of selectivity.[24,26,144]

For a complex VOC mixture, ideally the perfect separation can be performed by optimizing all the chromatographic variables, but the development of a μGC analytical system is often focused on rapid determination of chemicals. As a result, co-elution of vapors is likely, if not inevitable. Either fully time-resolved peaks corresponding to individual vapors or partially time-resolved peaks corresponding to two or three vapors can be found in chromatograms. Partially resolved peaks will reduce the ability to identify and quantify the components of a complex VOC mixture. Figure 1-4 presents the notion of partially resolved peaks.

MCR methods are often used in spectroscopic analysis of mixtures such as in vibrational spectroscopy and gas and liquid chromatography with a spectrometric detector (e.g., GC-MS, HPLC-diode array, etc.).[145-153] Without prior knowledge of the mixture composition, MCR methods can determine the number of components in overlapped chromatographic composite peaks and then can extract and recover the elution profile and spectrum of each component of the composite peak. Following MCR, the reconstituted spectra can then be compared to those in a library in order to determine the identities and concentrations of the individual analytes. Due to these reasons, various

MCR algorithms have been introduced and applied, such as AutoBTEM[154] for FT-IR, Raman, and IR imaging data, PARAFAC[155,156] for GC×GC and GC×GC-TOFMS, alternating least square (ALS)[157-159] for multiple applications, evolving factor analysis (EFA) with ALS[28] for microsensor array as mentioned above, etc.

In the μGCs with microsensor array detectors, it is logical to employ the multi-dimensional data analysis to detect hidden peaks in a chromatogram and to resolve overlapped peaks of any resolution. Very little research has been reported on the chemometrics required for using microsensor arrays as GC detectors.[27,160] There is only one study, reported by Dr. Zellers' group, addressing the issue of partially resolved peaks from microsensor array detectors.[28] The study used two different multivariate curve resolution techniques: evolving factor analysis (EFA) with alternating least squares (ALS). Extended disjoint principal component regression (EDPCR) was used to relate the results of EFA-ALS to vapor recognition probabilities. Seven vapor pairs spanning a range of pattern similarity are selected and modeled as Gaussian peaks whose magnitudes and degrees of overlap are varied by simulation. The study showed that EFA-ALS provides an effective means of extracting information about co-eluting components from the GC-microsensor array system, and the array provides sufficient diversity of responses to identify those components in most cases. However, the data set of binary mixtures used in the study was simulated using experimentally determined response patterns of individual vapors rather than experimentally generated. Therefore, it is very important to apply the EFA-ALS method for the deconvolution of overlapped peaks in real measurement data obtained from microsensor array.

Although numerous efforts have been mounted to develop chromatographic analytical systems for analyzing VOCs in complex mixtures, none of them has involved the use of a MEMS-based microsystem including all key components; micromachined sampling/injection module; micromachined separation column; and micromachined detector. We now discuss the results of the development of such a μGC, including 1) the development of the first fully integrated field deployable prototype μGC employing an array of microsensors as the detector that can determine TCE at low- or sub-ppb concentration level in the presence of multiple background interferences, including the results of meso-GC application for TCE-VI problem to guide the μGC development; 2) application of the developed μGC in the field to provide information about spatial and temporal variations of TCE in homes affected by VI from TCE-contaminated soil; 3) Application of EFA-ALS multivariate curve resolution method for real experimental data. This research would be one of the pioneers in the area of the development of microfabricated analytical systems.

1.3 References

1. U. S. EPA, OSWER Draft Guidance for Evaluating the Vapor Intrusion to Indoor Air Pathway from Groundwater and Soils (Subsurface Vapor Intrusion Guidance); EPA530-D-02-004; U.S. Environmental Protection Agency, 2002. Available at http://www.epa.gov/osw/hazard/correctiveaction/eis/vapor/complete.pdf
2. Zhong, Q.; Steinecker, W. H.; Zellers, E. T. *Analyst* **2009**, 134, 283-293.
3. Zhong, Q.; Veeneman, R. A.; Steinecker, W. H.; Jia, C.; Batterman, S. A.; Zellers, E. T. *J. Environ. Monit.* **2007**, 9, 440-448.
4. Lu, C. J.; Jin, C.; Zellers, E. T. *J. Environ. Monit.* **2006**, 8, 270-278.
5. Lu, C.-J; Whiting, J.; Sacks, R. D.; Zellers, E. T. *Anal. Chem.* **2003**, 75, 1400-1409.
6. Lu, C.-J.; Steinecker, W. H.; Tian, W.-C.; Oborny, M. C.; Nichols, J. M.; Agah, M.; Potkay, J. A.; Chan, H. K. L.; Driscoll, J.; Sacks, R. D.; Wise, K. D.; Pang, S. W.; Zellers, E. T. *Lab Chip* **2005**, 5, 1123-1131.
7. Kim, S. K.; Chang, H.; Bryant, J. G.; Burris, D. R.; Zellers, E. T. *Proc. Transducers '11*, Beijing, China, June 5-9 2011, pp. 799-802.
8. Chang, H.; Kim, S. K.; Sukaew, T.; Bohrer, F.; Zellers, E. T. *Procedia Engineering* **2010**, 5, 973-976.
9. Chang, H.; Kim, S. K.; Sukaew, T.; Bohrer, F.; Zellers, E. T. *Solid-State Sens., Actuator and Microsyst. Workshop*: Hilton Head, SC, June 6-10 2010, pp 278-281.
10. Zellers, E. T.; Reidy, S.; Veeneman, R. A.; Gordenker, R.; Steinecker, W. H.; Lambertus, G. R.; Kim, H.; Potkay, J. A.; Rowe, M. P.; Zhong, Q.; Avery, C.; Chan, H. K. L.; Sacks, R. D.; Najafi, K.; Wise, K. D. *Proc. Transducers '07*, Lyon, France, June 10-14 2007, pp 1491-1494.
11. Kim, H.; Steinecker, W. H.; Reidy, S.; Lambertus, G. R.; Najafi, A. A. A. K.; Zellers, E. T.; Bernal, L. P.; Washabaugh, P. D.; Wise, K. D. *Proc. Transducers '07*, Lyon, France, June 10-14 2007, pp 1505-1508.
12. Lu, C.-J.; Tian, W.-C.; Steinecker, W. H.; Guyon, A.; Agah, M.; Oborny, M. C.; Sacks, R.; Wise, K. D.; Pang, S. W.; Zellers, E. T. *7th lnternational Conference on Miniaturized Chemical and Biochemical Analysts Systems, uTAS '03*: Squaw Valley, CA, October 5-9 2003, pp 415-419.
13. Zellers, E. T.; Steinecker, W. H.; Lambertus, G.; Agah, M.; Lu, C.-J.; Chan, H. K. L.; Potkay, J. A.; Oborny, M. C.; Nichols, J. M.; Astle, A.; Kim, H. S.; Rowe, M.; Kim, J.; da Silva, L. W.; Zheng, J.; Whiting, J. *Solid-State Sens., Actuator and Microsyst. Workshop*: Hilton Head, SC, June 6-10 2004, pp 61-66.
14. Tian, W. C.; Tian, W.-C. *J. Microelectromech. Syst.* **2003**, 12, 264-272.
15. Tian, W. C.; Chan, K. L. H.; Lu, C.-J.; Pang, S. W.; Zellers, E. T. *J. Microelectromech. Syst.* **2005**, 14, 498-507.
16. Lu, C. J.; Zellers, E. T. *Analyst* **2002**, 127, 1061-1068.
17. Lu, C. J.; Zellers, E. T. *Anal. Chem.* **2001**, 73, 3449-3457.
18. Zellers, E. T.; Morishita, M., Cai, Q. –Y. *Sens. Actuators. B* **2000**, 67, 244-253.

19. Veeneman, R. A.; Zellers, E. T., *Solid-State Sensor, Actuator, Microsyst. Workshop*, Hilton Head, SC, June 1-5 2008; pp.252-255.
20. Serrano, G.; Reidy, S. M.; Zellers, E. T. *Sens. Actuators. B* **2009**, 141, 217-226.
21. Kim, S. K.; Chang, H.; Zellers, E. T. *Proc. Transducers '09*, Denver, CO, June 21-25 2009, pp 128-131.
22. Cai, Q.-Y.; Zellers, E. T. *Anal. Chem.* **2002**, 74, 3533-3539.
23. Steinecker, W. H.; Rowe, M.; Matzger, A.; Zellers, E. T. *Proc. Transducers '03* Boston, MA, June 9-13 2003, pp 1343-1346.
24. Hsieh, M.-D.; Zellers, E. T. *Anal. Chem.* **2004**, 76, 1885-1895.
25. Steinecker, W. H.; Rowe, M. P.; Zellers, E. T. *Anal. Chem.* **2007**, 79, 4977-4986.
26. Jin, C.; Kurzawski, P.; Hierlemann, A.; Zellers, E. T. *Anal. Chem.* **2008**, 80, 227-236.
27. Jin, C.; Zellers, E. T. *Anal. Chem.* **2008**, 80, 7283-7293.
28. Jin, C.; Zellers, E. T. *Sens. Actuators. B* **2009**, 139, 548-556.
29. Rairigh, D. J.; Warnell, G. A.; Xu, C.; Zellers, E. T.; Mason, A. J. *IEEE Trans. Biomedical Circuits and Systems* **2009**; 3, 267-276.
30. Covington, E.; Bohrer, F. I.; Xu, C.; Zellers, E. T.; Kurdak, Ç. *Lab Chip* **2010**, 10, 3058-3060.
31. Bohrer, F. I.; Covington, E.; Kurdak, Ç.; Zellers, E. T. *Anal. Chem.* **2011**, 83(10), 3687-3695.
32. Steinecker, W. H.; Kim, S. K.; Bohrer, F. I.; Farina, L.; Kurdak, Ç.; Zellers, E. T. *IEEE Sens. J.* **2011**, 11, 469-480.
33. Kim, S. K.; Chang, H.; Zellers, E. T. *Anal. Chem.* **2011**, 83, 7198-7206.
34. U. S. EPA, US Code, Federal Regulations, 40 CFR 51.100 – Definition – Volatile organic compounds (VOC), http://www.epa.gov/ttn/naaqs/ozone/ozonetech/def_voc.htm, as of March 31, 2009.
35. European Union Publications Office, Directive 2004/42/CE of the European Parliament and of the Council, EUR-Lex, http://eur-lex.europa.eu/LexUriServ/LexUriServ.do?uri=OJ:L:2004:143:0087:0087:EN:PDF
36. World Health Organization Regional Office for Europe, Air quality guidelines for Europe, 2nd ed. Copenhagen, 2000 (WHO Regional Publications, European Series, No. 91)
37. Wolkoff, P. *Indoor Air Suppl.* **1995,** 3, 1-73.
38. Brown, S. K.; Sim, M. R.; Abramson, M. J.; Gray, C. N. *Indoor Air* **1994,** 4, 123-134.
39. Brinke, J. T.; Selvin, S.; Hodgson, A. T.; Fisk, W. J.; Mendell, M. J.; Koshland, C. P.; Daisey, J. M. *Indoor Air* **1998,** 8, 140-152.
40. Edwards, R. *Atmospheric Environment* **2001,** 35, 4829-4841.
41. Lee, J. H. *Bulletin of the Korean chemical society* **2002,** 23, 488-496.
42. Minnesota Department of Health Fact Sheet, Volatile Organic Compounds (VOCs) in Your Home. **2010**, available at http://www.health.state.mn.us/divs/eh/indoorair/voc/vocfactsheet.pdf

43. U. S. EPA, Volatile Organic Compounds (VOCs), **2009**, available at http://www.epa.gov/iaq/voc.html#Health Effects
44. Hejazi, R. F.; Husain, T.; Khan, F. I. *J. of Hazardous Materials* **2003,** B99, 287-302.
45. Pekey, H.; Arslanbas, D. *Water Air Soil Pollut.* **2008,** 191, 113-129.
46. U. S. EPA, The 2008 Brownfields Technology Primer: Vapor intrusion considerations for redevelopment, EPA 542-R-08-001, **2008**, available at http://www.brownfieldstsc.org/pdfs/BTSC%20Vapor%20Intrusion%20Considerations%20for%20Redevelopment%20EPA%20542-R-08-001.pdf
47. Pankow, J.F.; Feenstra, S.; Cherry, J.A.; Ryan, M.C. Dense Chlorinated Solvents in Groundwater: Background and History of the Problem. In *Dense Chlorinated Solvents and Other DNAPLs in Groundwater*; Pankow, J.F.; Cherry, J.A., Ed.; Waterloo Press, Guelph, Ontario, 1996.
48. ATSDR, Tetrachloroethylene. **1997,** available at http://www.atsdr.cdc.gov/tfacts18.pdf.
49. U. S. EPA, NPL Site Narrative for Wurtsmith Air Force Base. **1994,** available at http://www.epa.gov/superfund/sites/npl/nar1416.htm.
50. ATSDR, Trichloroethylene. **2003,** available at http://www.atsdr.cdc.gov/tfacts19.pdf.
51. ATSDR, Toxicological Profile for Trichloroethylene (TCE), U.S. Department of Health and Human Services, September, 1997, available at http://www.atsdr.cdc.gov/toxprofiles/tp.asp?id=173&tid=30 , accessed August 2011.
52. U. S. Air Force, Guide for the Assessment of the Vapor Intrusion Pathway, 2006; available at http://airforcemedicine.afms.mil/idc/groups/public/documents/afms/ctb_050032.pdf.
53. McHugh, T.E.; Connor, J.A.; Ahmand, F. *Environ. Forensics* **2004**, 5, 33-44.
54. U.S. EPA Regions 3, 6, and 9 Risk-Based Regional Screening Levels; available at http://www.epa.gov/reg3hwmd/risk/human/rbconcentration_table/Generic_Tables/pdf/master_sl_table_bwrun_NOVEMBER2010.pdf
55. Mitigation Action Levels for Hill AFB, UT Indoor Air Sampling Program; available at http://www.hillrab.org/files/news/archive/2009/2009-03 Action Levels Change.htm
56. U.S. EPA OSWER, Review of the Draft 2002 Subsurface Vapor Intrusion Guidance, 2010; www.epa.gov/oswer/vaporintrusion/documents/review_of_2002_draft_vi_guidance_final.pdf
57. U. S. EPA, Compendium Method TO-15 Second Edition, available at http://www.epa.gov/ttnamti1/files/ambient/airtox/to-15r.pdf
58. U. S. EPA, Compendium Method TO-17 Second Edition, available at http://www.epa.gov/ttnamti1/files/ambient/airtox/to-17r.pdf
59. Odencrantz, J. E.; O'Neill, H.; Steinmacher, S. J.; Case, J. D.; Johnson, P. C. *Remediation* **2008**, 18, 49-54.
60. http://www.inficon.com

61. Gorder, K. A.; Dettenmaier, E. M. *Ground Water Monitoring and Remediation* **2011**, 31, 113-119.
62. Coffey, C.; Pearce, T.; Lawrence, R.; Hudnall, J.; Slaven, J.; Martin, S. *J. occupational and environmental hygiene* **2009**, 6, 1-8.
63. Thermo Scientific, Infrared Analyzer, MIRAN SapphIRe. available at http://www.thermo.com/com/cda/product/detail/1,,22553,00.html#MIRANXL.
64. Tarumi, T.; Small, G. W.; Combs, R. J.; Kroutil, R. T. *Vibrational Spectroscopy* **2005**, 37, 39-52.
65. Gasmet, Gasmet™ DX4030, available at http://www.gasmet.com
66. Taslakov, M.; Simeonov, V.; Bergh, H. V. D. *Journal of Physics - Conference Series* **2008**, 113, 012055.
67. Mulligan, C. C.; Justes, D. R.; Noll, R. J.; Sanders, N. L.; Laughlin, B. C.; Cooks, R. G. *Analyst* **2006**, 131, 556-567.
68. ICX, GRIFFIN 450 mobile GC/MS, available at http://www.griffinanalytical.com
69. Torion, Torion GC-TMS, available at http://www.torion.com
70. Hook, G.; Kimm, G. L.; Hall, T.; Smith, P. A. *Trends in Analytical Chemistry* **2002**, 21, 534-543.
71. Syage, J.; Nies, B. J.; Evans, M. D.; Hanold, K. A. *J. the American Society for Mass Spectrometry* **2001**, 12, 648-655.
72. Inficon, Hapsite ER Chemical Identification System, available at http://www.inficonchemicalidentificationsystems.com/
73. Persily, A.; Howard-Reed, C.; Nabinger, S. J. *Atmospheric Environment* **2003**, 37, 5505-5516.
74. Liu, X.; Pawliszyn, R; Wang, L. M. *Analyst* **2004**, 129, 55-62.
75. Agilent, 3000 Micro-GC, available at http://www.chem.agilent.com/en-us/products/instruments/gc/3000microgc/pages/default.aspx
76. Rasi, S.; Veijanen, A.; Rintal, J. *Energy* **2007**, 32, 1375-1380.
77. Services, G., Photovac Voyager, available at http://www.geotechnical.net/voyager.shtml
78. Arnold, N. S.; Dworzanski, J. P.; Sheya, S. A.; McClennen, W. H.; Meuzelaar, H. L. C. *Field Anal. Chem. & Technol* **2000**, 4, 219-238.
79. Femtoscan, available at http://www.femtoscan.com/pesticid.htm
80. Whalley, L. K.; Lewis, A. C.; McQuaid, J. B.; Purvis, R. M.; Lee, J. D.; Stemmler, K.; Zellweger, C.; Ridgeon, P. *J. Environ. Monit* **2004**, 6, 234-241.
81. Photovac Voyager, available at http://www.photovac.com/files/A4Voyager.pdf.
82. Schröoder, W.; Matz, G.; Kübler, J. *Field Analytical Chemistry & Technology* **1998**, 2, 287-297.
83. Defiant, Defiant gas chromatograph, http://www.defiant-tech.com/technology.php
84. U. S. EPA, Handheld detection system for TCE and PCE; EPD10021; U.S. Environmental Protection Agency, **2010**, available at

http://cfpub.epa.gov/ncer_abstracts/index.cfm/fuseaction/display.abstractDetail/abstract/9083

85. Kim, H.; Astle, A.; Najafi, K.; Bernal, L. P.; Washabaugh, P. D. *IEEE 20th Int'l Conf. Microelectromechanical System (MEMS)*: Kobe, Japan, January 21-25 2007; pp 131-134.
86. Kim, M.; Mitra, S. *J. Chrom.* **2003**, 996, 1-11.
87. Voiculescu, I.; McGill, R. A.; Zaghloul, M. E.; Mott, D.; Stepnowski, J.; Stepnowski, S.; Summers, H.; Nguyen, V.; Ross, S.; Walsh, K.; Martin, M. *IEEE Sens. J.* **2006**, 6, 1094-1104.
88. Camara, E. H. M.; Breuil, P.; Briand, D.; Guillot, L.; Pijolat, C.; de Rooij, N. F. *Sens. Actuators B* **2010**, 148, 610-619.
89. Manginell, R. P.; Adkins, D. R.; Moorman, M. W.; Hadizadeh, R.; Copic, D.; Porter, D. A.; Anderson, J. M.; Hietala, V. M.; Bryan, J. R.; Wheeler, D. R.; Pfeifer, K. B.; Rumpf, A. *J. Microelectromech. Syst.* **2008**, 17, 1396-1407.
90. Noh, H.; Hesketh, P. J.; Frye-Mason, G. C. *J. Microelectromech. Syst.* **2002**, 11, 718-725.
91. Dziuban, J. A.; Mroz, J.; Szczygielska, M.; Malachowski, M.; Gorecka-Drzazga, A.; Walczak, R.; Bula, W.; Zalewski, D.; Nieradko, L.; Lysko, J.; Koszur, J.; Kowalski, P. *Sens. Actuators A* **2004**, 115, 318-330.
92. Lambertus, G.; Elstro, A.; Sensenig, K.; Potkay, J.; Agah, M.; Scheuering, S.; Wise, K.; Dorman, F.; Sacks, R. *Anal. Chem.* **2004**, 76, 2629-2637.
93. Agah, M.; Potkay, J. A.; Lambertus, G.; Sacks, R.; Wise, K. D. *J. Microelectromech. Syst.* **2005**, 14, 1039-1050.
94. Bhushan, A.; Yemane, D.; Trudell, D.; Overton, E. B.; Goettert, J. *Microsyst. Technol.* **2007**, 13, 361-368.
95. Reidy, S.; Lambertus, G.; Reece, J.; Sacks, R. *Anal. Chem.* **2006**, 78, 2623-2630.
96. Stadermann, M.; McBrady, A. D.; Dick, B.; Reid, V. R.; Noy, A.; Synovec, R. E.; Bakajin, O. *Anal. Chem.* **2006**, 78, 5639-5644.
97. Potkay, J. A.; Lambertus, G. R.; Sacks, R. D.; Wise, K. D. *J. Microelectromech. Syst.* **2007**, 16, 1071-1079.
98. Radadia, A. D.; Masel, R. I.; Shannon, M. A.; Jerrell, J. P.; Cadwallader, K. R. *Anal. Chem.* **2008**, 80, 4087-4094.
99. Ali, S.; Ashraf-Khorassani, M.; Taylor, L. T.; Agah, M. *Sens. Actuators. B* **2009**, 141, 309-315.
100. Archibald, R.; Datskos, P.; Devault, G.; Lamberti, V.; Lavrik, N.; Noid, D.; Sepaniak, M.; Dutta, P. *Analytica Chimica Acta* **2007**, 584, 101-105.
101. Li, M.; Myers, E. B.; Tang, H. X.; Aldridge, S. J.; McCaig, H. C.; Whiting, J. J.; Simonson, R. J.; Lewis, N. S.; Roukes, M. L. *Nano Letters* **2010**, 10, 3899-3903.
102. Lu, C.-J.; Tian, W.-C.; Steinecker, W. H.; Guyon, A.; Agah, M.; Oborny, M. C.; Sacks, R.; Wise, K. D.; Pang, S. W.; Zellers, E. T. *7th lnternational Conference on Miniaturized Chemical and Biochemical Analysts Systems, uTAS '03*: Squaw Valley, CA, October 5-9 2003, pp 415-419.

103. Lewis, P. R.; Manginell, R. P.; Adkins, D. R.; Kottenstette, R. J.; Wheeler, D.; Sokolowski, S. S.; Trudell, D.; Byrnes, J. E.; Okandan, M.; Bauer, J. M.; Manley, R. G.; Frye-Mason, C. *IEEE Sens. J.* **2006**, 6, 784-795.
104. Zampolli, S.; Elmi, I.; Mancarella, F.; Betti, P.; Dalcanale, E.; Cardinali, G. C.; Severi, M. *Sens. Actuators. B* **2009**, 141, 322-328.
105. Terry, S. C.; Jerman, J. H.; Angell, J. B., A gas chromatographic air analyzer fabricated on a silicon wafer. *IEEE Trans. Electron Devices* **1979,** ED-26, 1880.
106. Varian Corp., C., CP-4900 Micro-GC. *on-line* **2004,** http://www.varianinc.com
107. C2V Concept to Volume, T. N., microDELTA. *on-line* **2004,** http://www.c2v.nl
108. Sandia-National-Labs, Micro-Scale Gas Separation Analyzer. *on-line* **2004,** http://www.darpa.gov
109. Kenda, A.; Drabe, C.; Schenk, H.; Frank, A.; Lenzhofer, M.; Scherf, W. In *Application of a micromachined translatory actuator to an optical FTIR spectrometer*, MEMS, MOEMS, and Micromachining II, Strasbourg, France, 2006; SPIE: Strasbourg, France, 2006; pp 618609-618611.
110. Yu, K.; Lee, D.; Krishnamoorthy, U.; Park, N.; Solgaard, O. *Sens. Actuators A* **2006,** 130-131, 523-530.
111. Kim, S.-S.; Young, C.; Mizaikoff, B. *Analytical and Bioanalytical Chemistry* **2008,** 390, 231-239.
112. Gao, L.; Sugiarto, A.; Harper, J. D.; Cooks, R. G.; Ouyang, Z. *Anal. Chem* **2008,** 80, 7198-7205.
113. Wapelhorst, E.; Hauschild, J.-P.; Müllera, J. *Sens. Actuators A* **2007,** 138, 22-27.
114. Lambertus, G. R.; Fix, C. S.; Reidy, S. M.; Miller, R. A.; Wheeler, D.; Nazarov, E.; Sacks, R. *Anal. Chem.* **2005**, 77, 7563-7571.
115. Serrano, G.; Chang, H.; Zellers, E. T. *Proc. Transducers '09*, Denver, CO, June 21-25 2009, pp 1654-1657.
116. Agah, M.; Lambertus, G. R.; Sacks, R.; Wise, K., High-speed MEMS-based gas chromatography. *Journal of microelectromechanical systems* **2006,** 15, (5), 1371.
117. Dziuban, J. A.; Mr, J.; Szczygielska, M.; Malachowski, M.; Gecka-Drzazga, A.; Walczak, R.; Bula, W.; Zalewski, D.; Nieradko, L.; Lysko, J.; Koszur, J.; Kowalski, P., Portable gas chromatograph with integrated components. *Sensors and Actuators A: Physical* **2004,** 115, (2-3), 318-330.
118. Staples, E. J.; Matsuda, T.; Viswanathan, S., Real Time Environmental Screening of Air, Water and Soil Matrices Using a novel Field Portable GC / SAW System. *Environmental Strategies for the 21st Century, Asia Pacific Conference* **1998**, 1-6.
119. Groves, W. A.; Zellers, E. T. *The Annals of Occupational Hygiene* **2001,** 45, 609-623.
120. Groves, W. A.; Zellers, E. T.; Frye, G. C. *Analytica Chimica Acta* **1998,** 371, 131-143.
121. Zellers, E. T.; Pan, T.-S.; Patrash, S. J.; Han, M.; Batterman, S. A. *Sensors and Actuators B: Chemical* **1993,** 12, 123-133.
122. WIMS^2 webpage, http://www.wimserc.org
123. Janata, J, Bezegh, A, *Anal. Chem*. 1988. 60. 62R-74R
124. Janata, J, Josowicz, M, *Anal. Chem*. 1998, 70, 179R-208R .

125. Szczurek, A.; Maciejewska, M.; Flisowska-Wiercik, B.; Bodzoj, L. *J. Environ. Monit.* **2009**, 11, 1942-1951.
126. Lee, D.S.; Jung, J.K.; Lim, J.W.; Huh, J. S, Lee. D.D. *Sens. Actuators B* **2001**, 77, 228-236.
127. Srivastava, A. K. *Sens. Actuators B* **2003**, 96, 24-37.
128. Tianshu, Z.; Hing, P.; Jiancheng, Z. *Sens. Actuators B* **1999**, 60, 208-215.
129. Hierlemann, A; et al., *Anal. Chem.*, **2000,** 72, 3696-3708.
130. Hierlemann, A; Zellers, E. T.; and Ricco, A. J.; *Anal. Chem.* **2001**, 73, 3458-3466.
131. Albert, K. J.; Walt, D. R.; Gill, D. S.; Pearce, T. C. *Anal. Chem.* **2001**, *73*(11), 2501-2508.
132. Grate, J. W. *Chem. Rev.* **2000**, *100*(7), 2627-2647.
133. Ballantine, D. S. Jr.; White, R. M.; Martin, S. J.; Ricco, A. J.; Zellers, E. T.; Frye, G. C.; Wohltjen, H., *Acoustic Wave Sensors. Theory, Design, and Physico-Chemical Applications;* Academic Press: San Diego, CA, 1997.
134. Patel, S. V.; Jenkins, M. W.; Hughes, R. C.; Yelton, W. G.; Ricco, A. J. *Anal. Chem.* **2000**, *72*(7), 1532-1542.
135. Severin, E. J.; Lewis, N. S. *Anal. Chem.* **2000**, *72*(9), 2008-2015.
136. Wohltjen, H.; Snow, A. W. *Anal. Chem.* **1998**, *70*(14), 2856-2859.
137. Rowe, M. P, Steinecker, W. H, and Zellers, E. T, *Anal. Chem*, 2007, 79, 1164-1172.
138. Jose, K A.; Biju, P; Ashwin, W.; *Smart materials and structures*, 2004, 13, 1045-1049
139. Srivastava, J. K.; Pandey, P.; Jha, S. K.; Mishra, V. N.; Dwivedri, R. *Sensors & Transducers* **2011**, 125, 42-48.
140. Chen, P. C.; Ishikawa, F. N.; Chang, H. K.; Ryu, K.; Zhou, C. *Nanotechnology* **2009**, 20, 155503.
141. Suslick, B. A.; Feng, L.; Suslick, K. S. *Anal. Chem.* **2010**, 82, 2067-2073.
142. Qi, X.; Crooke, E.; Ross, A.; Bastow, T. P.; Stalvies, C. *Analyst* **2011**, 136, 3731-3738.
143. Woodka, M. D.; Schnee, V. P. *Anal. Chem.* **2010**, 82, 9917-9924.
144. Park, J.; Groves, W. A.; Zellers, E. T. *Anal. Chem.* **1999,** 71, 3877-3885.
145. Jaumot, J.; Tauler, R. *Chemom. Intell. Lab. Syst.* **2010**, 103, 96-107.
146. De Juan, A.; Tauler, R. *J. Chromatog. A* **2007**, 1158, 184–195**.**
147. Manne, R. *Chemom. Intell. Lab. Syst.* **1995**, 27, 89-93.
148. Maeder, M. *Anal. Chem.* **1987**, 59, 527–530.
149. Gampp, H.; Maeder, M.; Meyer, C. J.; Zuberbuehier, A. D. *Talanta* **1985**, 32, 1133-1139.
150. Amrhein, M.; Srinivasan, B.; Bonvin, D.; Schumacher, M.M. *Chemom. Intell. Lab. Syst*.**1996**, 33, 17– 33.
151. Tauler, R.; Smilde, A.K.; Kowalski, B. J. *J. Chemom.***1995**, 9, 31– 58.
152. Tauler, R. *Chemom. Intell. Lab. Syst.* **1995**, 30, 133– 146.

153. Kowalski, B. R.; Sharaf, M. A. *Anal. Chem*. **1982**, 54, 1291-1296.
154. Xu, W.; Chen, K.; Liang, D.; Chew, W. *Anal. Biochem.* **2009**, 387, 42–53.
155. Hoggard, J. C.; Wahl, J. H.; Synovec, R. E.; Mong, G. M.; Fraga, C. G. *Anal. Chem.* **2010**, 82, 689–698.
156. Hoggard, J. C.; Siegler, W. C.; Synovec, R. E. *J. Chem.* **2009**, 23, 421–431.
157. Loszano, V. A.; Tauler, R.; Ibanez, G. A.; Olivieri, A. C. *Talanta* **2009**, 77, 1715–1723.
158. Szymanska, E.; Makuszewski, M. J.; Vander Heyden, Y.; Kaliszan, R. *Electrophoresis* **2009**, 30, 3573–3581.
159. Carneiro, R. L.; Braga, J. W. B.; Poppi, R. J.; Tauler, R. *Analyst* **2008**, 133, 774–783.
160. Jin, C.; Zellers, E. T.; Kurzawski, P.; Hierlemann, A. *Sensors, 2007 IEEE*, pp 1217-1220.

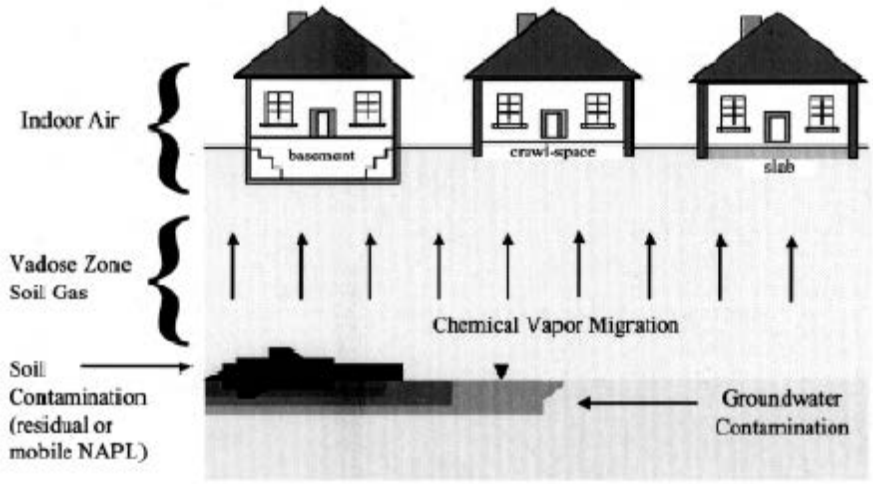

Figure 1-1. Generalized schematic of the pathway for subsurface vapor intrusion into indoor air.[1]

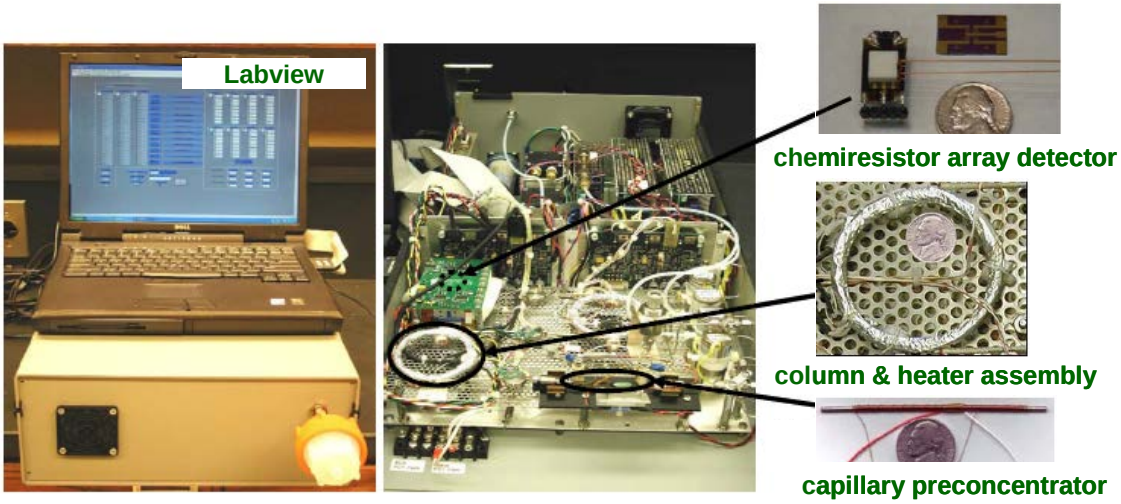

Figure 1-2. Meso-scale portable GC, consisting of a capillary preconcentrator/focusor, two non-polar separation columns, and a chemiresistor sensor array as the detector.

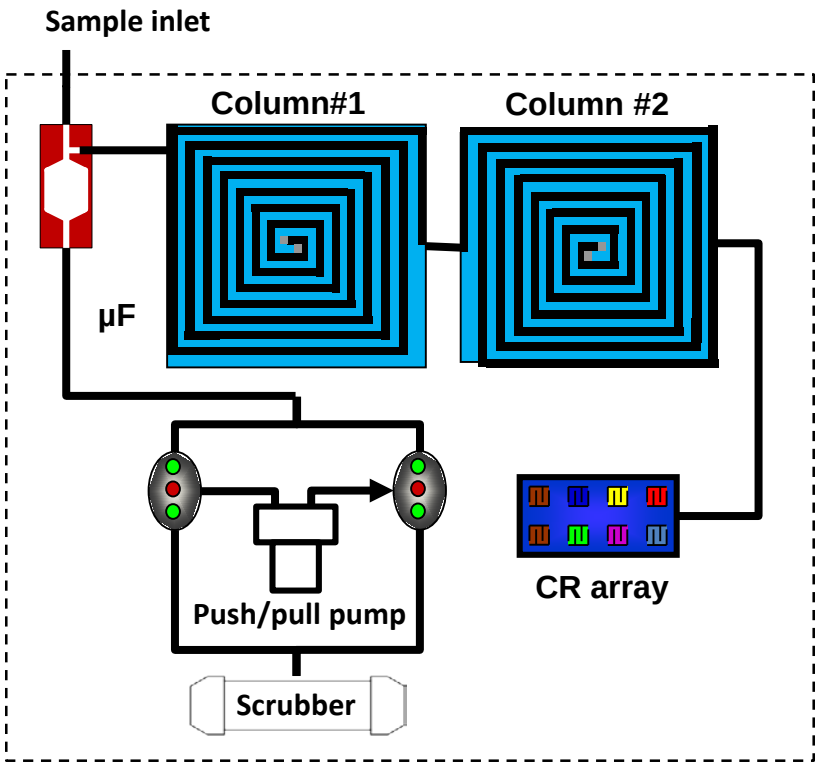

Figure 1-3. Concept diagram of WIMS^2 μGC.

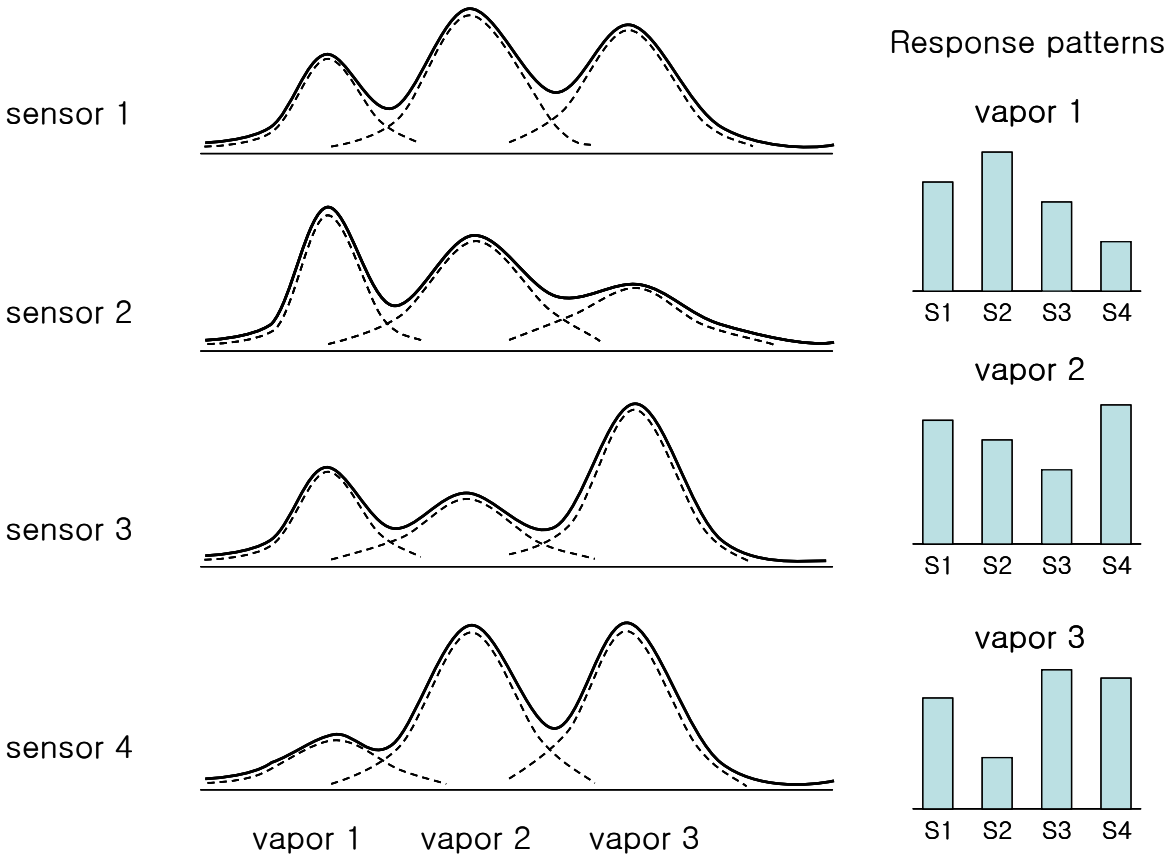

Figure 1-4. Deconvolution of overlapped peaks. Solid curves are the chromatograms obtained from different sensors, containing overlapped peaks of three partially overlapped pure components (dotted lines). Each pure component will correspond to a compound. Response patterns for individual vapors can be generated by using the pure components extracted by using EFA-ALS method.

CHAPTER II

Prototype Field-Portable GC with Nanoparticle-Coated Chemiresistor Array Detector for Sub-ppb Determinations of TCE Encountered in Homes Contaminated by Vapor Intrusion

2.1 Introduction

The term vapor intrusion (VI) is used to describe the mitigation of volatile organic chemicals (VOCs) into residential or office buildings from surrounding contaminated soils or groundwater. The pathways for VI contamination typically involve permeation or penetration through sub-surface walls by concentration or pressure gradients, and are considered as separate issues from indoor air contamination arising from sources within the building or from infiltration of ambient air contaminants.

The U.S. Department of Defense (DoD), regulators, private industry and others have recognized VI as an emerging problem. There are 10 DoD facilities currently known to have VI, including Hill Air Force Base (AFB), located in Utah (the site of our planned field study). Trichloroethylene (TCE) is the most common contaminant of concern (COC) at VI-impacted sites,[1] because of its use during 1960's and 1970's as a solvent for cleaning of metal parts and its release into the environment, either accidentally through leaks and spills or deliberately through dumping.[2-4] Once it is released into the environment, the problem is that it can migrate through the soil, can

reach the underlying groundwater because of its moderate solubility, and then can move a substantial distance with the groundwater from the original discharge point.[5] After spreading, it volatilizes into the overlying soil and can migrate through the soil, due to its relatively high vapor pressure (P_v = 69 torr at 25 °C). This pathway has been documented as the route of TCE VI into residences.[4] TCE is reported as a chemical that mainly affects the central nervous system acutely with symptoms including sleepiness, fatigue, headache, confusion, and euphoria.[6] Effects on the liver, kidneys, gastrointestinal system, and skin have also been noted as chronic problems, as well as the association with several types of cancers in humans, especially in the kidney, liver, cervix, and lymphatic system.[6] No standards have been set for VOCs in non-industrial settings, including TCE, while the threshold limit value (TLV, time-weighted-average) of TCE is 50 ppm for workplace environment.[7] Indoor air quality criteria for TCE vary among regulatory jurisdictions. The U.S. Air Force has implemented an environmental management program for hundreds of sites across the country, including both active and closed bases,[5] and has recently reset the mitigation action level (MAL) from 0.4 ppb to 2.3 ppb for residential buildings on or near bases (including Hill AFB).[8]

For low-level indoor VOC monitoring, U.S. EPA Method TO-15 has become the standard method to quantify and it uses Summa canisters for sample collection followed by GC-FID or GC-MS analysis.[9] U.S. EPA Method TO-17 is also used, but with lower frequency.[10] The method uses adsorbent-packed tubes for sampling followed by GC-FID/MS analysis. The time delay in obtaining results with these methods, however, can limit the quantity and quality of data available to guide VI investigations and interventions. The current convention of using 24-hour collection period for TO-15

precludes capture of the temporal variations in exposure to the residents. In addition, background VOCs from household products or human activities can make it difficult to differentiate such sources of TCE from that generated by VI. Efforts for mitigating VI are often made based on those monitoring results, but the inherent problem of those monitoring methods has an impact on the nature of such efforts implemented. Thus, there has been a demand for developing portable or permanently installed on-site analytical systems that can accurately determine TCE (or other VOCs of interest) at the low- or sub-ppb concentrations in the presence of other background VOCs. Various instruments might be considered for monitoring TCE, but few are suitable for routine *in situ* use because of reasons such as low sensitivity, limitation to determine components of multi-VOC mixtures, high cost, and high power consumption.

In response to the need, this study describes the adaptation of an existing prototype high performance portable GC to the determination of TCE in samples containing typical co-contaminants encountered in VI-impacted homes. An enhanced version of earlier prototypes,[11,12] this instrument incorporates a high-volume sampler to reduce LODs and sampling time; a single-stage adsorbent preconcentration/focuser (PCF); a tandem-column separation module with independent 'at-column' temperature-programming capabilities; and a detector comprising an array of microfabricated chemiresistor (CR) sensors with gold nanoparticle interface layers. In previous reports we characterized the prototype,[13] and described its use, for example, in environmental tobacco smoke (ETS) marker determination.[14]

This study was intended to guide the development of a field deployable microfabricated GC that can determine TCE vapors at sub-ppb concentration levels in the

presence of complex VOC mixtures in VI-impacted homes. As a preliminary result, a data set of 12 air samples was received from another research group (Kyle Gorder, U. S. Air Force, UT), which were collected in Summa canisters from VI-impacted homes near an U.S. Air Force base and analyzed by conventional methods (GC-MS) to identify and quantify TCE and the major co-contaminants. 10 most common interferences were selected based on the detection frequency and vapor pressures. A high-volume sampler was employed to capture sufficient TCE in a short time period to permit detection well below (~0.4 ppb) the MAL of 2.3 ppb in < 20 minutes.

To meet the purpose of this study, several tests were performed, including calibrations, LODs determination using the high volume sampler, chromatographic separation using mixtures of the 10 interferences, laboratory sample determinations such as blind sample, duplicate samples and sub-ppb level sample.

2.2 Prototype Description and Experimental Methods

2.2.1 Instrument Description and Operation

Since details of the instrument composition and operation have been provided in a previous report[13,14] only the salient features are provided here, along with modifications made during this study for adaptation to TCE determinations. The instrument weighs ~ 13.5 kg (including on-board power supply), measures 59 (l) x 32 (w) x 15 (h) cm, and operates on AC power. Air flow is provided by two small diaphragm pumps (UN86KTDC, KNF Neuberger Inc., Trenton, NJ) and is directed by four solenoid-actuated diaphragm valves (NResearch Inc., West Caldwell, NJ). The sequencing of functions is controlled by a laptop computer running routines written in LabView 7.1

(National Instruments, Austin, TX). The instrument automatically proceeds through a sequence of up to three operating modes whose timing, duration, and set-points can be user programmed.

Following a series of initial tests it was determined that a high-volume sampler was needed to be added to the front end of the original prototype in order to capture a sufficient quantity of TCE in a short enough time period to achieve the target LOD (~ 0.4 ppb) within the target analytical cycle time of 20 minutes. The sampler was fashioned from a TO-17 sampling tube packed with 200 mg of Carbopack X (specific surface area 250 m^2/g, Supelco, Bellefonte, PA) which was reported as an appropriate material to capture TCE[15] and wrapped with K-type thermocouple (Omega Engineering Inc., Stamford, CT) for temperature reading and Cu-wire coil (Consolidated Electronic Wire & Cable, Franklin Park, IL) for resistive heating. The sampler was mounted to the upstream of preconcentrator/focuser (PCF), as shown in Figure 2-1. The PCF is an insulated, thin-walled Inconel 600® tube (1.35 mm i.d., 7.5-cm long) (Accu-tube Corp., Englewood, CO) packed with graphitized carbon and wrapped with the K-type thermocouple for temperature reading and Cu-wire coil for resistive heating same as the sampler. For this study, the PCF tube was packed with 5 mg of 112-140 μm (sieved from 40/60-mesh) Carbopack X.

Both separation columns (4.5-m long, 0.25-mm i.d.) contain a wall-bonded polydimethylsiloxane stationary phase (DB-1, 0.5-μm thickness, Agilent, Wilmington, DE) in contrast to previous prototype which had a moderately polar second column with a wall-bonded polytrifluoropropylmethylsiloxane phase (RTX-200, 0.25-μm thickness, Restek, Bellefonte, PA). The reason for replacing the second column to another non-

polar column is that the polar column showed more than two times less efficiency than the non-polar column in terms of separation in the previous study.[13] The columns are heated independently using coiled 'at-column' heaters, (Agilent Technologies, Santa Clara, CA,).[12,16]

The detector, CR array consists of four sets of interdigital Au/Cr electrodes patterned on a single oxide-coated Si substrate. Each CR device contains 40 pairs of electrodes, 0.40-μm thick, and 5 μm wide with a 5 μm spacing and a 1.4 mm overlap.[17] Header pins bent at a 90º angle were soldered to the gold bonding pads and inserted into header sockets on a custom printed-circuit board (PCB) with multiple analog circuit trains for measuring resistance. Each CR sensor is coated with a different solvent-cast film of a gold-thiolate monolayer protected nanoparticle (MPN).[17-19] Film thicknesses were estimated to be ~200 nm, assuming 3 g/mL density.[17] The coated array is capped with a Macor® lid (cell volume ~ 1.5 μL) (Ceramic sheet, McMaster-Carr, Robbinsville, NJ) and fitted with inlet and outlet capillaries for fluidic interconnections. The cap is held in place with a patterned rectangular gasket of tape with adhesive on both sides that is 127-microns thick (VHB tape, 0.005 inch thickness, 3M, St. Paul, MN). MPNs derived from the following thiols were used in this study: n-octanethiol (C8), 1-mercapto-6-phenoxyhexane (OPH), methyl 6-mercaptohexanoate (HME), and 4-mercaptodiphenylacetylene (DPA).[14,20] A constant DC bias is applied to each sensor and the current is converted to a voltage, baseline corrected, amplified, and recorded with a D/A card on a laptop computer. In the CR array, vapors reversibly partition into each MPN film and cause it to swell, which changes the electron tunneling barrier and thereby the film resistance.[17,21] Since the structures of the MPN ligands differ on each sensor, the

affinities for a given vapor differ as well, and the array of CRs produces a different set of responses for each vapor. Baseline noise levels varied with the MPN film but were typically on the order of 10-20 mV. Since no other modification has been made on the instrument, more details about other components can be found elsewhere. [13,14]

In Sampling Mode, air is drawn by an on-board sampling pump through the sampler at 200 mL/min for 10 minutes. After sampling a pre-set air volume, the sampling pump is turned off and isolated from the system by an upstream valve. In Focusing Mode, the sampler is heated to 250 °C and the desorbed VOCs are focused to the PCF at 20 L/min for 5 min. An optional dry-air purge (Purge Mode) can then be performed in which the analysis pump draws ambient air in through a second inlet port and passes it through a scrubber cartridge located inside the instrument , which is packed with charcoal and 4A molecular sieves to remove VOCs and water vapor, respectively. The purified air is directed through the PCF and out through the sample inlet port, and serves to remove a portion of the water vapors from the adsorbents and to backflush residual VOCs from the fore line. In a typical sequence, the Purge Mode duration is about 60 sec.[12,15]

In Analysis Mode, the inlet valve is closed and ambient air, drawn into the system by the analysis pump, is scrubbed and then directed through the PCF, the separation columns, and the detector cell. After a 40-sec pressure stabilization period, the PCF is heated to 300 °C in < 2 sec and maintained at this temperature for up to 120 sec. The captured vapors are thereby injected into the first of the two separation columns. Eluting vapors are recognized and quantified by the CR array.

Following detection, the high volume sampler and PCF are re-conditioned by sequentially heating (300ºC) and backflushing with scrubbed air for 60 sec, and then

cooling actively with on-board fans prior to collecting the next sample. Assuming a 2-L sample volume at 200 mL/min sampling flow rate, a 5-min transfer step, and a 4-min separation, an entire analytical cycle (including post-sample PCF purge and cooling) can be completed in 20 min.

Custom-made software is run from a laptop computer and used to control the instrument and process the sensor output signals through separate 12 bit and 16 bit D/A data acquisition cards (Measurement Computing Corp., Middleboro, MA) at a rate of ≥ 50 Hz. The output voltages from the sensors are recorded in a text file and converted to chromatograms with Grams 32 software (Ver. 6.0, Thermo Scientific, Waltham, MA). Peaks were integrated with the same software.

2.2.2 Selection of Interferences and Test Atmosphere Generation

From the 12 sample data set for 75 compounds including TCE, the 10 most common interferences were selected based on the frequency measured among the 12 samples and on the vapor pressure (Table 1): selected interferences are 2-butanone, benzene, toluene, 2-hexanone, tetrachloroethylene, ethylbenzene, o-xylene, n-nonane, cumene and n-propylbenzene. These were found in at least 10-12 times of the 12 data sets and they have vapor pressures ranging from 3.4 torr (n-propylbenzene) to 95.2 torr (benzene). Concentrations of these co-contaminants ranged from 0.1 ppb for 2-hexanone to 58 ppb for toluene among the data sets provided. A mixture of TCE and the selected 10 interferences was analyzed with the portable GC.

Test atmospheres of TCE were generated by diluting samples taken from a certified compressed gas cylinder (Scott Specialty Gases Inc., Troy, MI) containing TCE

at 110 ppb (in N_2) with N_2 in Tedlar bags. For tests with the VOC interferences, the vapors were generated by injecting small volumes of the liquids into 12-L Tedlar® bags (SKC, Eighty-Four, PA) prefilled with a known volume of clean N_2 from a compressed-N_2 cylinder, and then samples of this test atmosphere were transferred by gas tight syringe to the bag containing TCE. For generating low-concentration test atmospheres, a process of one or two more dilutions was performed. Concentrations of test atmospheres were confirmed via a standard method, U.S. EPA method TO-15, by the analytical company, California Analytical Services (CAS, Simi Valley, CA).

2.2.3 Instrument Calibration and Laboratory Samples

Conditions required to separate TCE from the interferences were established using external sample loops with volumes ranging from 0.01-1 mL to cover the desired range of injected masses. Effective (mass-equivalent) vapor volumes were calculated according to the ratio of injection and sample volumes. For example, an aliquot of 1 mL from a sample loop containing 10 ppm of vapor is equivalent to 10 ppb in a 1-L sample volume. Mass-equivalent calibration concentrations ranged from 2.0 - 100 ppb-L.

Another calibration method was also employed by generating test atmospheres at four different concentrations ranging from 0.51 to 45 ppb. The calibration samples were also collected in TO-15 Summa canisters and then shipped immediately to CAS. The calibrated GC was then used for measuring TCE at a set of dynamic concentration range (0.42 - 28 ppb) samples, including duplicate samples and a blind sample (7.2 ppb) for accuracy test purpose. A test atmosphere for the mixture of interferences including TCE was also generated at ~10 ppb for the separation test purpose (also confirmed by CAS).

The samples generated in Tedlar bags were analyzed directly by the meso-GC and were also taken into evacuated 1-L canisters to be sent to CAS.

2.3 Results and Discussion

2.3.1 Calibration and Detection Limits

The instrument was calibrated with calibration samples in the range from 0.51 to 45 ppb, which were verified with TO-15 method. Figure 2-2 shows the calibration results. The sensitivities of C8, OPH, HME and DPA-coated CRs were calculated based on the slopes of the peak height results, 0.020, 0.024, 0.013, and 0.008 (V/ppb), respectively. Noise levels (standard deviation of the baseline) of the sensors were also determined in order to calculate the LODs, and were 0.0092, 0.0057, 0.0052, and 0.0035 (V), respectively. Using those sensitivity and noise data, LODs for the sensors assuming 1-L sample were calculated to be 1.4 ppb for C8, 0.7 ppb for OPH, 1.3 ppb for HME, and 1.3 ppb for DPA by the equation, LOD = sensitivity / 3 σ, where σ is standard deviation of baseline. To be conservative to detect TCE at sub-ppb concentration levels, the minimum sampling volume was determined to be more than 1 L (possibly up to 20 L). Assuming the sample volume of 6-L, calculated LODs for TCE would range from 0.12 ppb (OPH) to 0.23 ppb (C8), which satisfies the target LOD, 0.4 ppb. Note that the LODs do not necessarily correlate with the sensitivity values because of differences in the baseline noise for each sensor; the DPA and HME-coated sensors had particularly high baseline noise levels while the OPH-coated sensor had very low noise. The OPH-coated CR gave the lowest LOD and the highest sensitivity. C8-coated sensor gave a high sensitivity, but the noise level was also the highest. That is the reason why C8-coated sensor had the

highest LOD for TCE. These LODs are considered as minimum values because they are based on a single sensor. If responses are needed from the entire array for vapor recognition, then the LOD increases to 0.23 ppb for TCE, which is the highest among the four sensors. Compared to the earlier prototype,[12] the modifications made for this study lead to a 3-fold reduction in TCE LODs due to a larger sample volume.

2.3.2. Separation and Response Patterns

For the separation of TCE from interferences, two different concentration levels (0.44 ppb and 8.6 ppb, confirmed by TO-15) of mixtures were tested. First, the average concentrations of those samples determined by the meso-GC were 0.48 ppb and 9.0 ppb, respectively, showing the average error of 7.3 %. The relationship between TCE concentrations calculated from the sensors and those confirmed by TO-15 was linear, resulting linear regression r^2 values of >0.95 (forced zero). Interferences were added to be similar concentration as that of TCE. The separation of TCE from interferences is shown in Figure 2-3. TCE was fully separated from other compounds in ~ 1.3 min, while the latest eluting compound, n-propylbenzene, was analyzed within ~3.5 min.

In combination with the retention time, CR-array response patterns provide the means to recognize eluting vapors by reference to a library of calibrated patterns. The normalized response pattern for each vapor is shown in Figure 2-3. In TCE response pattern, C8-coated sensor showed the highest response followed by in the order of OPH, HME, and DPA-coated sensors. By visual inspection it is apparent that vapors from the same chemical class have patterns that are, in general, more similar than those for vapors from different classes.[18,19] Based on the correlation analysis (see Table 2), the TCE

response pattern is quite similar to benzene (0.974), tetrachloroethylene (0.961) and n-nonane (1.00). However, as seen in Figure 2-3, those vapors can be separated from TCE, chromatographically. Fortunately, chromatographic separation of homologues is also relatively easy. From the tabulation of relative response ratios within the sensor array in Table 2-2, the largest range of responses for any vapor is about 13-fold, with typical ranges being 1- to 5-fold.

2.3.3. Laboratory Sample Test

After calibration, the meso-GC was used for measuring TCE at a concentration range of 0.44 – 31 ppb and a blind sample at 7.2 ppb for accuracy test purpose. Duplicate samples were measured for 8.6 ppb test atmospheres. As expected for sorption-dependent sensors, sensitivity generally increases as the vapor pressure of the analyte decreases.[17,19] This is reflected in the within-sensor sensitivity ratios in Table 2-2. The functional-group interactions between the MPN ligands and the vapor also affect sensitivity as reflected in the response patterns. For example, the sensitivities of the C8-coated sensor (non-polar ligand) for n-nonane is much higher than that of the more polar HME-coated sensor.

Comparisons with TO-15 analyses are also shown in Figure 2-4 which shows that results from the meso-GC agree well with TO-15 results within 5 % of reference method for all different sensors, including blind sample, duplicates, and samples with 10 common interferences. Table 2-3 summarizes the result of laboratory sample test. All samples were determined to be within ±11 % of reference method results, except one low concentration (0.27 ppb) sample. Blind sample, which the operator was not informed

about, was also accurately determined showing the error of -7.2 %. Duplicate samples have the average error of 3%. Including the one exceptional sample, the overall error between meso-GC and TO-15 was ~ 10 %. Except the lowest concentration sample, the grand error rate was ~ 3.3 %.

To evaluate the capability of the instrument if it can detect a TCE sample at our targeted LOD concentration (0.4 ppb) in this study, a 6-L sample of 0.4 ppb sample was challenged to the system. Figure 2-5 presents the result of actual determination of TCE vapors at 0.4 ppb from all four different CR sensors.

2.4 Conclusions

The determination of TCE at trace ppt levels in moderately complex VOC backgrounds using a uniquely-equipped meso-GC prototype has been demonstrated through a series of laboratory experiments. Calculated LODs and dynamic ranges for TCE assuming a 6-L sample volume, are sufficient to guide efforts to monitor and remediate vapor intrusion of TCE in accordance with provisional action levels set by the U. S. Air Force for affected homes.

Several issues related to the adaptation of this instrument to VI-related TCE determinations were addressed and successfully resolved: 1) a high-volume sampler was developed and interfaced to the meso-GC to provide sufficient LODs while minimizing analytical cycle times; 2) a single-stage preconcentrator/injector was developed that provides quantitative trapping; 3) independent temperature programming of the dual-column separation module was used to separate TCE from prevalent interfering compounds in an elution time of < 3.5 min; and 4) an integrated chemiresistor array

employing functionalized gold nanoparticles interface layers was successfully used to accurately determine TCE at targeted concentration level. A complete sampling and analysis cycle can be completed every 20 minutes assuming 1-L sample volume. Results obtained from this study have been transferred to the development of a micro-scale GC used for the same purpose, as discussed in the next chapter.

2.5 References

1. Chiu, W. A.; Caldwell, J. C.; Keshava, N.; Scott, C. S. *Environ. Health Perspect.* **2006**, 114, 1445– 1449.
2. ATSDR, Tetrachloroethylene. **1997,** available at http://www.atsdr.cdc.gov/tfacts18.pdf
3. U. S. EPA, NPL Site Narrative for Wurtsmith Air Force Base. **1994,** available at http://www.epa.gov/superfund/sites/npl/nar1416.htm
4. ATSDR, Trichloroethylene. **2003,** available at http://www.atsdr.cdc.gov/tfacts19.pdf
5. U. S. Air Force, Guide for the Assessment of the Vapor Intrusion Pathway, 2006; available at http://airforcemedicine.afms.mil/idc/groups/public/documents/afms/ctb_050032.pdf
6. ATSDR, *Agency for Toxic Substances and Disease Registry. Toxicological Profile for Trichloroethylene (Update).* 1997. U.S. Public Health Service, U.S. Department of Health and Human Services, Atlanta, GA.
7. ACGIH TLV booklet, 2011.
8. Mitigation Action Levels for Hill AFB, UT Indoor Air Sampling Program; available at http://www.hillrab.org/files/news/archive/2009/2009-03 Action Levels Change.htm
9. U. S. EPA, Compendium Method TO-15 Second Edition, available at http://www.epa.gov/ttnamti1/files/ambient/airtox/to-15r.pdf
10. U. S. EPA, Compendium Method TO-17 Second Edition, available at http://www.epa.gov/ttnamti1/files/ambient/airtox/to-17r.pdf
11. Lu, C. J.; Jin, C.; Zellers, E. T. *J. Environ. Monit.* **2006**, 8, 270-278.
12. Lu, C.-J; Whiting, J.; Sacks, R. D.; Zellers, E. T. *Anal. Chem.* **2003**, 75, 1400-1409.
13. Zhong, Q.; Steinecker, W. H.; Zellers, E. T. *Analyst* **2009**, 134, 283-293.
14. Zhong, Q.; Veeneman, R. A.; Steinecker, W. H.; Jia, C.; Batterman, S. A.; Zellers, E. T. *J. Environ. Monit.* **2007**, 9, 440-448.
15. Lu, C. J.; Zellers, E. T. *Analyst* **2002**, 127, 1061-1068.
16. Agilent technologies, homepage, http://www.chem.agilent.com/en-US/products/instruments/gc/ltmrapidheatingcoolingforgc/pages/default.aspx

17. Steinecker, W. H.; Rowe, M. P.; Zellers, E. T. *Anal. Chem.* **2007**, 79, 4977-4986.
18. Lu, C.-J.; Steinecker, W. H.; Tian, W.-C.; Oborny, M. C.; Nichols, J. M.; Agah, M.; Potkay, J. A.; Chan, H. K. L.; Driscoll, J.; Sacks, R. D.; Wise, K. D.; Pang, S. W.; Zellers, E. T. *Lab Chip* **2005**, 5, 1123-1131.
19. Cai, Q.-Y.; Zellers, E. T. *Anal. Chem.* **2002**, 74, 3533-3539.
20. Rowe, M. P.; Plass, K. E.; Kim, K.; Kurdak, Ç.; Zellers, E. T.; Matzger, A. *Chem. Mater.* **2004**, 16, 3513-3517.
21. Wohltjen, H.; Snow, A.W. *Anal. Chem.* **1998**, 70, 2856-2859.

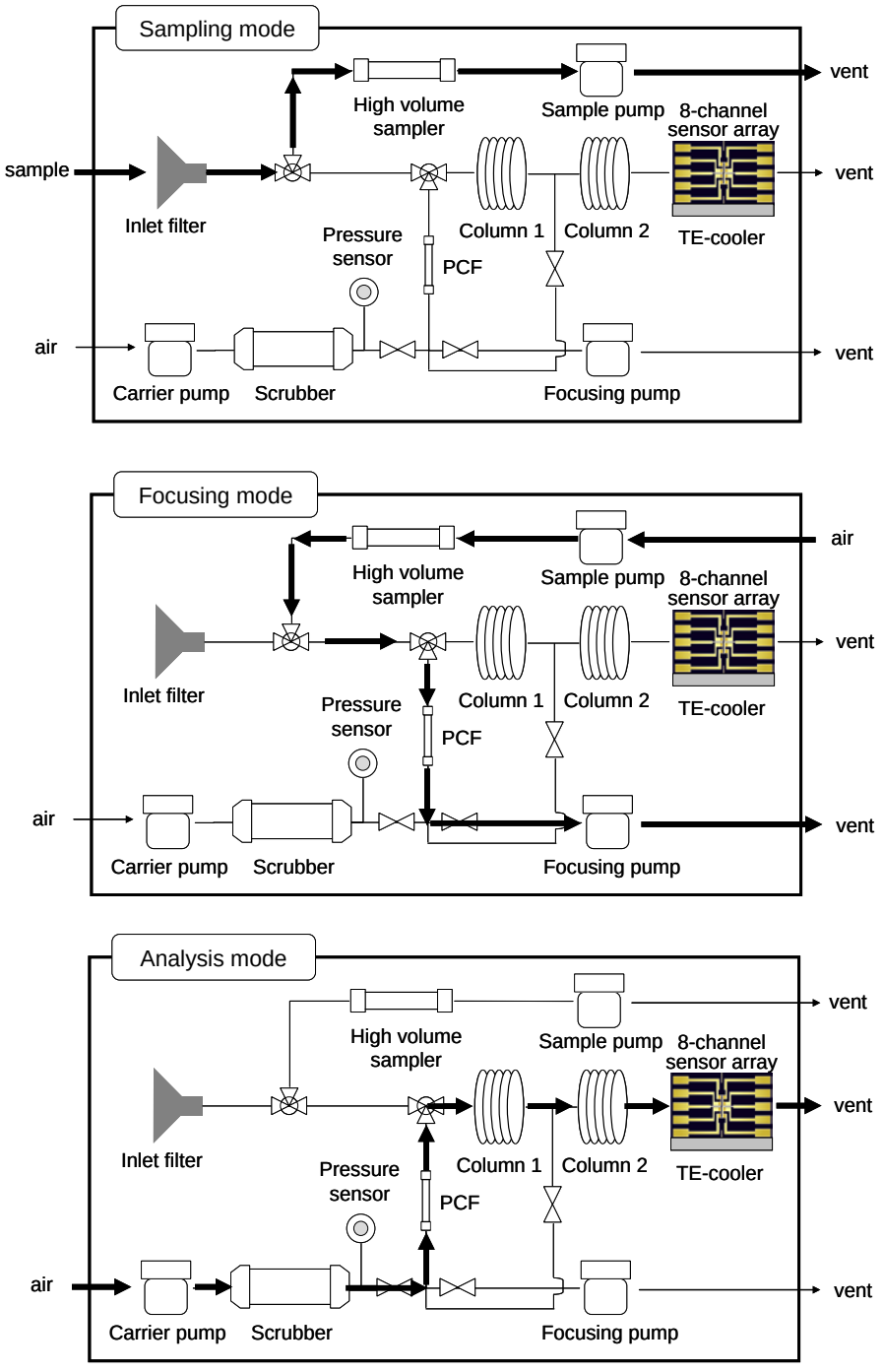

Figure 2-1. Block diagram of instrument and flow direction at each operation mode; sampling mode (upper), focusing mode (middle), and analysis mode (bottom).

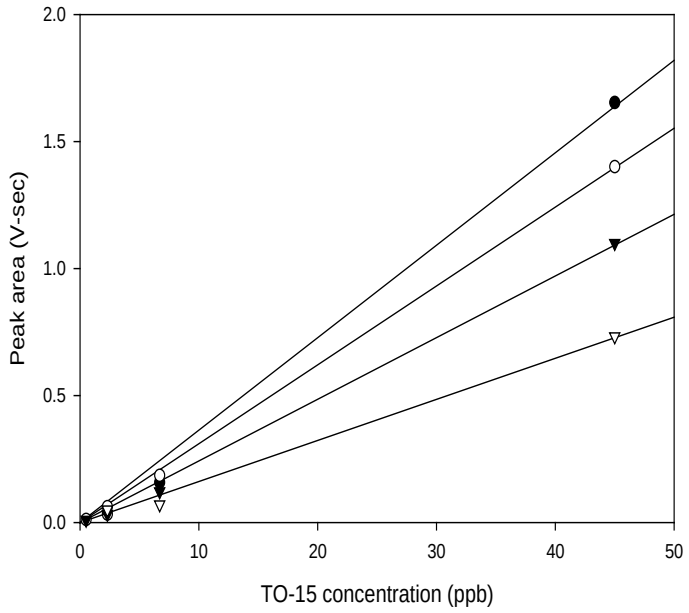

Figure 2-2. Calibration result of the CR sensor array with TCE samples ranging from 0.51 ppb to 54 ppb. Legend: filled circles: C8 (y=0.0305x); unfilled circles: OPH (y=0.0260x); filled triangles: HME (y=0.0203x); filled triangles: DPA (y=0.0135x).

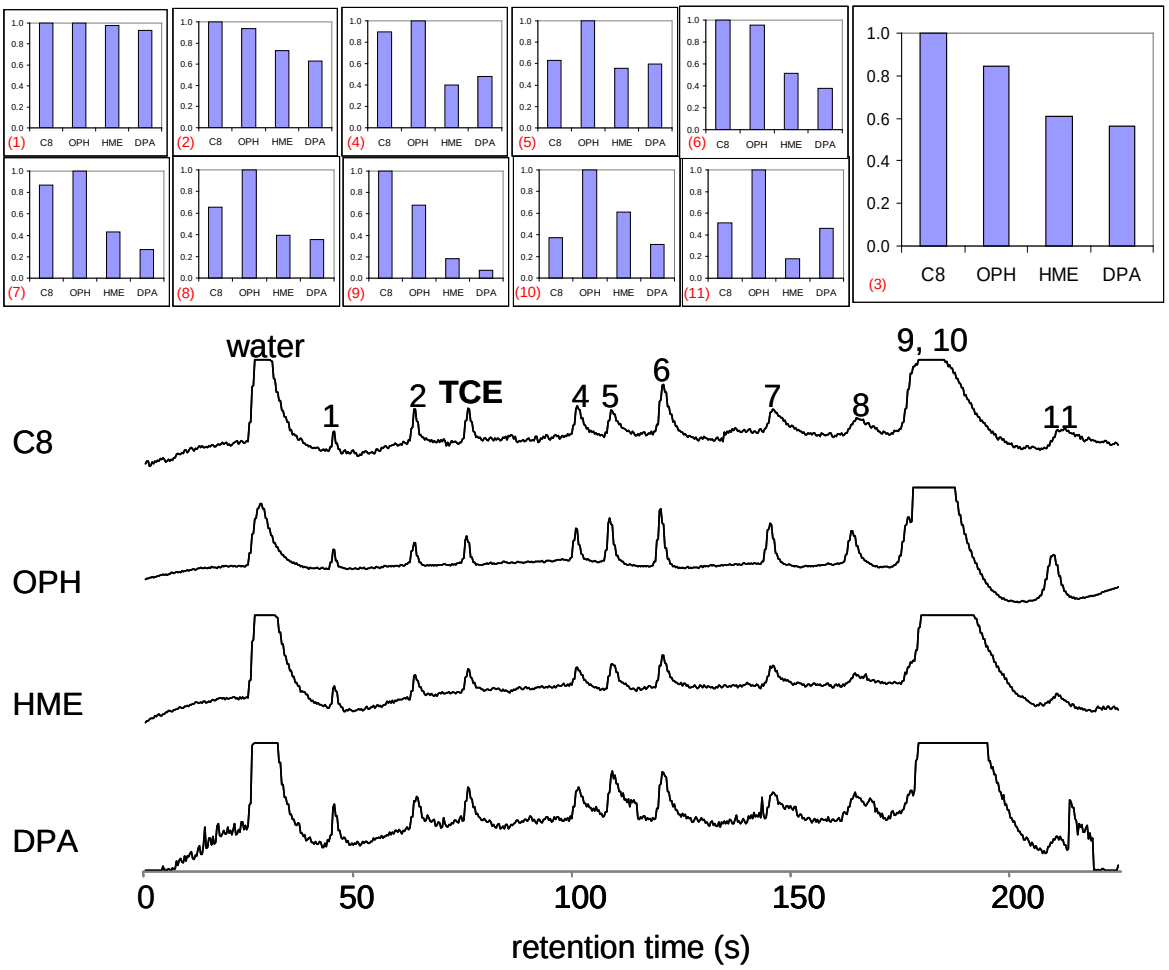

Figure 2-3. Chromatogram traces of TCE and 10 common VOCs found in indoor air at homes near an air force base. Normalized responses shown above the chromatograms illustrate the additional selectivity provided by the CR-array detector. The acronyms in the response patterns refer to the structures of the ligands of the MPNs: n-octanethiolate (C8), 1-mercapto-6-phenoxyhexane (OPH), methyl 6-mercaptohxanoate (HME), and 4-mercaptodiphenylaccetylene (DPA). Numbers on the chromatogram refer to the compounds: (1) 2-butanone, (2) benzene, (4) toluene, (5) 2-hexanone, (6) tetrachloroethylene, (7) ethylbenzene, (8) o-xylene, (9) n-nonane, (10) cumene and (11) n-propylbenzene.

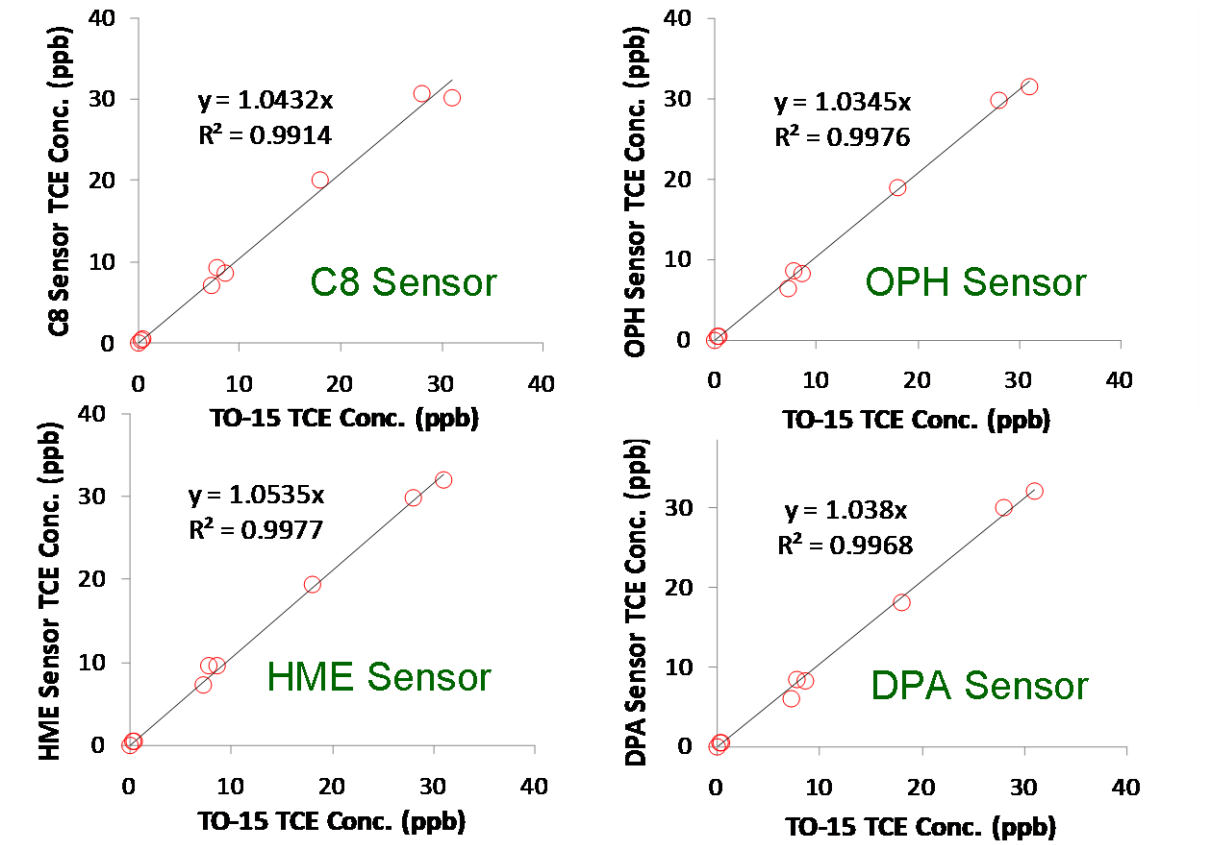

Figure 2-4. Comparison results of the GC performance versus US EPA Method TO-15.

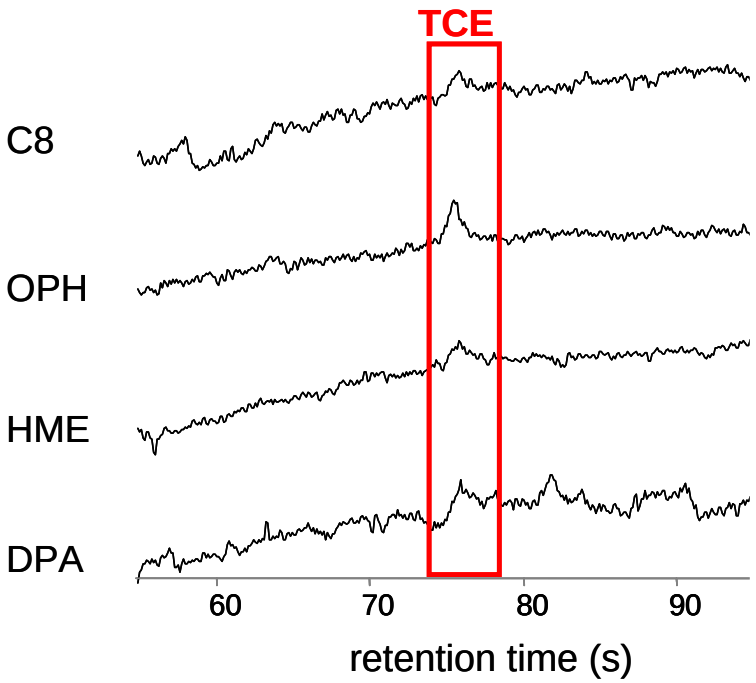

Figure 2-5. Sub-ppb level (0.4 ppb) TCE determination with the GC. The sample volume collected was 6 L. Acronyms for the thiolate ligands: n-octanethiolate (C8), 1-mercapto-6-phenoxyhexane (OPH), methyl 6-mercaptohexanoate (HME), and 4-mercaptodiphenylaccetylene (DPA).

Table 2-1. Target compound and interferences detected in homes near an Air Force base.

No.	Compound	Frequency [a]	P_v (torr) [b]
1	2-butanone	12	89
2	benzene	12	95.2
3	trichloroethene (TCE)	12	69
4	toluene	12	28.4
5	2-hexanone	10	12
6	tetrachloroethene	12	18.6
7	ethylbenzene	12	9.6
8	o-xylene	12	6.61
9	n-nonane	11	4.45
10	cumene	11	3.5
11	n-propylbenzene	11	3.4

[a] Detected frequency among 12 TO-15 data sets, [b] Vapor pressure at 25°C.

Table 2-2. Relative response patterns, response ratio, and correlation coefficient of TCE and other vapors from the GC analysis of an 11-vapor mixture including TCE and 10 other interferences.

		Sensor response (V·sec)[a]				Normalized sensor response[b]					
No.	Vapor	C8	OPH	HME	DPA	C8	OPH	HME	DPA	Ratio[c]	Corr.[d]
1	2-butanone	0.15	0.15	0.15	0.14	1.00	1.00	0.98	0.93	1.1	0.834
2	benzene	0.26	0.25	0.19	0.17	1.00	0.94	0.73	0.63	1.6	0.974
3	TCE	0.31	0.26	0.19	0.18	1.00	0.84	0.61	0.56	1.8	1.000
4	toluene	0.35	0.39	0.16	0.19	0.90	1.00	0.40	0.48	2.5	0.877
5	2-hexanone	0.35	0.56	0.31	0.33	0.63	1.00	0.55	0.60	1.8	0.399
6	PCE	0.78	0.75	0.40	0.29	1.00	0.96	0.51	0.38	2.7	0.961
7	ethylbenzene	0.65	0.74	0.32	0.20	0.87	1.00	0.43	0.27	3.7	0.886
8	o-xylene	0.53	0.81	0.32	0.29	0.66	1.00	0.40	0.36	2.8	0.685
9	n-nonane	1.15	0.79	0.21	0.087	1.00	0.68	0.18	0.08	13	1.000
10	cumene	9.04	24.4	14.9	7.52	0.37	1.00	0.61	0.31	3.2	0.169
11	n-propylbenzene	0.70	1.37	0.25	0.63	0.51	1.00	0.18	0.46	5.5	0.485

[a] Peak area. [b] For each vapor, the largest response (peak area) was assigned a value of 1.00 and all other responses were scaled accordingly. [C] within-sensor array response ratio for each vapor (largest response/smallest response). [d] Correlation coefficients of response patterns of TCE and other 10 vapors.

Table 2-3. Result of laboratory sample test with meso-GC, including blind sample, duplicate samples.

TO-15	meso-GC (ppb)					avg. error	Remark
(ppb)	C8	OPH	HME	DPA	avg.	(%)	
0.27	0.31	0.45	0.44	0.50	0.42	57	
0.44	0.49	0.46	0.47	0.51	0.48	9.5	
7.2	7.0	6.4	7.3	6.0	6.7	-7.2	blind sample
8.6	9.3	8.6	9.5	8.5	9.0	4.7	duplicates
8.6	8.7	8.3	9.6	8.2	8.7	1.2	duplicates
18	20	19	19	18	19	6.2	
28	30	31	32	32	31	12	
31	31	30	30	30	30	-3.2	

CHAPTER III

Microfabricated Gas Chromatograph for the Selective Determination of Trichloroethylene Vapor at Sub-Parts-Per-Billion Concentrations in Complex Mixtures

3.1 Introduction

Gas chromatographic microsystems (μGC) fabricated using Si-micromachining batch processing techniques have been the subject of a resurgence of interest over the past decade, and represent perhaps the most promising technology for meeting the need for small, low-power field instruments capable of analyzing volatile organic compounds (VOC) in moderately complex mixtures. Some prominent target applications include ambient air monitoring, worker exposure assessment, military surveillance, homeland security, and biomedical diagnostics.

Most of the research on μGC over this period of time has focused on the individual components of such microsystems, including micropumps,[1] micropreconcentrators,[2] microcolumns,[3] and microsensor or microsensor-array detectors.[4] Several reports have described subsystems that combine a microcolumn with one other micro-scale component.[3k, 5, 6] Yet, only a handful of studies have addressed complete μGC systems,[7] defined here as comprising a fluidically interconnected ensemble of at least the following three essential components, all of which are

microfabricated: a preconcentrator or other injector, a separation column, and a detector. The small number of such reports attests to the challenges associated with microsystem integration.

The earliest of these reports concerned a laboratory prototype μGC produced in our laboratory, which was capable of determining the components of moderately complex VOC mixtures at ppb concentrations.[7a-c] It included a multi-stage microfabricated preconcentrator/focuser (μPCF), which served as both a trap and an injector, a microcolumn with a 3-m-long separation channel, and a detector consisting of an integrated array of four chemiresistors (CR) that employed thiolate-monolayer-protected gold nanoparticles (MPN) as the sorptive interface layers. Performance tradeoffs were explored as a function of several operating variables. Combining the response pattern generated from the microsensor array with the corresponding chromatographic retention time facilitated the differentiation and identification of the components of the 11-VOC mixture that was analyzed.[7c] Since then, in collaboration with our colleagues,[8] we have improved the design and performance of several of the original μGC components, [3k,4l,n,o,9,10] developed new components,[11-14] and made further progress toward integrating them into microsystems for the quantitative analysis of VOC mixtures.[3k,6,7f,h,i,15,16]

The specific application for which the prototype described here has been optimized concerns the measurement of trichloroethylene (TCE) vapors arising from a phenomenon called vapor intrusion (VI). VI refers to indoor air contamination arising from the migration of volatile organic compounds (VOC) into occupied structures from underlying contaminated soil or ground water.[17] TCE is a common soil contaminant

found in proximity to numerous hazardous waste sites around the U. S. due to its historically widespread use as a degreasing solvent, indiscriminant disposal, environmental persistence, and volatility.[18] Indoor air concentrations of TCE arising from VI are often in the low- or sub-parts-per-billion (ppb) range,[19-21] which is also the range within which many common indoor air contaminants are typically encountered.[22] Therefore, determining TCE in locations potentially affected by VI requires preconcentration and separation from such co-contaminants.

Among the few currently available direct-reading instruments capable of *in situ* determinations of TCE at such low concentrations in the presence of numerous possible co-contaminants, the portable GC-MS appears to be the most effective due to its combination of chromatographic separation and spectrometric detection.[23,24] However, the utility of GC-MS for continuous, long-term assessments of indoor air contamination in multiple locations is severely limited by its cost and operating complexity. Thus, there remains a need for portable instruments capable of determining trace levels of specific VOCs in complex mixtures, yet small, simple, and inexpensive enough to be used for routine monitoring.

In this article we describe the design, development, assembly, and laboratory characterization of a high-performance μGC field prototype adapted specifically for TCE determinations in VI-impacted homes. An overview of the key components of the system as well as the application-specific variables that dictated their design, configuration, and operating conditions are provided in the next section. Descriptions of the materials, methods, and components used, along with their physical and functional integration are then provided, followed by results demonstrating the performance of the assembled

prototype.

3.1.1 Analytical Subsystem Design and Operating Conditions

Figure 3-1a shows a schematic diagram of the primary analytical components and fluidic pathways of the instrument. A commercial mini-pump (sample pump) draws an air sample through the manifold-mounted pre-trap and sampler at a high flow rate, bypassing the other components. Then, the appropriate valves are actuated and the sample pump draws scrubbed ambient air in the opposite direction through the sampler as it is resistively heated and backflushed to desorb and transfer the captured VOCs (including TCE) to the microfocuser (μF) at a lower flow rate. Following another set of valve actuations, the analysis mini-pump draws scrubbed air in and pushes it through the μF as the μF is heated rapidly to backflush and inject the captured VOC mixture into the first of two series-coupled microcolumns for analyte separation and detection by the array of nanoparticle-coated CR microsensors.

This laboratory study was performed in preparation for field testing in several residences near a U. S. Air Force base where TCE VI has been documented.[25] An indoor air concentration of 2.3 parts-per-billion (ppb) was established as a "mitigation action level" (MAL) for homes near this site, and historical monitoring indicated that TCE concentrations were most commonly between 0.2 and 8 ppb. On this basis we established a target limit of detection (LOD) of 0.06 ppb, a corresponding limit of quantitation (LOQ) of 0.2 ppb, and a calibration concentration range of ~40-fold for the prototype. Preliminary testing with the CR array detector installed downstream from the microcolumns yielded a provisional LOD for TCE of 1.2 ppb from a 1-L preconcentrated air sample.[7h] This corresponds to an integrated volume of 1.2 ppb-L and a mass of 6.4 ng

of captured TCE. Therefore, a sample volume of 20 L would be required to detect 0.06 ppb of TCE.

Our previous work with μPCFs[2b,c, 7c] and other miniaturized preconcentrators[4b, 26] suggested that such a large air sample volume would likely result in some degree of breakthrough of TCE, even at the low concentrations expected in the field. The narrow cross section and small volume of this device would also limit the maximum volumetric flow rates that could be passed through it, which would lead to excessively long sampling periods. In addition, any semi-volatile organic compounds (SVOCs) present in the air would be expected to adsorb strongly to all exposed surfaces, and only slowly desorb from the μPCF at normal desorption temperatures.[4k,27] Furthermore, the finite peak capacity of the relatively short microcolumns employed would limit the capability to chromatographically separate TCE from co-contaminants in captured samples.

To address this set of constraints, we developed a front-end preconcentrator-focuser (PCF) module consisting of a pre-trap of conventional design (i.e., an adsorbent-packed metal tube) for capturing interferences with vapor pressures (p_v) < 3 torr and a high-volume sampler, also of conventional design, for capturing (and transferring) TCE and other compounds with p_v values within the range of ~3-95 torr. Compounds with higher p_v values are allowed to pass through largely unretained. The sampler then transfers the captured VOCs to the μF chip for focusing and injection into the separation module. This PCF module provides the means to selectively, and quantitatively capture, transfer, and inject TCE vapor samples at the required concentrations in the presence of common indoor air contaminants.[10] It also greatly reduces the time required for a complete sampling and analysis cycle; although somewhat arbitrary, a target of roughly two

measurements per hour was set to provide a level of temporal resolution sufficient for guiding assessment and remediation efforts in the field.

Prior tests with the two 3-m microcolumns, both wall-coated with a polydimethylsiloxane (PDMS) stationary phase, indicated that ~3 min would be required for TCE and the most common co-contaminants that might be captured and injected along with TCE to elute with good chromatographic resolution.[7i] An estimate of the number of theoretical plates, N, required for such separations under the analytical conditions employed is consistent with this finding (see Appendix 1). Allowing a few minutes for the focusing step and for subsequent sensor baseline stabilization prior to injection, a sampling flow rate of ~1 $L \cdot min^{-1}$ was determined to be sufficient to meet the overall analysis time limit of ~30-40 min for samples requiring the maximum anticipated volume of 20 L.

3.2 Experimental Methods

3.2.1 Materials

The compounds used as potential interferences are a subset of the 63 VOCs found (by GC-MS) in a series of 12 air samples collected from VI-impacted residences near the site where field tests were ultimately conducted. These ranged in p_v values from 0.085 to > 5,000 torr. Since most of the 27 detected compounds with p_v values > 100 Torr are (by design) not captured efficiently by the adsorbent in the sampler, all but a few of them were eliminated from the test set. Some of the moderate- and low-volatility compounds were replaced with other compounds of similar structure and volatility often found as contaminants in indoor air that were available in the laboratory. The resulting set of 45

co-contaminants, which was considered sufficient to demonstrate selective TCE determinations, is presented in Table 3-1.

All VOCs were purchased from Sigma-Aldrich/Fluka (Milwaulkee, WI) or Acros/Fisher (Pittsburgh, PA) in >95% (most > 99%) purity and were used as received. The adsorbents used were graphitized carbons obtained from Supelco (Bellefonte, PA): Carbopack B (C-B, specific surface area = 100 m^2/g) was used in the pre-trap and Carbopack X (C-X, 250 m^2/g) was used in the sampler and the μF. Samples of C-B and C-X (60/80 mesh) were sieved and the fractions with nominal diameters in the range of 212-250 μm were isolated and packed in the appropriate device. The PDMS stationary phase polymer was obtained from Ohio Valley (OV-1, Marietta, OH) and the surface pre-treatment agent hexamethyldisilazane was obtained from Acros Organics (Geel, Belgium). MPNs derived from the following thiols were taken from existing supplies that were synthesized by the method reported by Rowe et al.:[28] n-octanethiol (C8), 6-phenoxyhexane-1-thiol (OPH), 4-(phenylethynyl)-benzenethiol (DPA), and methyl-6-mercaptohexanoate (HME). The MPNs had core diameters in the range of 3.4-4.7 nm.[4n]

3.2.2 PCF Module Components

The pre-trap and sampler were constructed from thin-walled stainless-steel tubes (0.64-cm o.d.; 0.54-cm i.d.; 6 cm long). A 50-mg bed of C-B was used in the pre-trap and a 100-mg bed of C-X was used in the sampler. The pre-trap does not retain TCE, and the 10% breakthrough volume of TCE through the sampler at 1 $L \cdot min^{-1}$ is > 30 L in the presence of 23 interferences (each at ~ 50 ppb) at high humidity.[10] Both devices were

heated with coils of insulated Cu wire and monitored with thermocouples held snugly against the tube walls.

The μF chip has dimensions of 9.76 × 4.18 × 0.6 mm. Deep-reactive-ion-etching (DRIE) was used to form a 3.2 (w) × 3.45 (l) × 0.38 mm (h) cavity with additional tapered sections leading to the inlet and outlet ports at opposing ends of the Si substrate, a set of pillars near the inlet and outlet ports to retain the adsorbent within the cavity, and inlet and outlet channels one of which has a right-angle tee-branch. The device was capped with an anodically bonded Pyrex plate. Cr/Au contact pads were evaporated onto the backside of the substrate for bulk resistive heating, and a Ti/Pt resistive temperature device (RTD) was patterned near the contacts for monitoring temperature. C-X (~2.3 mg) was loaded into the μF using gentle suction. Deactivated fused-silica interconnection capillaries (0.25-mm i.d., 0.32-mm o.d., Restek Corp., Belafonte, PA) were secured with adhesive (Duraseal® 1531, Cotronics, Brooklyn, N.Y). Electrical connections to a custom printed circuit board (PCB) were made via Al wire-bonds.

The maximum μF desorption temperature of 225 °C employed was sufficient to desorb TCE rapidly and completely, while low enough to minimize the risk of thermal degradation of the C-X, which we have found to shed small particles after repeated thermal cycling at > 250 °C in air. During injection the μF was heated at 440 °C/s for 0.45 s, maintained between 225 and 250 °C for 120 s, and then allowed to cool (see Figure 3-2 for a representative heating profile).

3.2.3 Microcolumns

Each microcolumn chip has a 3 × 3 cm footprint, and comprises a convolved square-spiral channel 3 m long with a rectangular cross section, 150 × 240 μm, formed in Si by DRIE and sealed by an anodically bonded Pyrex cover plate.[3f,l] The peripheral inlet and outlet ports accommodate deactivated fused-silica capillaries (250 μm i.d.) that were sealed with epoxy (Hysol® Epoxy Patch 1C, Henkel Corp., Rocky Hill, CT). Two meander-line Cr/Au heaters and a Ti/Pt RTD evaporated onto the backside of the microcolumns were used for programmed heating during separations. In this study, one set of microcolumns was modified by chamfering the corners within the spiral by using a different DRIE mask during fabrication and enlarging the heaters to improve the heat-transfer efficiency and uniformity. The microcolumns were individually pre-treated with HMDS, coated with a PDMS stationary phase from solution using a static deposition method, and then cross-linked using dicumyl peroxide (calc. avg. film thickness = 0.15 μm).[3l]

The maximum N produced by the microcolumns with chamfered corners is 4,550 plates/m, which is ~20% greater than that produced from microcolumns with right-angle corners (see Appendix 1 for Golay plots and a representative chromatogram). For all separations, microcolumn temperatures were maintained ≤ 120 °C to minimize stationary phase bleed.[4l]

3.2.4 Chemiresistor (CR) Array

Responses from MPN-coated CRs derive from the swelling induced changes in inter-particle distance as well as any changes in the dielectric constant accompanying

reversible vapor sorption.[4f] The CR array used in the prototype is the same as that used in a meso-scale instrument reported on previously.[4j,25] The array chip has dimensions of 2.0 × 1.2 cm and consists of 8 Au/Cr interdigital electrodes (IDEs) deposited in a 4×2 pattern on a thermal-SiO_x/Si substrate. Each IDE has 24 finger pairs (5 μm widths/spaces, 450 μm length, 410 μm overlap). A Macor® lid with inlet/outlet ports was sealed to the substrate using a gasket of VHB tape (3M, St. Paul, MN) to create a detector cell volume of 1.6 μL (0.3 (w) × 0.4 (l) × 0.013 cm (h)). Deactivated fused-silica capillaries were sealed into the ports with Hysol® epoxy. Two sensors were coated with each type of MPN by drop casting from solution with a 0.5-μL syringe to create multi-layer films with baseline resistances within the range of 1-10 MΩ (note: thicknesses were not determined). The CR array temperature was monitored via a calibrated on-chip RTD.

3.2.5 Device Mounting and System Integration

The assembled prototype has dimensions of 44 (w) × 25.5 (d) × 14.5 cm (h) and weighs 4.5 kg. Photographs of the key fluidic and analytical components are provided in Figure 3-1b-h. A stainless-steel manifold was created with top-surface access ports designed to match those on each of six 2-way latching micro-solenoid valves (Lee Co., Westbrook, CT) which were bolted in place (Figure 3-1g). The pre-trap and sampler were also mounted on the manifold using Teflon® Swagelok® fittings tapped into opposing sidewalls (Figure 3-1f, g). The two miniature diaphragm pumps (NMS020, KNF Neuburger, Trenton, NJ) (Figure 3-1h) were located beside the manifold and connected to the appropriate ports via flexible tubing.

The μF, CR array, and the dual-microcolumn separation module (Figure 3-1b-e) were mounted and wire-bonded on separate carrier PCBs which, in turn, were mounted on standoffs to the floor of the prototype. Cut-outs in the microcolumn PCB reduced the distances among these devices, which were connected by use of glass press-fits (Agilent Technologies, Palo Alto, CA). Two large, cylindrical scrubbers (Restek), each containing Drierite® and 5Å molecular sieves, as well as two smaller scrubbers containing activated charcoal (SKC Inc., Eighty Four, PA), were mounted to the external walls of the prototype chassis and used to remove water vapor and background organic vapors, respectively, during focusing and analysis. Additional components included two power supplies, three cooling fans. The custom circuit boards and associated DAQ cards used to monitor and control the prototype components are described in the Appendix 1.

3.2.6 Device Control and System Operation

Each measurement cycle consisted of sampling, focusing, stabilization, and analysis steps. User-defined pump, valve, and heater actuation timing and temperature settings, as well as the temperature program for each microcolumn, could be entered at the start of a run through the graphic user interface of the custom instrument control program written in LabView® and automatically implemented. However, manual operation of each step was also possible, and was often used during testing.

The sampler and pre-trap were preconditioned at 300 ^{o}C for 30 min under N_2 before initial use, and were periodically heated with backflushing under N_2 thereafter to remove residual trapped VOCs. VOCs were desorbed from the sampler to the μF at 220 °C by application of a constant dc voltage bias to the heater coil. The μF was heated to

225 °C by the application of a high initial dc voltage bias followed by a lower maintenance voltage. The microcolumns were temperature programmed using a pulse-width-modulation (PWM) method with a proportional-integral-derivative (PID) algorithm incorporated into a LabView sub-routine. Up to 6 settings and ramp rates could be specified for each microcolumn in a given run.

Resistance changes of the CR sensors were measured indirectly by applying a constant dc voltage to each CR through a 1-MΩ reference resistor, forming a voltage divider. The voltage drop across each CR was recorded by the DAQ card at 20 Hz after amplification of the signal difference between baseline and measured values. The methods used for data analysis and subsequent chemometric analysis are described in the Appendix 1.

3.2.7 Test-Atmosphere Generation

Test atmospheres of TCE were generated by diluting samples taken from a certified compressed gas cylinder (Scott Specialty Gases Inc., Troy, MI) containing TCE vapor at either 11 or 20 ppb (in N_2) with N_2 in Tedlar® bags. For certain tests, concentrations of the test atmospheres were confirmed by collecting samples in Summa® canisters and analyzing by GC-MS according to EPA Method TO-15[29] (analyses performed by Columbia Analytical Services, Simi Valley, CA). For tests run with other VOC interferences, a small volume (2.5 µL to 30 µL depending on the compound) of headspace from a vial of each pure liquid was drawn into a gas-tight syringe and injected on a background of clean air into the system through the septum port in a temporary tee connector placed in line upstream from the inlet.

3.3 Results and Discussion

3.3.1 System Integration

Due to flow restrictions in the manifold, the maximum flow rate achievable during sampling was 0.78 $L \cdot min^{-1}$. Therefore, collecting the largest anticipated sample volume of 20 L required 26 min. Focusing at 18 $mL \cdot min^{-1}$ for 3 min was sufficient to transfer TCE quantitatively to the μF (i.e., subsequent blank analyses yielded no measurable TCE) without breakthrough of the μF adsorbent bed.[10] For the stabilization step the flow through the microcolumns and sensor array was set at 1.2 $mL \cdot min^{-1}$ (discussed immediately below) and a minimum period of 3 min was required in order to regain stable sensor baseline signals. Although it required < 1 min for TCE to elute during the analysis step, up to 3.5 min was allowed for elution of the remaining mixture components to illustrate their full or partial resolution (note: this time period could be reduced by increasing the rate of heating). Thus, the maximum total sampling and analytical cycle time was ~36 min.

Reconciling flow rates among the devices in the analytical subsystem required tradeoffs in the various aspects of performance.[7b] Previous work had shown that the injection band width of TCE from the μF decreased sharply between 0.2 and 1 $mL \cdot min^{-1}$ and then more gradually up to 2 $mL \cdot min^{-1}$, reaching a minimum full-width-at-half-maximum (*fwhm*) value of 1s by FID.[10] Although the optimal efficiency for the dual column ensemble occurs at 0.22 $mL \cdot min^{-1}$ in air or N_2, the *fwhm* of the injection band at this low flow rate is > 2.7 s, which precludes the separation of TCE from early-eluting co-contaminants. Increasing the flow rate to 2 $mL \cdot min^{-1}$ minimizes the injection band width but also decreases N from 4,500 to ~700 plates/meter. The peak areas and *fwhm*

values from the CR sensors have been shown to decrease sharply up to a flow rate of 1.0 $mL \cdot min^{-1}$, followed by a more gradual decrease up to 3.3 $mL \cdot min^{-1}$.[4k] Thus, although lower flow rates yield higher sensitivities, they also yield broader peaks and incur a very high *sensitivity* to flow rate, which are undesirable. Notably, peak height shows a much smaller dependence on flow rate, which argues for using peak height as the sensitivity parameter.[4k] The analytical flow rate of 1.2 $mL \cdot min^{-1}$ adopted for all subsequent testing represents a compromise among the efficiency, resolution, speed, and sensitivity of the analysis.

3.3.2 Chromatographic Resolution and Array Response Patterns

A subset of 11 VOCs with p_v values ranging from 3.5 to 150 torr, bracketing that of TCE (p_v = 69 torr), was selected to develop the separation conditions and to illustrate the performance of the prototype. The set of chromatograms in Figure 3-3a was generated from the analysis of a 20-L spiked air sample with the prototype. As shown, TCE was separated from the 11 interferences in 45 s and the entire mixture eluted in < 3 min. The temperature program used for each microcolumn was determined empirically. A more aggressive heating ramp (i.e., > 7.6 $°C \cdot s^{-1}$) could be implemented after the first 45 s to reduce the analysis time, with a consequent loss of resolution of the later eluting compounds. This particular separation did not require the more elaborate temperature programming capability built in to the instrument.

The chromatogram from the HME-coated sensor shows an exceptionally large artifact peak at a retention time of ~25 s with a long tail that overlaps the TCE peak. This was eventually determined to be due to water vapor drawn in to the system during

focusing by a small leak in the downstream Teflon® fitting of the sampler. Separate testing confirmed that the water sensitivity of the HME sensor is significantly greater that of the other sensors in the array, consistent with the data shown in Figure 3-3a. Despite the overlap with the tail of this peak, it was possible to obtain sensitive and reproducible TCE responses from the HME sensor.

The mixture component eluting most closely to TCE is benzene. For the measured retention time (t_R) values of 39.1 and 45.3 s and *fwhm* values of 2.1 ± 0.3 and 2.0 ± 0.2 s (among all 4 sensors) for benzene and TCE, respectively, the resolution is 1.7. This is comparable to the resolution provided by the FID (top trace in Figure 3-3a); however, since the latter was placed downstream from the CR array it was subject to the band broadening associated with the array detector cell and interconnecting capillary (~40 cm). Regardless, it is interesting to note the differences in the relative magnitudes of various peaks between the sensors and the FID. For example, the benzene:TCE peak area ratio of 3.9 for the FID reflects the low sensitivity of the FID to chlorinated hydrocarbons, whereas the ratio of 1.1 for the C8 sensor (similar to the other sensors) reflects the similarity in partition coefficients of the two vapors in the MPN films.[4n]

CR array response patterns are presented in Figure 3-3b for TCE and the subset of 4 compounds eluting most closely to TCE. The TCE response pattern is quite distinct from those of n-hexane and MIBK but rather similar those of benzene and toluene, consistent with previous reports of microsensor arrays employing polymer or MPN interface layers.[4p,q] To assess the ability to recognize TCE and differentiate it from the other vapors in the set on the basis of its response pattern, retention time notwithstanding, Monte Carlo simulations coupled with EDPCR analyses were performed with the relative

response patterns generated from the data in Figure 3-3b. Details of the methodology and the resulting confusion matrix are presented in Table 3-2.

For TCE, the recognition rate (RR) value is only 80%, with the error being due almost entirely to confusion with benzene (i.e., excluding benzene, the RR value for TCE is > 99.5%). The RR values for n-hexane, benzene, MIBK, and toluene are 100, 83, 99, and 99 %, respectively. The low value for benzene is due to its confusion with TCE. Thus, while this confirms the value of the CR array to help identify TCE (and other analytes) it also emphasizes the need for chromatographic separation in utilizing the CR array (or any other microsensor array) for multi-vapor analyses.

3.3.3 Calibration, Detection Limits, and Accuracy

Figure 3-4 shows a set of calibration curves for TCE obtained by collecting samples of different volumes from two test atmospheres generated in Tedlar® bags from a compressed gas cylinder containing a low TCE concentration. The TCE bag concentrations were found to be 0.83 ppb and 18 ppb from duplicate canister samples analyzed by GC-MS. Ambient temperature and relative humidity during testing were 25 °C and 20%, respectively. Sample volumes of 2-8 L were collected and analyzed, resulting in a range of captured TCE masses from 9-390 ng and integrated vapor volumes of 1.7-72 ppb-L.

As shown, responses (peak areas) vary linearly with concentration. The corresponding plots of peak height show similar relative sensitivities and the same degree of linearity. TCE LODs calculated on the basis of these data are presented in Table 3-3 for assumed sample volumes of 1 and 20 L. For the latter, the LODs range from 0.04 ppb

(OPH) to 0.12 ppb (DPA). For reference, single-point estimates of the sensitivities for a subset of other vapors from Figure 3-3a were used to derive rough estimates of their LODs, as well: using the sensor that provided the lowest LOD value in the array for a given vapor, these range from 0.010 ppb for m-xylene (OPH) to 15 ppb for 2-propanol (C8) assuming a 20-L sample (note: n-nonane and cumene were excluded because of significant retention by the pre-trap, which also occurs to a lesser extent for compounds eluting after TCE).

The inset of Figure 3-4 shows the raw response data from all four sensors for a 20-L sample collected from a test atmosphere containing 0.12 ppb TCE (confirmed by GC-MS). Using the aforementioned calibration data, the average value obtained with the prototype using the peak areas from the four sensors was 0.12 ± 0.033 ppb (0 % error) and that using peak heights was 0.14 ± 0.035 ppb (+17% error). An additional 4-L sample of a test atmosphere containing 11 ppb of TCE (also confirmed by GC-MS) gave an average of 11 ± 0.40 ppb (0 %error) on the basis of the peak area calibrations and 12 ± 0.70 ppb (+9% error) on the basis of peak height. This degree of accuracy is sufficient for any practical purpose.

The preconcentration factor (PF) achieved by use of the high-volume sampler can be evaluated by taking the ratio of the sample volume to the volume of the peak measured at the detector, assuming that the same mass of TCE is contained in both (i.e., that the transfer efficiency is 100%). This corresponds to the ratio of the atmospheric concentration to the concentration delivered to the sensor array. For a *fwhm* value of 2.0 s at 1.2 $mL \cdot min^{-1}$ (0.02 $mL \cdot s^{-1}$) the volume of the TCE peak is ~0.04 mL. For a 20-L sample volume, PF = 500,000.

3.3.4 Stability

Previous reports have noted that the responses from MPN-coated CR sensors can drift over time, often significantly.[4k,o] The short-term stabilities of the retention times, responses, and response patterns were examined by replicate analyses of 2-L samples of 11 ppb of TCE (n = 10). Results are summarized in Table 3-4. The retention times varied by < 1% (RSD) for all 4 sensors (t_R = 45.3 sec) and the variation in peak areas ranged from 3.7% (OPH) to 9.1% (C8) (avg = 6.1%) for signal-to-noise ratios ranging from 25 (C8) to 94 (OPH). Similar results were obtained when using peak height values.

The stability of the response pattern was assessed using the pairwise correlation coefficients (*r*) between the pattern for the first sample and those of each subsequent sample. The *r* values ranged from 0.97 to 1.00 (peak area or height) for the first nine replicates and decreased to 0.95 for the last sample due to an anomalously low response from the HME sensor. Another set of replicates (n=6) collected for mixtures of benzene, toluene, ethylbenzene, and m-xylene spiked into each 20-L air sample gave RSDs of 0.4-0.9% and 13-30% (avg = 23%) for retention time and peak height, respectively. The relatively large variation in peak height values is attributed to the use of manual (syringe) injections to spike the air samples and to partial retention of the latter three compounds on the pre-trap adsorbent.

Medium-term stability was also examined by analyzing replicate 2-L samples of 11 ppb of TCE every few days for 4 weeks (Table 3-4). Within a given day, the RSD values among the responses (peak heights) from all sensors (n=4) were < 9.3 % and averaged 6.6% over the 15 days on which tests were run. Over the month, the RSDs of the grand averages of the 15 daily (average) values ranged from 7.7% (OPH) to 13%

(DPA) among the four sensors. The largest amount of drift was observed over the first week, after which sensitivities changed by < 10%. Net drifts ranged from -26 to +15% of the starting sensitivity values. Accordingly, the pairwise correlations between the relative response pattern for TCE from the first day and those from subsequent samples decreased over the first week (i.e., from r = 1.00 to 0.95), but then stabilized over the subsequent 3 weeks (i.e., r > 0.99). (Note: drift of a similar magnitude is apparent between the TCE responses in Figures 3-3 and 3-4, which were collected 2 weeks apart).

3.3.5 Complex Mixture Analysis

To test the ability of the prototype to analyze TCE in the presence of a large number of interferences, a mixture of 46 VOCs was introduced on a background of 20 L of clean air. Focusing, separation, and detection proceeded as described above and the microcolumn temperature programs were the same as those used to generate the chromatograms in Figure 3-3a. Firuge 3-5 shows the traces with each of the 38 other compounds not (completely) retained in the pre-trap designated by number. Eight of the 10 compounds with p_v values < 3 torr were effectively captured by the pre-trap, while two broke through to the sampler and were focused and analyzed. As shown, TCE is completely resolved and elutes in 45 s, and the entire mixture elutes within ~3.5 min. The tailing peak seen in the HME-sensor trace is a combination of water vapor (primarily) and a few of the more volatile, polar interferences to which the (polar) HME MPN has the most affinity.

Notably, benzene, toluene, ethylbenzene, and m-xylene are also resolved in this analysis, which suggests that they could be analyzed effectively with the prototype,

following some modifications to the pre-trap to ensure that they are transferred from the atmosphere to the sampler quantitatively. This bodes well for adapting the prototype to the quantitative analysis of multiple target compounds in the vapor pressure range of ~3-95 torr.

3.4 Conclusions

This is the first report of a field-deployable μGC prototype employing microsensor array detection that is capable of selective multi-VOC determinations at sub-ppb concentrations. Optimized for TCE, the instrument relies on selective high-volume preconcentration; microfocuser injection; rapid, temperature-programmed, dual-microcolumn separation; and microsensor-array recognition and quantification to analyze TCE in the presence of a complex mixture of background VOCs. The sensitivity, selectivity, accuracy, stability, and analytical cycle time demonstrated here, coupled with the capability for automated operation, indicate that this type of instrument would be effective in guiding efforts to monitor and mitigate TCE vapor intrusion in affected residences. In addition, it appears feasible to extend its use to the simultaneous analysis of other VOCs at sub-ppb concentrations, such as benzene, toluene, ethylbenzene, and xylene.

All of the analytical components of this μGC were microfabricated using standard processing methods and materials, which affords several inherent advantages, including: simple, high-yield, modular (interchangeable) components; small fluidic path dimensions and low dead volumes; rapid, low-power heating (for the μF and microcolumns); and low-profile multi-dimensional (spectrometric) detection. However, this study revealed

that the collective demands of the specific application addressed here, i.e., quantitative analysis of a relatively volatile target vapor at trace-level concentrations in the presence of numerous co-contaminants in a short period of time, could not be met by the microsystem alone, and required the use of a (selective) front-end preconcentration module made from non-microfabricated components.

Since completing this study, we have deployed two prototypes of this design in the field for tests in a home impacted by TCE arising from vapor intrusion. Results of these studies, which demonstrate the use of these instruments for monitoring spatial and temporal variations in TCE concentrations, will be reported in the near future.

3.5 References

1. Kim, H.; Astle, A.; Najafi, K.; Bernal, L. P.; Washabaugh, P. D. *IEEE 20th Int'l Conf. Microelectromechanical System (MEMS)*: Kobe, Japan, January 21-25 2007; pp 131-134.
2. (a) Kim, M.; Mitra, S. *J. Chrom.* **2003**, 996, 1-11. (b) Tian, W. C.; Tian, W.-C. *J. Microelectromech. Syst.* **2003**, 12, 264-272. (c) Tian, W. C.; Chan, K. L. H.; Lu, C.-J.; Pang, S. W.; Zellers, E. T. *J. Microelectromech. Syst.* **2005**, 14, 498-507. (d) Voiculescu, I.; McGill, R. A.; Zaghloul, M. E.; Mott, D.; Stepnowski, J.; Stepnowski, S.; Summers, H.; Nguyen, V.; Ross, S.; Walsh, K.; Martin, M. *IEEE Sens. J.* **2006**, 6, 1094-1104. (e) Camara, E. H. M.; Breuil, P.; Briand, D.; Guillot, L.; Pijolat, C.; de Rooij, N. F. *Sens. Actuators B* **2010**, 148, 610-619. (f) Manginell, R. P.; Adkins, D. R.; Moorman, M. W.; Hadizadeh, R.; Copic, D.; Porter, D. A.; Anderson, J. M.; Hietala, V. M.; Bryan, J. R.; Wheeler, D. R.; Pfeifer, K. B.; Rumpf, A. *J. Microelectromech. Syst.* **2008**, 17, 1396-1407. (g) Veeneman, R. A.; Zellers, E. T., *Solid-State Sensor, Actuator, Microsyst. Workshop*, Hilton Head, SC, June 1-5 2008; pp.252-255.
3. (a) Noh, H.; Hesketh, P. J.; Frye-Mason, G. C. *J. Microelectromech. Syst.* **2002**, 11, 718-725. (b) Dziuban, J. A.; Mroz, J.; Szczygielska, M.; Malachowski, M.; Gorecka-Drzazga, A.; Walczak, R.; Bula, W.; Zalewski, D.; Nieradko, L.; Lysko, J.; Koszur, J.; Kowalski, P. *Sens. Actuators A* **2004**, 115, 318-330. (c) Lambertus, G.; Elstro, A.; Sensenig, K.; Potkay, J.; Agah, M.; Scheuering, S.; Wise, K.; Dorman, F.; Sacks, R. *Anal. Chem.* **2004**, 76, 2629-2637. (d) Agah, M.; Potkay, J. A.; Lambertus, G.; Sacks, R.; Wise, K. D. *J. Microelectromech. Syst.* **2005**, 14, 1039-1050. (e) Bhushan, A.; Yemane, D.; Trudell, D.; Overton, E. B.; Goettert, J. *Microsyst. Technol.* **2007**, 13, 361-368. (f) Reidy, S.; Lambertus, G.; Reece, J.; Sacks, R. *Anal. Chem.* **2006**, 78,

2623-2630. (g) Stadermann, M.; McBrady, A. D.; Dick, B.; Reid, V. R.; Noy, A.; Synovec, R. E.; Bakajin, O. *Anal. Chem.* **2006**, 78, 5639-5644. (h) Potkay, J. A.; Lambertus, G. R.; Sacks, R. D.; Wise, K. D. *J. Microelectromech. Syst.* **2007**, 16, 1071-1079. (i) Radadia, A. D.; Masel, R. I.; Shannon, M. A.; Jerrell, J. P.; Cadwallader, K. R. *Anal. Chem.* **2008**, 80, 4087-4094. (j) Ali, S.; Ashraf-Khorassani, M.; Taylor, L. T.; Agah, M. *Sens. Actuators. B* **2009**, 141, 309-315. (k) Kim, S. K.; Chang, H.; Zellers, E. T. *Proc. Transducers '09*, Denver, CO, June 21-25 2009, pp 128-131. (l) Serrano, G.; Reidy, S. M.; Zellers, E. T. *Sens. Actuators. B* **2009**, 141, 217-226.

4. (a) Cai, Q.-Y.; Zellers, E. T. *Anal. Chem.* **2002**, 74, 3533-3539. (b) Lu, C.-J.; Whiting, J.; Sacks, R. D.; Zellers, E. T. *Anal. Chem.* **2003**, 75, 1400-1409. (c) Steinecker, W. H.; Rowe, M.; Matzger, A.; Zellers, E. T. *Proc. Transducers '03* Boston, MA, June 9-13 2003, pp 1343-1346. (d) Hsieh, M.-D.; Zellers, E. T. *Anal. Chem.* **2004**, 76, 1885-1895. (e) Archibald, R.; Datskos, P.; Devault, G.; Lamberti, V.; Lavrik, N.; Noid, D.; Sepaniak, M.; Dutta, P. *Analytica Chimica Acta* **2007**, 584, 101-105. (f) Steinecker, W. H.; Rowe, M. P.; Zellers, E. T. *Anal. Chem.* **2007**, 79, 4977-4986. (g) Jin, C.; Kurzawski, P.; Hierlemann, A.; Zellers, E. T. *Anal. Chem.* **2008**, 80, 227-236. (h) Jin, C.; Zellers, E. T. *Anal. Chem.* **2008**, 80, 7283-7293. (i) Jin, C.; Zellers, E. T. *Sens. Actuators. B* **2009**, 139, 548-556. (j) Rairigh, D. J.; Warnell, G. A.; Xu, C.; Zellers, E. T.; Mason, A. J. *IEEE Trans. Biomedical Circuits and Systems* **2009**; 3, 267-276. (k) Zhong, Q.; Steinecker, W. H.; Zellers, E. T. *Analyst* **2009**, 134, 283-293. (l) Covington, E.; Bohrer, F. I.; Xu, C.; Zellers, E. T.; Kurdak, Ç. *Lab Chip* **2010**, 10, 3058-3060. (m) Li, M.; Myers, E. B.; Tang, H. X.; Aldridge, S. J.; McCaig, H. C.; Whiting, J. J.; Simonson, R. J.; Lewis, N. S.; Roukes, M. L. *Nano Letters* **2010**, 10, 3899-3903. (n) Bohrer, F. I.; Covington, E.; Kurdak, Ç.; Zellers, E. T. *Anal. Chem.* **2011**, 83(10), 3687-3695. (o) Steinecker, W. H.; Kim, S. K.; Bohrer, F. I.; Farina, L.; Kurdak, Ç.; Zellers, E. T. *IEEE Sens. J.* **2011**, 11, 469-480. (p) Lu, C. J.; Jin, C.; Zellers, E. T. *J. Environ. Monit.* **2006**, 8, 270-278. (q) Zhong, Q.; Veeneman, R. A.; Steinecker, W. H.; Jia, C.; Batterman, S. A.; Zellers E. T. *J. Environ. Monit.* **2007**, 9, 440-448.
5. Lambertus, G. R.; Fix, C. S.; Reidy, S. M.; Miller, R. A.; Wheeler, D.; Nazarov, E.; Sacks, R. *Anal. Chem.* **2005**, 77, 7563-7571.
6. Serrano, G.; Chang, H.; Zellers, E. T. *Proc. Transducers '09*, Denver, CO, June 21-25 2009, pp 1654-1657.
7. (a) Lu, C.-J.; Tian, W.-C.; Steinecker, W. H.; Guyon, A.; Agah, M.; Oborny, M. C.; Sacks, R.; Wise, K. D.; Pang, S. W.; Zellers, E. T. *7th lnternational Conference on Miniaturized Chemical and Biochemical Analysts Systems, uTAS '03*: Squaw Valley, CA, October 5-9 2003, pp 415-419. (b) Zellers, E. T.; Steinecker, W. H.; Lambertus, G.; Agah, M.; Lu, C.-J.; Chan, H. K. L.; Potkay, J. A.; Oborny, M. C.; Nichols, J. M.; Astle, A.; Kim, H. S.; Rowe, M.; Kim, J.; da Silva, L. W.; Zheng, J.; Whiting, J. *Solid-State Sens., Actuator and Microsyst. Workshop*: Hilton Head, SC, June 6-10 2004, pp 61-66. (c) Lu, C.-J.; Steinecker, W. H.; Tian, W.-C.; Oborny, M. C.; Nichols, J. M.; Agah, M.; Potkay, J. A.; Chan, H. K. L.; Driscoll, J.; Sacks, R. D.; Wise, K. D.; Pang, S. W.; Zellers, E. T. *Lab Chip* **2005**, 5, 1123-1131. (d) Lewis, P. R.; Manginell, R. P.; Adkins, D. R.; Kottenstette, R. J.; Wheeler, D.; Sokolowski, S. S.; Trudell, D.; Byrnes, J. E.; Okandan, M.; Bauer, J. M.; Manley, R. G.; Frye-Mason, C. *IEEE Sens.*

J. **2006**, 6, 784-795. (e) Kim H.; Steinecker, W. H.; Reidy, S.; Lambertus, G. R.; Najafi, A. A. A. K.; Zellers, E. T.; Bernal, L. P.; Washabaugh, P. D.; Wise, K. D. *Proc. Transducers '07,* Lyon, France, June 10-14 2007, pp 1505-1508. (f) Zellers, E. T.; Reidy, S.; Veeneman, R. A.; Gordenker, R.; Steinecker, W. H.; Lambertus, G. R.; Kim, H.; Potkay, J. A.; Rowe, M. P.; Zhong, Q.; Avery, C.; Chan, H. K. L.; Sacks, R. D.; Najafi, K.; Wise, K. D. *Proc. Transducers '07*, Lyon, France, June 10-14 2007, pp 1491-1494. (g) Zampolli, S.; Elmi, I.; Mancarella, F.; Betti, P.; Dalcanale, E.; Cardinali, G. C.; Severi, M. *Sens. Actuators. B* **2009**, 141, 322-328. (h) Chang, H.; Kim, S. K.; Sukaew, T.; Bohrer, F.; Zellers, E. T. *Solid-State Sens., Actuator and Microsyst. Workshop*: Hilton Head, SC, June 6-10 2010, pp 278-281. (i) Chang, H.; Kim, S. K.; Sukaew, T.; Bohrer, F.; Zellers, E. T. *Procedia Engineering* **2010**, 5, 973-976.

8. http://www.wimserc.org/
9. Beach, K. T.; Reidy, S.; Gordenker, R. J.; Wise, K. D. *Proc. IEEE Micro Electro Mechanical Systems (MEMS),* Cancun, Mexico, January 23-27 2011. pp 813-816.
10. Sukaew, T.; Chang, H.; Serrano, G.; Zellers, E. T. *Analyst* **2011**, 136, 1664-1674.
11. Wallner, J. Z.; Hunt, K. S.; Obanionwu, H.; Oborny, M. C.; Bergstrom, P. L.; Zellers, E. T. *Physica Status Solidi A* **2007**, 204, 1449-1453.
12. Kim, S.-J.; Reidy, S. M.; Block, B. P.; Wise, K. D.; Zellers, E. T.; Kurabayashi, K. *Lab Chip* **2010**, 10, 1647-1654.
13. Kim, S.-J.; Serrano G.; Wise K. D.; Kurabayashi K.; Zellers E. T. *Anal. Chem.* **2011**, published on web, DOI: 10.1021/ac200336e.
14. Seo, J. H.; Kim, S. K.; Zellers, E. T.; Kurabayashi, K. *Proc. IEEE Microelectromech. Syst.*, Cancun, Mexico, January 23-27 **2011**, pp 825-828.
15. Kim, S. K.; Chang, H.; Bryant, J. G.; Burris, D. R.; Zellers, E. T. *Proc. Transducers '11,* Beijing, China, June 5-9 2011, pp. 799-802.
16. Zellers, E. T.; Serrano, G.; Chang, H.; Amos, L. K. *Proc. Transducers '11,* Beijing, China, June 5-9 2011, pp 2082-2085 .
17. U. S. EPA, Draft Guidance for Evaluating the Vapor Intrusion to Indoor Air Pathway from Groundwater and Soils, U. S. EPA: Washington DC, 2002, available at http://www.epa.gov/osw/hazard/correctiveaction/eis/vapor/complete.pdf.
18. Chiu, W. A.; Caldwell, J. C.; Keshava, N.; Scott, C. S. *Environmental Health Perspectives* **2006**, 114, 1445.
19. Fitzpatrick, N. A.; Fitzgerald, J. J. Presented at *Proc. 11th Annual Conference on Contaminated Soils,* Amherst, MA, October 21-24 1996, pp.1-15.
20. ATSDR, Public Health Assessment: Hill Air Force Base, Utah, Davis and Weber Counties, Utah, Federal Facilities Assessment Branch, Division of Health Assessment and Consultation, ATSDR, 2003, available at http://www.atsdr.cdc.gov/hac/pha/pha.asp?docid=795&pg=0, accessed June 2011.
21. Folkes, D.; Wertz, W.; Kurtz, J.; Kuehster, T. *Ground Water Monit. & Remed.* **2009**, 29, 70-80.
22. McHugh, T.; Connor, J.; Ahmad, F. *Environ. Forensics* **2004**, 5, 33-44.
23. Inficon, Hapsite, available at http://www.inficonchemicalidentificationsystems.com, accessed June 2011.
24. Fair, J. D.; Bailey, W. F.; Felty, R. A.; Gifford, A. E.; Shultes, B.; Volles, L. H. *J. Environ. Sciences* **2009**, 21, 1005-1008.

25. U. S. Air Force (AFIOH), Guide for the Assessment of the Vapor Intrusion Pathway, 2006; available at http://airforcemedicine.afms.mil/idc/groups/public/documents/afms/ctb_050032.pdf.
26. Lu, C. J.; Zellers, E. T. *Analyst* **2002**, 127, 1061-1068.
27. Zhong, Q.; Veeneman, R. A.; Steinecker, W. H.; Jia, C.; Batterman, S. A.; Zellers, E. T. *J. Environ. Monit.* **2007**, 9, 440-448.
28. Rowe, M. P.; Plass, K. E.; Kim, K.; Kurdak, Ç.; Zellers, E. T.; Matzger, A. *Chem. Mater*. **2004**, 16, 3513-3517.
29. U. S. Environmental Protection Agency (EPA), Compendium Method TO-15 Second Edition, available at http://www.epa.gov/ttnamti1/files/ambient/airtox/to-15r.pdf

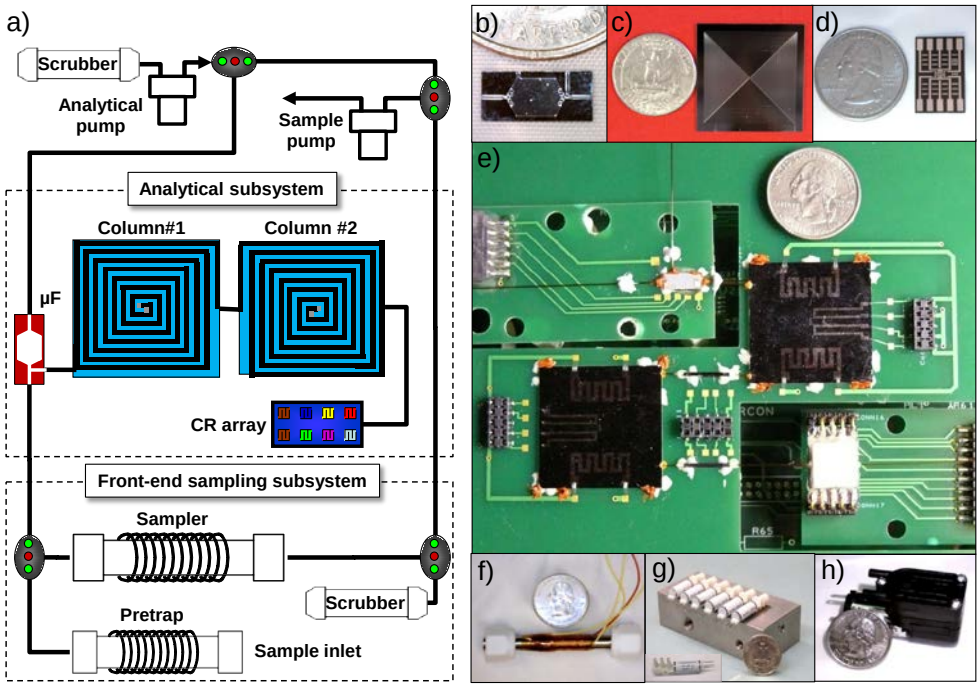

Figure 3-1. Fluidic diagram of the µGC prototype and photographs of the major components: a) schematic diagram showing fluidic pathways; b) microfocusor (µF); c) 3-m microcolumn; d) microsensor array; e) integrated micro-analytical subsystem; f) high-volume sampler/pretrap; g) valve and valve manifold; h) miniature diaphragm pump.

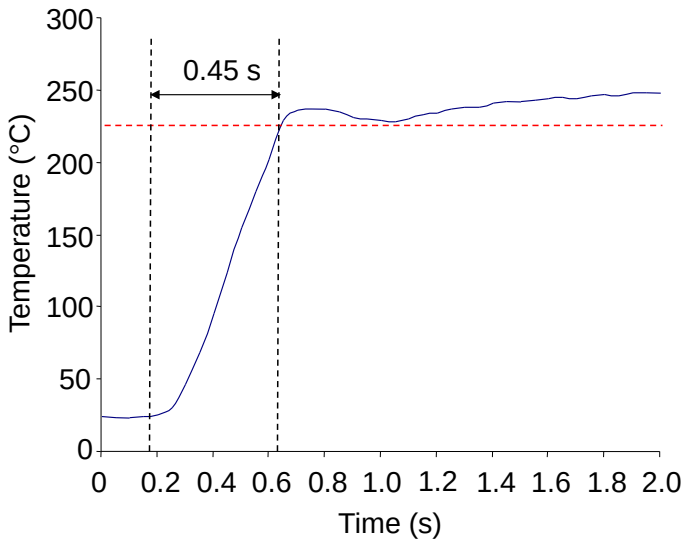

Figure 3-2. Representative (experimental) heating profile for the μF during desorption/ injection. Application of 36 V leads to an increase 25 to 225°C in 0.45 s (440 °C/s). Subsequent application of 16 V maintains the μF between 225 and 250 °C.

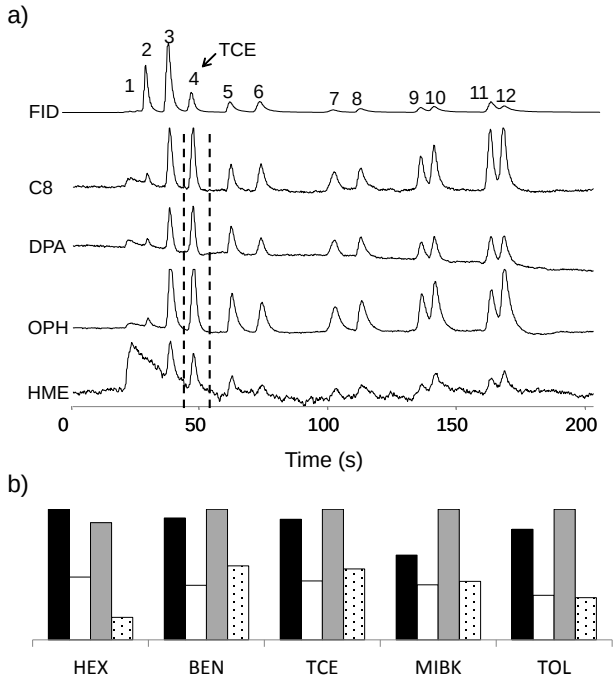

Figure 3-3. (a) 3-min chromatograms from the four CR microsensors and a downstream FID generated from the analysis of a 20-L air sample spiked with TCE and 11 VOC interferences by the μGC prototype. Peak assignments are as follows: 1, 2-propanol; 2, n-hexane (HEX); 3, benzene (BEN); 4, TCE; 5, 4-methyl-2-pentanone (MIBK); 6, toluene (TOL); 7, perchloroethylene; 8, butylacetate; 9, ethylbenzene; 10, m-xylene; 11, nonane; 12, cumene. The mixture composition was adjusted so that the range of sampled masses (34-1700 ng) decreased with decreasing analyte volatility (increasing retention time) and peaks of comparable size were obtained for all components in the chromatograms. Temperature program of 1st microcolumn: hold at 25 °C for 40 s, heat to 50 °C at 1.25 °C/s, heat to 120 °C at 0.58 °C/s, hold at 120 °C for 60 s. Temperature program of 2nd microcolumn: hold at 25 °C for 45 s, heat to 60 °C at 0.64 °C/s, heat to 120 °C at 0.75 °C/s, hold at 120 °C for 60 s. b) Normalized CR array response patterns for TCE and proximate interferences (black: C8, white: DPA, gray: OPH, dotted filled: HME).

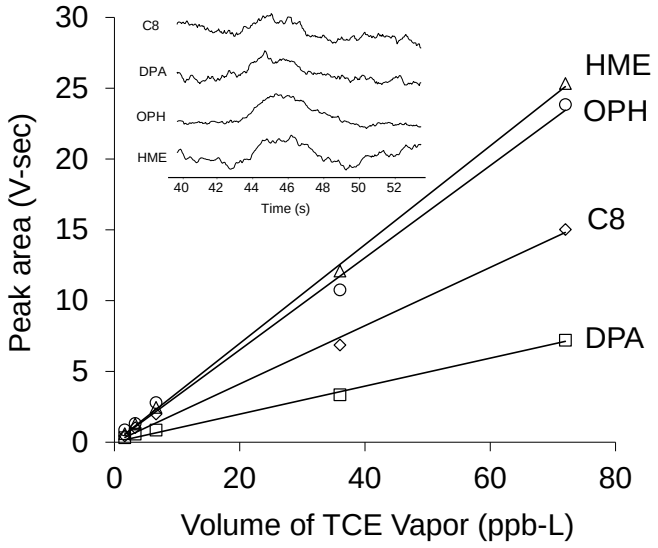

Figure 3-4. Calibration curves generated from sampling different volumes of test atmospheres of TCE in air. The net TCE volumes ranged from 1.7-72 ppb-L (9-390 ng): linear regression (forced zero) r^2 values are all > 0.99. Concentrations were confirmed by independent GC-MS analysis. Inset shows chromatograms from the analysis of a test atmosphere containing 0.12 ppb of TCE in air (sample volume: 20 L; TCE volume: 2.4 ppb-L; TCE mass: 13 ng).

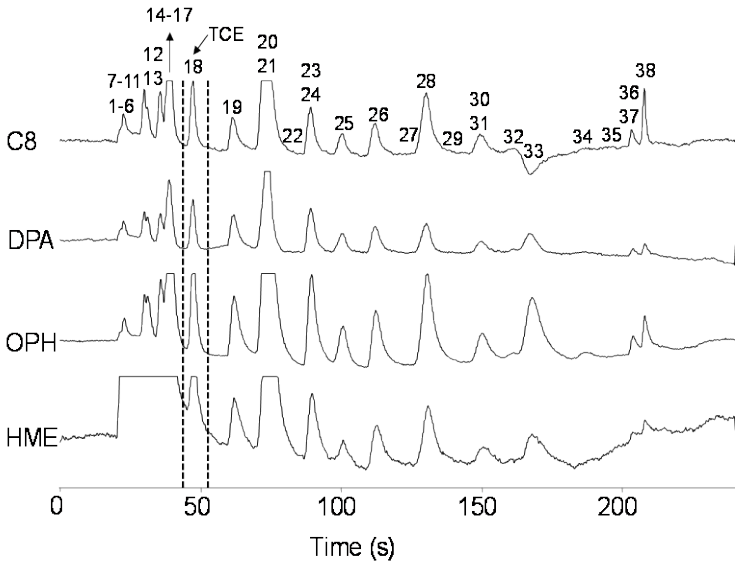

Figure 3-5. Chromatograms from the four CR microsensors generated from the analysis of a 20-L air sample spiked with TCE and 45 interferences. Eight of the interferences were (by design) retained by the pretrap and therefore do not appear in the chromatograms. Numbers correspond to the compounds listed in Table 3-1.

Table 3-1. List of 46 test compounds and their vapor pressures (p_v).

ID	Compound	p_v (torr)[a]	ID	Compound	p_v (torr)[a]
1	Pentane	514	24	n-Octane	14.1
2	1,2-Dichloroethane	333	25	n-Butyl Acetate	15
3	Methylene Chloride	349	26	Chlorobenzene	11.8
4	Acetonitrile	73	27	Ethylbenzene	9.6
5	2-Propanol (Isopropyl Alcohol)	44	28	m,p-Xylenes	8.29
6	Acrylonitrile	97	29	Bromoform	5
7	2-Butanone (MEK)	89	30	o-Xylene	6.61
8	n-Hexane	150	31	Styrene	6.4
9	Ethanol	60	32	n-Nonane	4.45
10	Tetrahydrofuran (THF)	162	33	Cumene	3.5
11	Chloroform	200	34	alpha-Pinene	4.75
12	Acetone	231	35	n-Propylbenzene	3.42
13	1,1,1-Trichloroethane	100	36	1,2,4-Trimethylbenzene	2.1
14	Ethyl Acetate	93.7	37	4-Ethyltoluene	3
15	Carbon Tetrachloride	113	38	1,3,5-Trimethylbenzene	2.48
16	Benzene	95.2	39	d-Limonene	1.98
17	Cyclohexane	98	40	1,2,4-Trichlorobenzene	0.5
18	Trichloroethylene (TCE)	69	41	1,4-dichlorobenzene	1.76
19	4-Methyl-2-pentanone	20	42	Naphthalene	0.08
20	1,1,2-Trichloroethane	17	43	n-Decane	1.4
21	Toluene	28.4	44	n-Undecane	0.564
22	2-Hexanone	12	45	n-Dodecane	0.21
23	Tetrachloroethylene (PCE)	18.6	46	n-Tridecane	0.081

Table 3-2. Confusion matrix for single-vapor discrimination.[a]

Compound	HEX	BEN	TCE	MIBK	TOL
HEX	500	0	0	0	0
BEN	0	415	97	0	0
TCE	0	85	402	1	0
MIBK	0	0	1	496	5
TOL	0	0	0	3	495
Recognition rate (%)	100	83.0	80.4	99.2	99.0

[a] Based on Monte Carlo simulations and EDPCR classification models (see text); HEX = n-hexane, BEN = benzene, TCE = trichloroethylene, MIBK = 4-methyl-2-pentanone, TOL = toluene; actual identities are listed in the top row and assigned identities are listed in the first column; n = 500 iterations for each vapor.

Table 3-3. Limits of detection for TCE from each sensor in the array for two assumed sample volumes.

Sensor	LOD[a] (ppb)	
	1 L	20 L
C8	1.7	0.08
DPA	2.4	0.12
OPH	0.8	0.04
HME	1.4	0.07

[a] LOD = 3s/sensitivity, where s = standard deviation of baseline noise determined for each sensor and sensitivity was taken as the slope of the calibration curve in Figure 3-4.

Table 3-4. Short- and medium-term stability of retention times and sensor responses.

Period	Sensor	RSD (%)[a]		
		Peak area	Peak height	t_R
Short-term[b]	C8	9.1	8.1	0.9
	DPA	3.9	2.7	1.0
	OPH	3.7	2.2	0.9
	HME	5.6	9.5	0.9
	avg	5.6	5.6	1.0
Medium-term[c]	C8	8.2	9.5	1.4
	DPA	15	13	1.4
	OPH	10	7.7	1.3
	HME	10	9.4	1.4
	avg	11	9.9	1.4

[a] relative standard deviation

[b] n = 10 replicates within a single day

[c] n = 15 replicates over one month

CHAPTER IV

Microfabricated Gas Chromatograph for On-Site Determination of Trichloroethylene in Indoor Air Arising from Vapor Intrusion Part I: Field Evaluation

4.1 Introduction

Trichloroethylene (TCE) is a common groundwater contaminant due to its former widespread use as a degreasing solvent, inappropriate disposal, low rate of biodegradation under aerobic conditions and appreciable aqueous solubility.[1] These factors, in addition to its relative high vapor pressure (p_v; 69 Torr) have led to increased concern about TCE vapor intrusion (VI) into occupied buildings overlying contaminated soils or groundwater.[2,3]

Indoor air quality criteria for TCE vary among regulatory jurisdictions. The U.S. EPA 2002 Draft Subsurface VI Guidance Document sets a generic screening level of 0.41 ppb (at 10^{-4} cancer risk),[4] whereas the EPA Regional Screening Level for TCE in residential indoor air for Regions 3, 6, and 9 is 0.22 ppb.[5] In the vicinity of Hill Air Force Base (AFB), where the field testing described in this study was performed, the TCE Mitigation Action Level (MAL) is 2.3 ppb.[6] A recent EPA review of the 2002 Draft

Subsurface VI Guidance Document suggests an increased reliance on indoor air concentrations in future VI evaluations.[7]

Determinations of TCE from VI must be made in the presence of the numerous other volatile organic compounds (VOCs) normally found in indoor air at concentrations in the low- or sub-ppb range.[8,9] Traditional methods, such as EPA TO-15 and TO-17, which entail canister or sorbent tube sample collection, respectively, followed by off-site analysis by gas chromatography with mass spectrometric detection (GC-MS),[10,11] can provide such determinations. But they are not well-suited for VI assessments involving extended indoor air monitoring or the identification of major VI entry points or non-VI indoor sources of VOCs. Portable instruments capable of analyzing the components of such complex mixtures at low concentrations, such as the Inficon Hapsite portable GC-MS,[12] can be effective for on-site assessments and source location tasks,[3,13,14] but their cost, size, and complexity limit their use in many routine or multi-site investigations.

Microfabricated gas chromatographic instrumentation (μGC), made from micromachined Si components, may provide a suitable option for addressing on-site VOC analysis needs due to the small size and low power requirements, potentially low cost, and capability for analyzing specific components of multi-VOC mixtures. Although a significant amount of research has been reported on μGC components in the past 10 years,[15-25] relatively few reports have appeared on complete μGC systems, which include at least the following three essential *microfabricated* components: a preconcentrator or other injector, a separation column, and a detector.[26-29] As with most VOC monitoring instruments, preconcentration is typically required to achieve detection limits (LOD) in the low- or sub-ppb range. Since short separation columns are employed in a μGC,

resolution is inherently constrained; multiple analytes may co-elute, which limits the complexity of the mixtures amenable to quantitative analysis. In response, some researchers have incorporated microsensor arrays as detectors;[23,26,27,29] the response pattern afforded by such an array constitutes a crude spectrum that can assist in *identifying* fully resolved vapor peaks and the components of partially overlapping peaks in a manner analogous to that used in GC-MS systems.[23,26,29-35]

We recently reported on a μGC field prototype that we developed and optimized specifically for the determination of TCE in indoor air for VI investigations.[29] Laboratory characterizations demonstrated the quantitative capture, selective preconcentration, separation, and (array) detection of TCE in the presence of up to 45 common indoor VOCs. Test atmospheres containing 120 parts-per-trillion (ppt) of TCE were accurately determined, with a projected LOD of 40 ppt (4.2 ng captured, 20-L sample, 36-min total sampling and analysis time). Response patterns from the sensor-array detector were used to confirm the identity of TCE.

In this article and the companion article that follows, we report on the first results generated in field demonstrations of two identical μGC prototype units (Proto 1 and Proto 2) in a house above a TCE groundwater plume with active vapor intrusion. This article describes the instrument features and operation, results of field calibrations, and comparisons of measurements between the two prototypes and between the prototypes and a standard reference method. The use of array response patterns to reveal the presence of co-eluting interferences is highlighted. The following article describes the application of the μGC prototypes to monitoring spatial and temporal changes in TCE concentrations.

4.2 Instrumentation and Methodology

4.2.1 μGC Prototype Description and Operation

Figure 4-1 shows a fluidic layout diagram of the μGC and images of the assembled prototype and the key micro-scale components. Each instrument measures 44 (w) × 25.5 (d) × 14.5 cm (h), weighs 4.5 kg, and operates on AC mains power. The rationale for the system design as well as details of the fabrication methods and structures of the micro-scale components, front-end preconcentration module, and supporting hardware and software have been presented elsewhere.[29, 36]

There are four operating modes: sampling, focusing, stabilization, and analysis. In sampling mode, an air sample is drawn at ~0.78 L/min through the pre-trap and sampler with the sample pump (Figure 4-1a). The former is a steel tube (6.4 mm o.d.) wrapped with insulated heater wire and packed with 50 mg of Carbopack B (C-B, Supleco, Bellefonte, CA). It effectively captures compounds with p_v values < 3 Torr. The latter is an identically wrapped tube packed with 100 mg of Carbopack X (C-X, Supelco). It captures compounds within a p_v range of ~3-95 torr, which includes TCE, and allows more volatile compounds to pass through largely unretained. The 10% breakthrough volume for TCE in the presence of interferences is > 30 L.[36] Both of these devices are mounted to a stainless steel manifold that also supports and integrates the six 3-way latching mini-valves used for directing air flow (Figures 4-1a and b). In this study, the pretrap was regenerated as needed by heating for 5 minutes at 250 °C while backflushing with scrubbed air at 0.78 L/min to prevent accumulation of low volatility interferences on the adsorbent bed. Scrubbers (Figure 4-1a) mounted to the outside of the

instrument chassis were packed with Drierite® and 5Å molecular sieves to remove water vapor and activated charcoal to remove background VOCs.

In focusing mode, the sampler is heated to 220 °C for 3 minutes while the sample-pump flow is redirected to desorb the trapped VOCs and transfer them at 18 mL/min to the microfocuser (μF). The μF is a micromachined-Si chip with a cavity packed with ~2.3 mg of C-X, fluidic ports, and an anodically bonded Pyrex cap (Figure 4-1c). It has integrated thin-metal-film heater contact pads and a temperature sensor patterned on its surface.

Prior to sample injection, the analysis pump pushes scrubbed ambient air through the microanalytical subsystem at 1.0 - 1.2 mL/min for 3 min to establish stable baseline signals from the four microsensors in the array (stabilization mode). Then, the μF is heated to 225°C in 0.45 s and maintained at that temperature for 2 min. The injected VOC mixture passes through the series-coupled microcolumns (Figure 4-1d) which have identical wall coatings of the non-polar stationary phase, polydimethylsiloxane (0.15 μm thickness, OV-1, Ohio Valley, Marietta, OH). Each microcolumn chip contains a 3-m long spiral channel with cross-sectional dimensions of 140 × 150 μm (3 × 3 cm footprint) and an integrated thin-film meander-line heater and temperature sensor. The microcolumns are independently temperature programmed and conditions were established to achieve the highest resolution of TCE from a set of typical VOC indoor air contaminants in the shortest amount of time. [29]

Vapors eluting from the second microcolumn are detected by an integrated array of four chemiresistors (CR) (Figure 4-1e), each coated with a different thiolate-monolayer-protected Au nanoparticle (MPN) film. Responses in these devices arise from

the transient change in film resistance accompanying sorption/desorption of vapors into the MPN films. Differences in the extent of sorption, swelling efficiency, and dielectric constant yield the array response pattern used to assist in recognizing and differentiating the eluting vapors.[26,32] The MPNs employed here were taken from existing stocks synthesized from the following starting thiols: n-octanethiol (C8), 6-phenoxyhexane-1-thiol (OPH), 4-(phenylethynyl)-benzenethiol (DPA), and methyl-6-mercaptohexanoate (HME).[37]

Following elution of TCE and other injected VOCs, the prototype returns to sampling mode and the cycle starts again. The prototype can proceed through multiple cycles automatically but for most of the measurements collected in this study this option was not selected. The time required for one complete cycle varies with the sample volume and ranges from 11 to 36 min for samples of 0.5 to 20 L, respectively.

4.2.2 Control, Data Acquisition, and Data Processing

All μGC functions were controlled by a laptop computer running a program written in-house in LabVIEW (version 8.5, National Instruments, Austin, TX) that was interfaced to a microsystem control printed circuit board (PCB) via two 16-bit DAQ cards (National Instruments, Austin, TX) mounted beneath the microanalytical and sampling subsystems. Resistance changes of the CR sensors were measured indirectly by applying a constant dc voltage to each CR through a 1-MΩ reference resistor, forming a voltage divider. The voltage drop across each CR after amplification of the signal difference between baseline and measured sensor response values was amplified and recorded at 20 Hz.

The text file containing retention times and sensor responses was imported into GRAMS/32 AI (Ver. 6.0, Thermo Scientific, Waltham, MA) for off-line data analysis. TCE peak heights and areas were extracted from the raw chromatograms using a Fourier self-deconvolution routine in GRAMS.[38] Subsequent data analysis was performed using Excel or (Matlab, Ver. R2010a, MathWorks, Inc., Natick, MA). Response pattern matching employed the correlation coefficient, r, derived from a comparison of the vector-sum of the responses from the (three or) four sensors in the array for a given TCE measurement to that determined during calibration. System blanks and field blanks were analyzed by the prototypes without sample collection and after collecting 2-L of VOC-free air from a cylinder, respectively. No detectable TCE was found in any of these samples.

4.2.3 Field Calibration and Reference Method

Samples used for field calibration and single-point standardizations were collected directly from a certified compressed-gas cylinder containing 11 ppb of TCE vapor in N_2 (Air Liquide, Plumsteadville, PA) through a tee-fitting inserted downstream from the tank regulator. For calibration, sample volumes of 0.5–8 L were collected, resulting in captured TCE masses ranging from 30–470 ng, which correspond to integrated TCE vapor volumes of 5.5–88 ppb·L.

The concentration of the tank standard was confirmed periodically (n = 7) by partially filling a 45-L Tedlar bag, drawing a sample into an evacuated 6-L Summa canister, and analyzing by GC-MS according to EPA Method TO-15. Reference canister samples were also collected periodically within 30 cm of one of the prototype inlets while

that prototype was also collecting a sample. Using a flow restrictor it was possible to extend the collection time of the canister sample to more closely match those of the prototypes. All canister samples were shipped promptly to Columbia Analytical Services (CAS, Simi Valley, CA) for GC-MS analysis. For most analyses only TCE was quantified; however, a subset of samples was analyzed for TCE along with 74 other compounds on the CAS target list.

4.2.4. Field Demonstration Site

The testing reported here was conducted in a house in Layton, UT overlying a shallow TCE groundwater plume originating at Hill AFB. This is a VI study house managed by researchers from Arizona State University (ASU) for a Strategic Environmental Research and Development (SERDP) project.[39] Following an initial set-up period, measurements were collected on each of 18 days over a 3-week period.

Samples were collected throughout the study house, but the majority was collected in the basement near a significant VI entry location consisting of a crack at the juncture of the cement-slab floor and the cinder-block wall. The magnitude of TCE VI was modulated using a variable speed exhaust fan placed in a second-floor bedroom window, which was sufficient to induce a negative pressure differential between the sub-slab and the basement. Periodically the basement windows were opened and outside air was drawn in to reduce TCE concentrations prior to subsequent measurements. The indoor temperature was 25 ± 3 °C and relative humidity was within the range of 20-60%.

4.3 Results and Discussion

4.3.1 Field Calibration and Detection Limits

The standard tank TCE concentration of 9.6 ± 0.43 ppb (51.7 μg/m^3, n = 7) determined by the reference method (i.e., EPA TO-15) over the course of the study period was within 1 % of the concentration determined by the tank supplier (i.e., 9.7 ppb, 52.3 μg/m^3) after correcting for the difference in atmospheric pressure between the test site (12.7 psi) and the site where the tank was prepared (14.4 psi). For calibration, sample volumes ranging from 0.5–6 L and 0.5–8 L were collected for Proto 1 and Proto 2, respectively. The corresponding ranges of collected masses (integrated vapor volumes) were 26–310 ng (4.8–58 ppb·L) and 26–414 ng (4.8–77 ppb·L). With the amplification circuit configuration employed, the most TCE-sensitive sensors (i.e., HME and OPH) would saturate at masses of ~330 ng (61 ppb·L) and ~430 ng (80 ppb·L) for Proto 1 and 2, respectively. Two full (i.e., 6-7 points) calibrations and seven single-point standardization checks (2-L tank sample) were performed over the 3-week study. One set of calibration curves is presented in Figure 4-2. The forced-zero linear regression r^2 values are ≥ 0.98 for all sensors in both prototypes. Response patterns for TCE derived from the peak-height sensitivity values (Figure 4-2 insets) differ somewhat between the two instruments because of small differences in sensitivities among the MPN-coated CRs in the arrays installed in each prototype.

LODs for TCE calculated on the basis of these calibration data are presented in Table 4-1 for assumed sample volumes of 4 L (minimum volume collected during the field tests) and 20 L (maximum possible sample volume), since the LOD is inversely proportional to sample volume. For a 20-L sample, the lowest LOD among the

individual sensors in the two prototypes is 0.021 ppb. Differences in LOD values for a given type of sensor between the two prototypes arise from a combination of different sensitivities and baseline noise levels. Although the LOD for the array as whole is dictated by the highest LOD among the sensors, it is possible to use only three of the four sensors and still perform effective vapor recognition from the array response patterns.[33-35] Sample volumes collected for the tests described below were ≤ 10 L (typically 4–8 L) due to concerns over exceeding the dynamic range of the more sensitive sensors at larger sample volumes. For an 8-L sample, the lowest LOD values are 0.052 ppb (HME in Proto 1) and 0.073 ppb (OPH in Proto 2). If the three most sensitive sensors are considered collectively (i.e., minimum required for pattern recognition), the LOD values are 0.18 ppb and 0.25 ppb for Proto 1 and 2, respectively (~10% of the MAL).

4.3.2 TCE Standardizations and Inter-Prototype Comparisons

Figures 4-3a and b summarize the standardization data collected every few days for Proto 2 in the form of bar charts. The variations in TCE sensitivity (Figure 4-3a, rsd = 17%) were ≤ 11% except for the last day (-32%) and there was no temporal trend in the sign or magnitude of the drift. The concentration-normalized response patterns in Figure 4-3b show that the pattern fidelity was quite good, as reflected in the r values relating the pattern on each day to that determined from the mid-study full calibration (i.e., day 12). Over the first week the HME sensor response drifted downward, but then stabilized. As a result, the r value of 0.85 for the first day is exceptionally low compared to all other days, for which r ≥ 0.95. With the possible exception of the first day, this indicates that the fluctuations in sensitivity (Figure 4-3a) arise from a ‘common mode’ effect, such as a

shift in the array temperature or pump flow rate during sampling. To account for the changes in apparent sensitivity, prototype responses obtained on a given day were corrected using the most recent standardization value; that is, measured values were multiplied by the ratio of the original calibration value to that of the standardization value. The same standardization method was applied to the data for Proto 1.

A total of 23 indoor air samples analyzed concurrently by both prototypes while operating in close proximity gave TCE values > LOD. The range of concentrations among these samples was from 1-11.4 ppb. Figure 4-4 shows good consistency between the measurements from the two prototypes: the forced-zero, linear regression r^2 value is 0.88 and the slope is 1.12. Proto 2 yielded slightly higher values than Proto 1 on average. Note that if the three samples above the MAL showing the largest differences (open symbols in Figure 4-4), are removed, then the slope and r^2 become 1.06 and 0.94, respectively.

A set of representative chromatograms obtained from one of the indoor air samples analyzed by Proto 1 is presented in Figure 4-5a. Although several later eluting peaks are apparent, there were no closely eluting interferences detected in this particular field sample. The absence of peaks at elution times shorter than that of TCE reflects the selectivity against more volatile compounds designed into the high-volume sampler. On the basis of the limited number of TO-15 samples for which expanded analyses were performed over the course of the study, there were 26 possible interferences found that would have eluted before TCE; average concentrations ranged from 0.06 to 42 ppb. TCE in this sample was detected by all four sensors, providing a response pattern very similar to the TCE calibration pattern (Figure 4-5b, r = 0.998). The TCE concentration

determined by Proto 1 from the average of the four sensors was 10 ppb, while that from a simultaneously collected reference sample was 12 ppb (-17% error). Traces from a representative Proto 2 analysis are presented in Figure 4-6, for which the TCE concentration of 5.8 ppb differed from that of the reference method by 15%.

Response patterns for the six most prominent additional peaks in the chromatograms of Figure 4-5a are presented in Figure 4-5b along with the r values derived from comparisons with the TCE calibration pattern, which range from r = 0.46 to 0.98. The identities of these compounds were not determined. As shown, the ability to differentiate TCE from interferences on the basis of response patterns varies. However, many patterns are sufficiently different from that of TCE to enhance the reliability of the TCE analysis significantly, particularly when considered in conjunction with the retention times. Stated differently, it is evident that these prototypes could be used to selectively determine other VOCs with proper calibration and adjustment of operating conditions.

The utility of the array response pattern is perhaps of greater value when interfering VOCs are present that fully or partially co-elute with TCE. For this preliminary study we applied a simple pattern matching test to identify cases where there was reason to suspect the presence of one or more co-eluting co-contaminants; that is, for a set of peaks eluting at the retention time expected for TCE, if the correlation of the sample-pattern vector to the calibration-pattern vector for TCE yielded a value of $r < 0.85$, then it was assumed that one or more co-eluting interferences was present. Samples with $r < 0.85$ would therefore be expected to yield positively biased (apparent) TCE concentrations relative to those found with the reference method.

Figure 4-7 presents extracted sections of three chromatograms from Proto 1 in which peaks were detected at the TCE retention time and patterns derived therefrom. For brevity only a single, representative, sensor trace is presented along with the 4-sensor response pattern (insets). The first panel (Figure 4-7a) shows a slightly tailing peak and a response pattern for which r = 0.997. The concentration determined with the prototype was 8.3 ppb, which is within 5% of that of the parallel sample analyzed by the reference method (i.e., 8.7 ppb). The second panel shows a peak with some distortion suggesting the presence of more than one component. Indeed, the response pattern gave an r = 0.830 and the TCE concentration estimated with the prototype had a positive bias of 52% (i.e., 4.1 ppb vs. 2.7 ppb). For the third panel, again some distortion is apparent in the peak, and the concentration estimate was positively biased by 64%, but the response pattern gave an r = 0.984. In this case it appears as if the response pattern(s) of the co-eluting interference(s) was not sufficiently different from that of TCE to exceed the threshold for a mismatch.

4.3.3 Accuracy of μGC TCE Determinations

All of the 60 TO-15 reference samples collected and analyzed during the study gave detectable levels of TCE, with concentrations ranging from 0.047 to 16 ppb. Of these, 42 were above the LODs for at least three of the sensors: 30 for Proto 1; and 12 for Proto 2. Figure 4-8 plots the pooled TCE concentration estimates from the two prototypes against the matching reference values. The slope and (force-zero) linear regression r^2 value are 0.90 and 0.87, respectively, indicating generally good agreement with the reference method. Above the MAL, 21 of the 26 TCE values were within 25%

of the reference values. Deviations are larger and more prevalent below the MAL. Overall, Figure 4-8 reveals a slight tendency toward underestimation at high concentrations and a stronger tendency toward overestimation at low concentrations for the prototypes.

By dividing the data set into values falling above and below the MAL, and above and below the pattern matching threshold of r = 0.85, a more detailed assessment of performance is possible. Results are summarized in Table 4-2 and the relevant plots are presented in Figures 4-9. For measurements ≥ MAL with patterns giving r > 0.85 (n=25), regression onto the reference measurements gave a slope of 0.90 (r^2 = 0.72). Errors in measured TCE concentrations ranged from -43 to +50, averaging -6.6%. Over the same concentration range there was just one sample that gave a pattern with r < 0.85, which had a large positive error in the TCE concentration estimate (i.e., 51%), implying a significant concentration of co-eluting interference(s) with pattern(s) different from that of TCE. Thus, pattern matching appears to add reliability over this range of concentrations.

Below the MAL, for the 11 samples with patterns giving r > 0.85 the correlation between prototype and reference TCE values was somewhat lower (i.e., linear regression r^2 = 0.69) and all of the measurements were positively biased; the slope = 1.66 and the range of errors was 24-119%, averaging 74%. In this concentration range the pattern matching criterion was not as effective in detecting the presence of co-eluting VOCs, which suggests that the interferences had response patterns similar to that of TCE. Still, for those samples not meeting the pattern matching threshold (Table 4-2, r < 0.85, n = 5), the errors were generally much larger (i.e., range = 75-285%; average = 147%),

indicating that the response pattern was useful in identifying the more extreme cases of co-eluting interferences.

Table 4-3 presents data from the four reference samples subjected to expanded GC-MS analysis. Among all four reference samples a total of 52 other VOCs were detected at least once, and 17 compounds were found in all four samples. As many as 37 interfering compounds were identified in a single reference sample (Case 1). In subsequent laboratory testing with the prototypes, only three of these compounds were determined to fully or partially overlap with TCE under the prototype operating conditions used in the field: bromodichloromethane (BDCM), 1,2-dichloropropane (DCP), and n-heptane (nC7). Comparing the response patterns of these three compounds with that of TCE (also determined in subsequent laboratory analyses) gave r values of 0.986, 0.971, and 0.799 for BDCM, DCP, and nC7, respectively, which means that only nC7 would be differentiated from TCE on this basis and only at a relatively high concentration.

The concentrations of these compounds and TCE measured by the reference method are listed in Table 4-3. For the two cases with TCE concentrations < MAL, Case 1 ($r = 0.789$) fell below the minimum pattern matching threshold and Case 2 ($r = 0.975$) exceeded the threshold. In the former case, the prototype indicated a TCE concentration of 1.4 ppb, ~6 times that of the reference method, while in the latter case, the prototype indicated a concentration (1.9 ppb) ~2 times higher than that of the reference method. Although the r values correctly indicate greater levels of interferences in Case 1, in neither case is the extent of positive bias observed accounted for by the indicated interference concentrations.

We surmise that there were additional interferences present that were not targeted in the GC-MS analysis. To the extent that nC7 is a marker of fuel vapors, it is reasonable to suspect that other fuel hydrocarbons (e.g., other heptane isomers) may have been present. As it turns out, there are several heptane isomers with p_v values and expected GC elution times similar to that of TCE, which may have gone undetected, such as 2-methylhexane (p_v = 65 Torr), 3-methylhexane (p_v = 63 Torr), 2,3-dimethylpentane (p_v = 66 Torr), 3,3-dimethylpentane (p_v = 77 Torr). Since their response patterns are likely to resemble to that of nC7, the pattern mismatch reflected in the r value for Case 1 in Table 4-3 suggests significant concentrations of such compounds in the composite peak. For Case 2, consistent with the higher r value and smaller positive bias, the concentrations of such interferences were likely to have been lower. For Cases 3 and 4, with TCE concentrations > MAL, the high r values and relative small errors in TCE concentration are consistent with much lower concentrations of interferences.

4.4 Conclusions

In conclusion, we have described the first field deployment of a microfabricated gas chromatograph (μGC) employing microsensor array detection for trace-level determinations of targeted environmental VOC air contaminants. The instrument relies on selective high-volume preconcentration; microfocuser injection; rapid, temperature-programmed, dual-microcolumn separation; and microsensor-array recognition and quantification. All key components are modular and interchangeable. Two prototype μGC units adapted specifically for the measurement of low-/sub-ppb concentrations of TCE were tested in a VI-impacted house. Results showed consistent performance

between the prototypes, good medium-term stability, and selective determinations of TCE at concentrations of 0.31 to 16 ppb in the presence of up to 43 background VOCs. The on-board high-volume pre-trap and sampler devices facilitated the rapid collection of detectable quantities of TCE while preventing more- and less-volatile interferences (including ambient water vapor) from being transferred to the downstream microanalytical subsystem. The LOD and dynamic range of TCE measurement were sufficient to assess the need for mitigation in a total sampling and analytical cycle time of ~20 min (8-L sample). The accuracy of TCE determinations was reasonably good above the 2.3-ppb mitigation action level applicable to this site. At lower concentrations, significant positive biases were observed, owing to the presence of co-eluting VOC interferences. A simple pattern-matching criterion applied to the response patterns obtained from the array detector revealed those samples with high levels of co-eluting co-contaminants. A more sophisticated multivariate curve resolution algorithm is being explored to improve the detection of lower levels of co-eluting interferences.[23] Actively thermostatting the microsensor array and modifying the signal processing circuitry to expand the dynamic range are expected to further enhance performance. With slight modifications, it appears feasible to extend the use of this instrumentation to the simultaneous analysis of other VOCs. The companion article that follows (Part II) demonstrates the use of the prototype μGCs described here for monitoring spatial and temporal variations in indoor TCE concentrations in support of VI assessments.

4.5 References

1. Pankow, J. F.; Feenstra, S.; Cherry, J. A.; Ryan, M. C. Dense chlorinated solvents in groundwater, background and history of the problem. In *Dense Chlorinated Solvents and other DNAPLs in Groundwater*; History, Behavior, and Remediation, Pankow, J. F., Cherry, J. A., eds. Waterloo Press, Portland, OR, United States, 1996, pp. 1-52.
2. ATSDR, Trichloroethylene. 2003, available at http://www.atsdr.cdc.gov/tfacts19.pdf.
3. McHugh, T.; Kuder, T.; Fiorenza, S.; Gorder, K.; Dettenmaier, E.; Philp, P. Application of CSIA to distinguish between vapor intrusion and indoor sources of VOCs, *Environ. Sci. Technol.* **2011**, 4, 5952-5958.
4. U.S. EPA OSWER, OSWER Draft Guidance for Evaluating the Vapor Intrusion to Indoor Air Pathway from Groundwater and Soils (Subsurface Vapor Intrusion Guidance); EPA530-D-02-004; U.S. Environmental Protection Agency, 2002.
5. U.S. EPA Regions 3, 6, and 9 Risk-Based Regional Screening Levels; available at http://www.epa.gov/reg3hwmd/risk/human/rbconcentration_table/Generic_Tables/pdf/master_sl_table_bwrun_NOVEMBER2010.pdf
6. Mitigation Action Levels for Hill AFB, UT Indoor Air Sampling Program; available at http://www.hillrab.org/files/news/archive/2009/2009-03 Action Levels Change.htm
7. U.S. EPA OSWER, Review of the Draft 2002 Subsurface Vapor Intrusion Guidance, 2010; available at www.epa.gov/oswer/vaporintrusion/documents/review_of_2002_draft_vi_guidance_final.pdf
8. McHugh, T.E.; Connor, J.A.; Ahmand, F. An empirical analysis of the groundwater-to-indoor-air exposure pathway: The role of background concentrations to indoor air. *Environ. Forensics* **2004**, 5, 33-44.
9. Dawson, H. E.; McAlary, T. A compilation of statistics for VOCs from post-1990 indoor air concentration studies in North American residences unaffected by subsurface vapor intrusion *Ground Water Monitoring & Remediation* **2009**, 29, 60-69.
10. U. S. Environmental Protection Agency (EPA), Compendium Method TO-15 Second Edition, Determination Of Volatile Organic Compounds (VOCs) In Air Collected In Specially-Prepared Canisters And Analyzed By Gas Chromatography/Mass Spectrometry (GC-MS), available at http://www.epa.gov/ttnamti1/files/ambient/airtox/to-15r.pdf
11. U. S. Environmental Protection Agency (EPA), Compendium Method TO-17 Second Edition, Determination of Volatile Organic Compounds in Ambient Air Using Active Sampling Onto Sorbent Tubes, http://www.epa.gov/ttnamti1/files/ambient/airtox/to-17r.pdf
12. Inficon, Hapsite, available at http://www.inficonchemicalidentificationsystems.com.
13. Fair, J. D.; Bailey W. F.; Felty, R. A.; Gifford, A. E; Shultes, B.; Volles, L. H. Method for rapid on-site identification of VOCs, *J. Environ. Sciences* **2009**, 21, 1005-1008.
14. Gorder, K. A; Dettenmaier, E. M. Portable GC/MS methods to evaluate sources of VOC contamination in indoor air *Ground Water Monitoring & Remediation* **2011**, 31, 113-119.

15. Bhushan, A.; Yemane, D.; Trudell, D.; Overton, E. B.; Goettert, J. Fabrication of micro-gas chromatograph columns for fast chromatography *J. Microsyst. Technol.* **2007**, 13, 361-368.
16. Agah, M.; Potkay, J. A.; Lambertus, G.; Sacks, R.; Wise, K. D. High-performance temperature-programmed microfabricated gas chromatography columns *J. Microelectromech. Syst.* **2005**, 14, 1039-1050.
17. Ali, S.; Ashraf-Khorassani, M.; Taylor, L. T.; Agah, M. MEMS-based semi-packed gas chromatography columns *Sens. Actuators. B* **2009**, 141, 309-315.
18. Lambertus, G.; Elstro, A.; Sensenig, K.; Potkay, J.; Agah, M.; Scheuering, S.; Wise, K.; Dorman, F.; Sacks, R. Design, fabrication, and evaluation of microfabricated columns for gas chromatography *Anal. Chem.* **2004**, 76, 2629-2637.
19. Tian, W. C.; Chan, K. L. H.; Lu, C.-J.; Pang, S. W.; Zellers, E. T. Multiple-stage microfabricated preconcentrator-focuser for micro gas chromatography system *J. Microelectromech. Syst.* **2005**, 14, 498-507.
20. Li, M.; Myers, E. B.; Tang, H. X.; Aldridge, S. J.; McCaig, H. C.; Whiting, J. J.; Simonson, R. J.; Lewis, N. S.; Roukes, M. L. Nanoelectromechanical resonator arrays for ultrafast, gas-phase chromatographic chemical analysis *Nano Letters* **2010**, 10, 3899-3903.
21. Radadia, A. D.; Morgan, R. D.; Masel, R. I.; Shannon, M. A. Partially buried microcolumns for micro gas analyzers *Anal. Chem.* **2009**, 81, 3471-3477.
22. Serrano, G.; Reidy, S.; Zellers, E. T. Assessing the reliability of wall-coated microfabricated gas chromatographic separation columns *Sens. Actuator B* **2009**, 141, 217-226.
23. Jin, C.; Zellers, E. T. Chemometric analysis of gas chromatographic peaks measured with a microsensor array: methodology and performance assessment *Sens. Actuator B* **2009**, 139, 548-556.
24. Manginell, R. P.; Adkins, D. R.; Moorman, M. W.; Hadizadeh, R.; Copic, D.; Porter, D. A.; Anderson, J. M.; Hietala, V. M.; Bryan, J. R.; Wheeler, D. R.; Pfeifer, K. B.; Rumpf, A. Mass-sensitive microfabricated chemical preconcentrator *J. Microelectromech. Syst.* **2008**, 17, 1396-1407.
25. Reidy, S.; Lambertus, G.; Reece, J.; Sacks, R. High-performance, static-coated silicon microfabricated columns for gas chromatography *Anal. Chem.* **2006**, 78, 2623-2630.
26. Lu, C.-J.; Steinecker, W. H.; Tian, W.-C.; Oborny, M. C.; Nichols, J. M.; Agah, M.; Potkay, J. A.; Chan, H. K. L.; Driscoll, J.; Sacks, R. D.; Wise, K. D.; Pang, S. W.; Zellers, E. T. First-generation hybrid MEMS gas chromatograph *Lab Chip* **2005**, 5, 1123-1131.
27. Lewis, P. R.; Manginell, R. P.; Adkins, D. R.; Kottenstette, R. J.; Wheeler, D.; Sokolowski, S. S.; Trudell, D.; Byrnes, J. E.; Okandan, M.; Bauer, J. M.; Manley, R. G.; Frye-Mason, C. Recent advancements in the gas-phase MicroChemLab *IEEE Sens. J.* **2006**, 6, 784-795.
28. Zampolli, S.; Elmi, I.; Mancarella, F.; Betti, P.; Dalcanale, E.; Cardinali, G. C.; Severi, M. Real-time monitoring of sub-ppb concentrations of aromatic volatiles with a MEMS-enabled miniaturized gas-chromatograph *Sens. Actuators. B* **2009**, 141, 322-328.

29. Kim, S. K.; Chang, H.; Zellers, E. T. Microfabricated gas chromatograph for the selective determination of trichloroethylene vapor at sub-parts-per-billion concentrations in complex mixtures *Anal. Chem.* **2011**, 83, 7198-7206.
30. Lu, C. J.; Whiting, J.; Sacks, R. D.; Zellers, E. T. Portable GC with tunable retention and microsensor array detection for the determination of complex vapor mixtures *Anal. Chem*. **2003**, 75, 1400-1409.
31. Jin, C.; Zellers, E. T. Limits of recognition for binary and ternary vapor mixtures determined with multitransducer arrays *Anal. Chem.* **2008**, 80, 7283-7293.
32. Zhong, Q.; Steinecker, W. H.; Zellers, E. T. Characterization of a high-performance portable GC with a chemiresistor array detector *Analyst* **2009**, 134, 283-293.
33. Hsieh, M.-D.; Zellers, E. T. Limits of recognition for simple vapor mixtures determined with a microsensor array *Anal. Chem.* **2004**, 76, 1885-1895.
34. Park, J.; Groves, W. A.; Zellers, E. T. Vapor recognition with small arrays of polymer-coated microsensors: a comprehensive analysis *Anal. Chem.* **1999**, 71, 3877-3886.
35. Cai, Q-Y; Zellers, E. T. Dual-chemiresistor GC detector employing monolayer-protected metal nanocluster interfaces *Anal. Chem.* **2002**, 71, 3877-3886.
36. Sukaew, T.; Chang, H.; Serrano, G.; Zellers, E. T. Multi-stage preconcentrator/focuser module designed to enable trace level determinations of trichloroethylene in indoor air with a microfabricated gas chromatograph *Analyst* **2011**, 136, 1664-1674.
37. Rowe, M. P.; Plass, K. E.; Kim, K.; Kurdak, Ç.; Zellers, E. T.; Matzger, A. Single-phase synthesis of functionalized gold nanoparticles *Chem. Mater.* **2004**, 16, 3513-3517.
38. Kauppinen, J. K.; Moffatt, D. J.; Mantsch, H. H.; Cameron, D. G. Fourier self-deconvolution: A method for resolving intrinsically overlapped bands *Appl. Spectrosc.* **1981**, 35, 271-276.
39. *Integrated field-scale, lab-scale, and modeling studies for improving the ability to assess the groundwater to indoor air pathway at chlorinated solvent-impacted groundwater sites*, ESTCP ER-1686; Strategic Environmental Research and Development Program in the Department of Defense/Environmental Security Technology Certification Program (SERDP/ESTCP); Arlington, VA, 2011; http://estcp.org/Program-Areas/Environmental-Restoration/Contaminated-Groundwater/Emerging-Issues/ER-1686

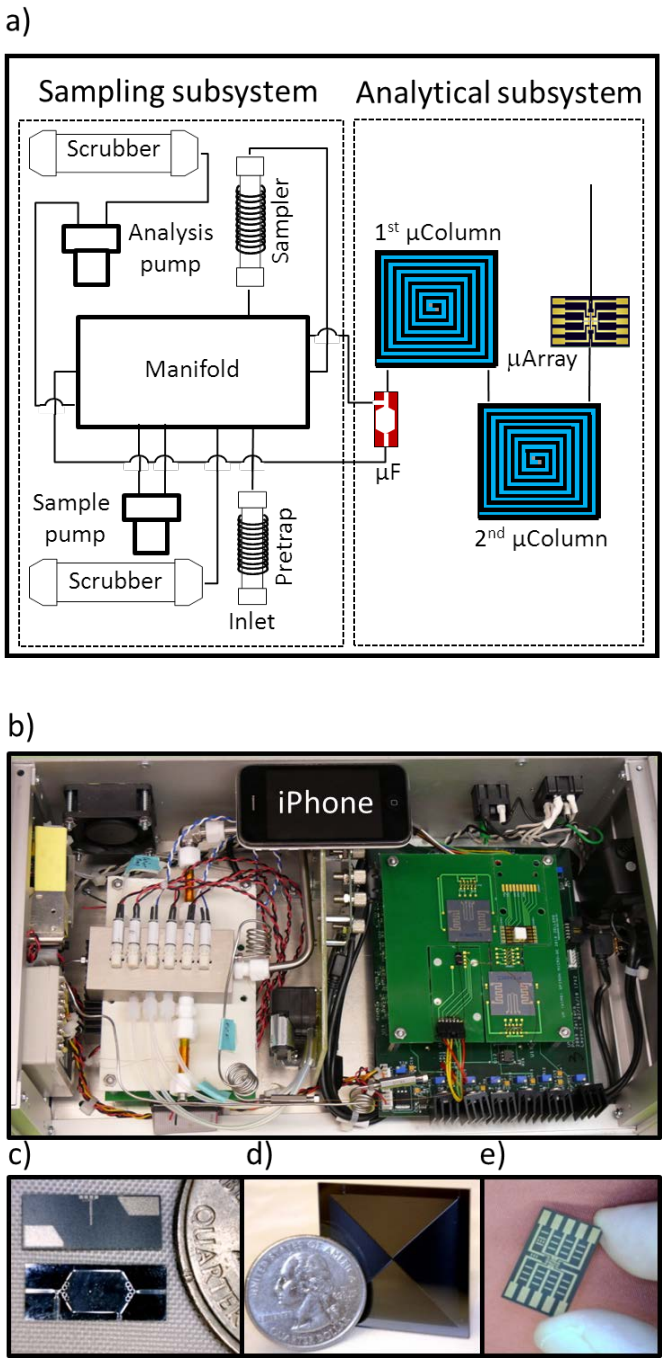

Figure 4-1. Prototype µGC system and components: (a) layout diagram showing subsystems and fluidic pathways; (b) top view of Proto 1 with cover panel removed (iPhone included for scale); (c) µfocuser; (d) µcolumn; and (e) micro-scale chemiresistor array.

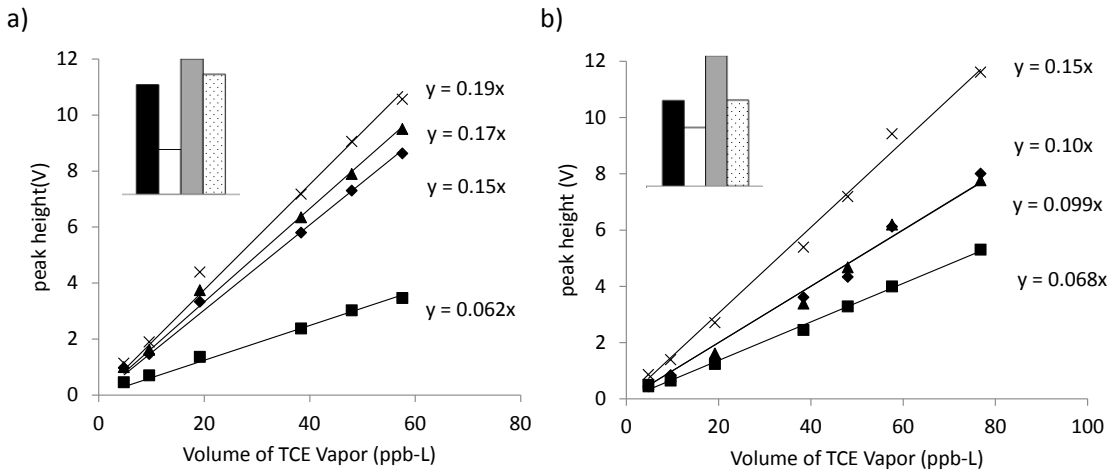

Figure 4-2. Field calibration curves for a) Proto 1 and b) Proto 2. All regression lines have r^2 values > 0.99, except HME in Proto 2 (r^2 = 0.98). Insets show the normalized response pattern for TCE from the CR arrays (bars, from left to right, refer to the following nanoparticle sensor coatings: C8, DPA, OPH, and HME; see text for acronym definitions).

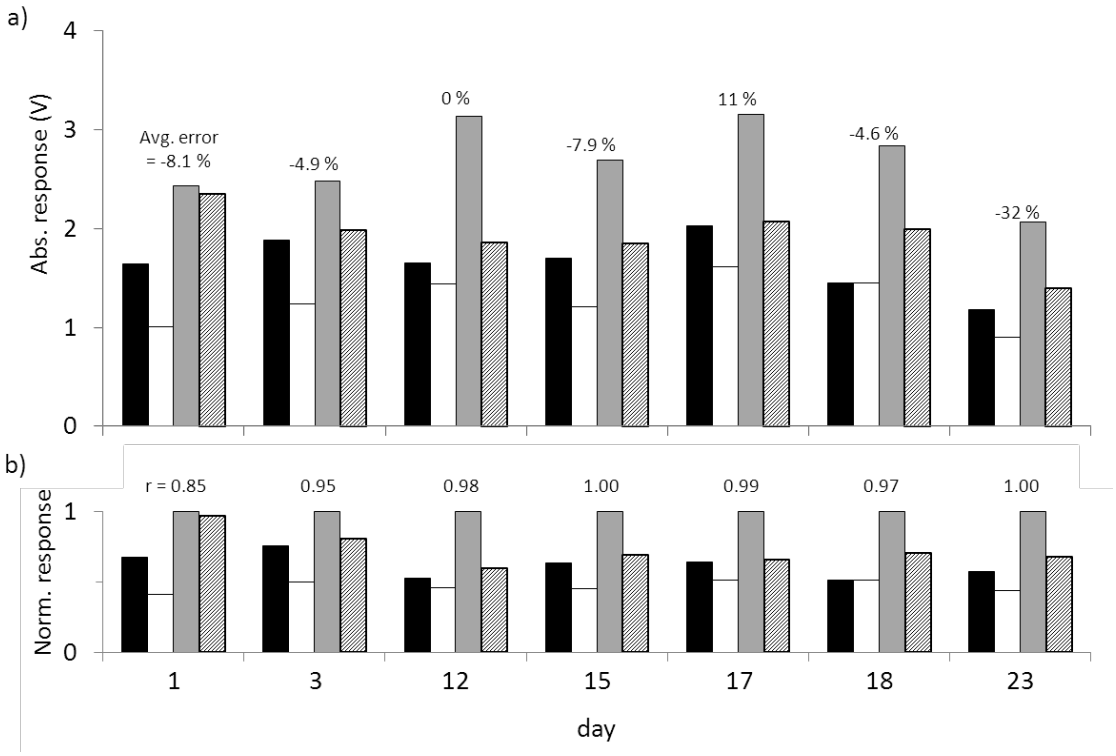

Figure 4-3. Results of periodic analysis (standardization check) of the TCE tank standard (2-L sample; 9.6 ppb TCE) showing stability of responses and relative response patterns over the 3-week study (RSD = 17%). a) Actual (absolute) responses from each sensor in the array; error (%) between each sample estimate of TCE concentration (avg. of four sensors) and that determined from the calibration performed on day 12 is shown above each set of responses. b) Normalized response patterns obtained by dividing each response by the maximum response among all four sensors; the correlation coefficient (r) derived from a comparison of the pattern on each day to that on day 15 is shown above each set of responses. Bars, from left to right, refer to the following nanoparticle sensor coatings: C8, DPA, OPH, and HME; see text for definitions of acronyms.

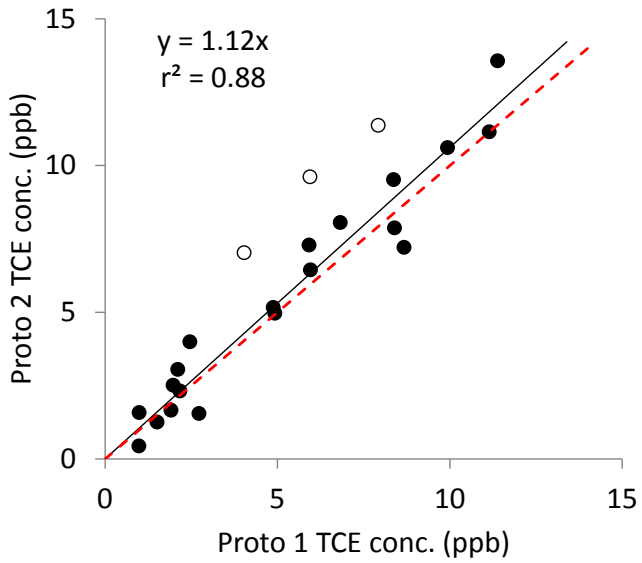

Figure 4-4. Inter-prototype comparison of TCE concentrations for 23 side-by-side air samples. Force-zero linear regression slope and r^2 are shown; dashed line is the 1:1 correlation. Points designated with open symbols show the greatest deviation above the MAL of 2.3 ppb. Removal of these outliers results in a slope of 1.06 and r^2 of 0.94.

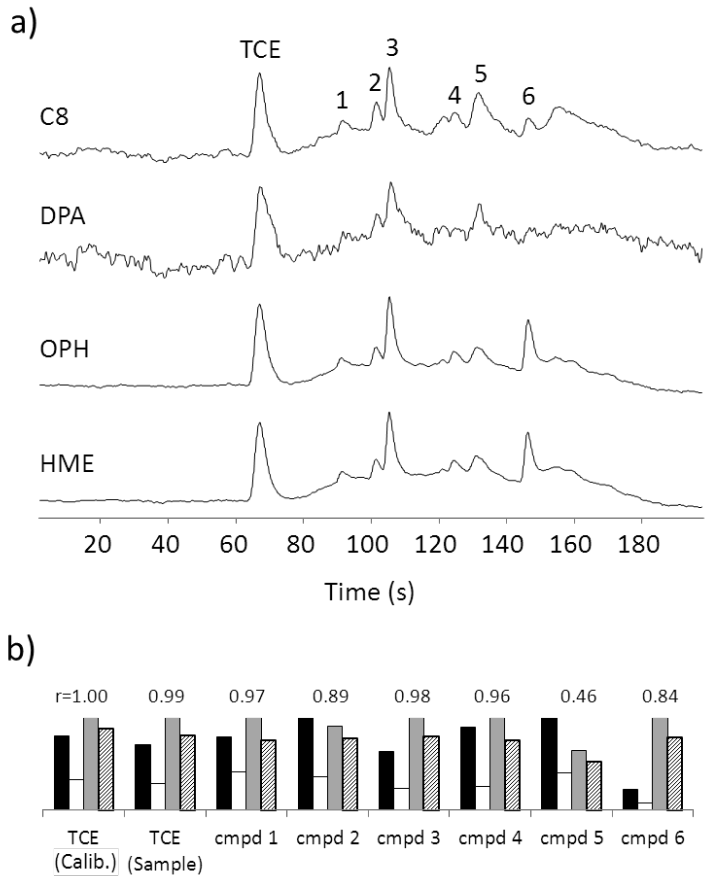

Figure 4-5. (a) Representative chromatograms from the MPN-coated CR array for a measurement obtained from Proto-1 having a TCE concentration of 12 ppb; (b) Normalized response patterns (bar charts) for TCE and the selected (unknown) VOCs designated in (a). Bars in each chart correspond to specific sensors in the array, from left to right: C8, DPA, OPH and HME (see text for definitions of acronyms). The pattern-matching correlation coefficients (r values) above each response pattern reflect the similarity with the pattern for TCE determined from the calibration (see Figure 4-2).

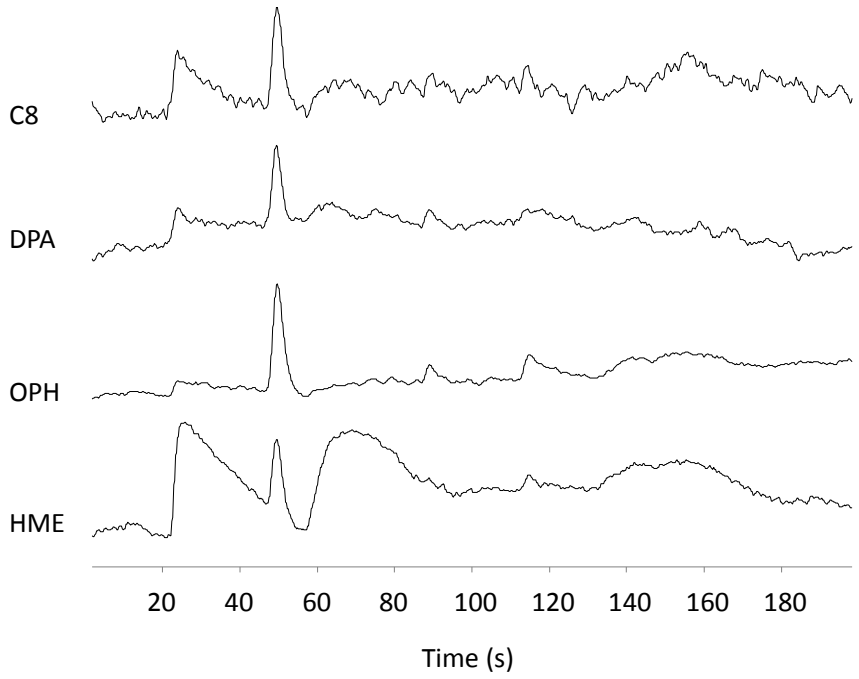

Figure 4-6. Chromatograms obtained from Proto 2 for an indoor air sample containing TCE. The concentration determined with the prototype was 6.7 ppb, while that from a matched reference sample analyzed by GC-MS was 5.8 ppb (15% error). Note that this sample was collected prior to repairing a leak discovered upstream from the μF, which allowed water vapor to enter the μF during the focusing step. It is presented to illustrate that atmospheric water vapor affects the TCE measurement only for the HME sensor, and that accurate quantification was possible nonetheless (see reference 29 in the main article).

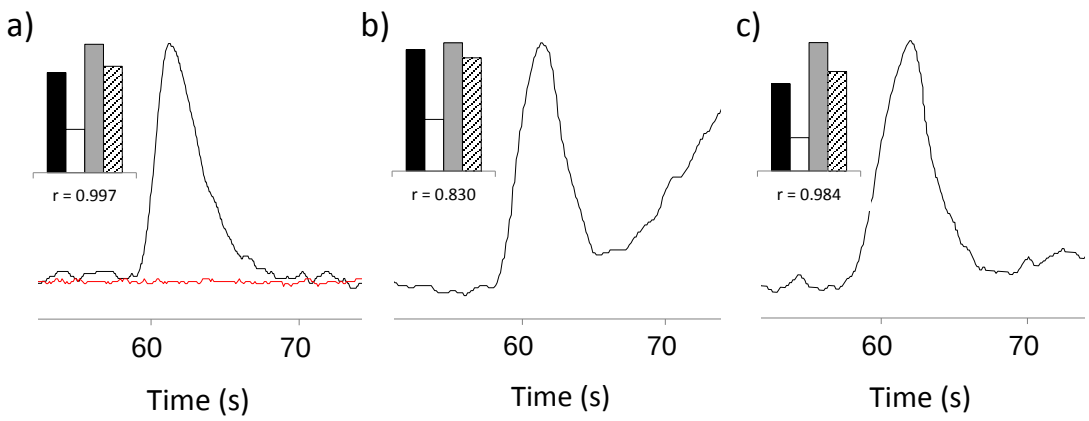

Figure 4-7. Extracted subsections of several chromatograms from the OPH sensor of Proto 1 and corresponding normalized response patterns from the CR array (insets) for TCE peaks with and without co-eluting interferences, illustrating the utility of the pattern-matching criterion (note: scale of each panel was adjusted separately for ease of visualization). a) Chromatogram trace with no apparent interferences: pattern-matching r = 0.997; prototype TCE concentration = 8.3 ppb, reference method TCE concentration = 8.7 ppb (-5% error). Trace for a 2-L blank sample is shown in red superimposed on the trace for the TCE peak. b) Chromatogram trace with partially-co-eluting interference(s) indicated by the distortion in the peak shape: pattern-matching r = 0.830; prototype TCE concentration = 4.1 ppb; reference method TCE concentration = 2.7 ppb (+52% error). c) Chromatogram trace with partially-co-eluting interference(s) as indicated by the distortion in the peak shape: pattern matching r = 0.984; prototype TCE concentration = 2.3 ppb; reference method TCE concentration = 1.4 ppb (+64% error); lack of pattern mismatch indicates the presence of interferences with response patterns similar to that of TCE.

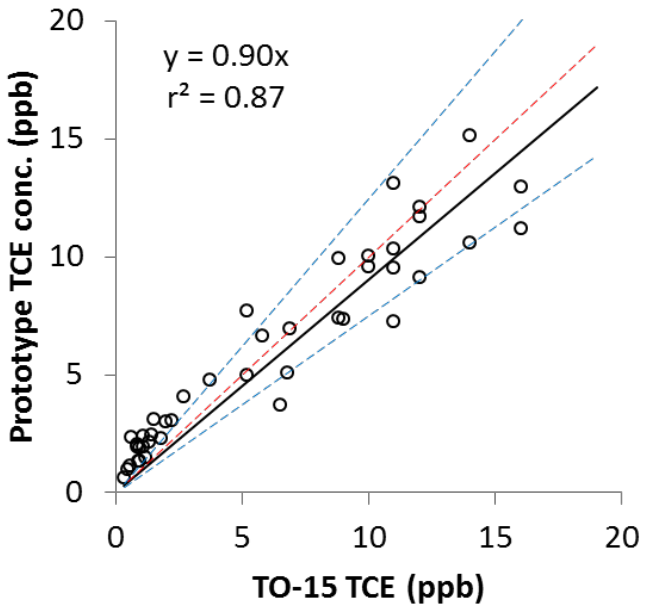

Figure 4-8.Correlation of the pooled measurements from the μGC prototypes with the corresponding canister samples analyzed by GC-MS (reference method; EPA TO-15). The black solid line is from linear regression with forced zero (slope and r^2 shown), the red dotted line is the 1:1 correlation, and the blue dashed lines show the ± 25% limits around the 1:1 correlation.

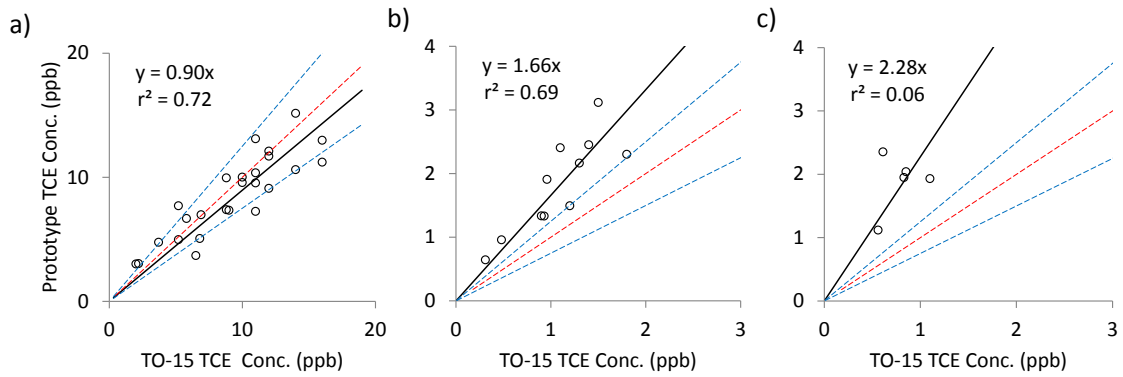

Figure 4-9.Comparison of TCE measurements from the prototypes and from the reference method (TO-15) for matched samples. In each panel, the black solid line is from linear regression with forced zero (slope and r^2 shown), the red dotted line is the 1:1 correlation, and the blue dashed lines show the ± 25% limits around the 1:1 correlation. a) Subset of data with TCE concentrations > MAL and r > 0.850. b) Subset of data with TCE concentrations < MAL and r > 0.850. c) Subset of data with TCE concentrations < MAL and r < 0.850. Note that there was only 1 sample with TCE concentration > MAL and r < 0.850 (see text in the main article for discussion).

Table 4-1. Limit of Detection (LOD, ppb) for TCE with both prototypes for assumed sample volumes of 4 L (20 L).[a]

Sensor	LOD	
	Proto 1	Proto 2
C8	0.37 (0.073)	0.65 (0.13)
DPA	0.95 (0.19)	0.50 (0.099)
OPH	0.11 (0.022)	0.15 (0.029)
HME	0.11 (0.021)	0.30 (0.060)

[a] Calculations are based on sensitivities and noise levels obtained from the calibration curves shown in Figure 4-2. See text for definitions of MPN acronyms. LOD=3σ/sensitivity, where σ is the standard deviation of baseline noise, which ranged from 0.023 V (HME) to 0.077 V (DPA) for Proto 1 and from 0.030 V (OPH) to 0.085 (C8) for Proto 2. To convert from ppb to μg/m^3, multiply by 5.4.

Table 4-2. Comparison of TCE measurements obtained concurrently from the μGC prototypes and from canister samples analyzed by GC-MS (reference method).

				Difference (%)[c]		
case	conc.	r[a]	n[b]	min.	max.	avg.
1	> MAL[d]	> 0.85	25	-43	50	-6.6
2	> MAL	< 0.85	1	51	51	51
3	< MAL	> 0.85	11	24	119	74
4	< MAL	< 0.85	5	75	285	147

[a] Correlation coefficient between response patterns from air samples and from calibration. [b] Number of samples. [c] Difference between TCE concentrations determined by prototypes and reference method. [d] Mitigation Action Level (2.3 ppb).

Table 4-3. Concentrations of TCE and co-eluting interferences from reference samples subjected to expanded GC-MS analysis (TO-15), and the corresponding TCE concentrations from the μGC prototypes (matched samples).

	TO-15 (ppb)					prototype (ppb)
case	TCE	BDCM[a]	DCP[b]	nC7[c]	r[d]	TCE
1	0.24	nd[e]	nd	0.20	0.789	1.4
2	1.0	nd	0.068	0.095	0.975	1.9
3	12	0.056	0.055	0.068	0.996	13
4	16	0.076	0.055	0.088	0.986	12

[a] Bromodichloromethane. [b] 1,2-dichloropropane. [c] n-heptane. [d] Correlation coefficient between response patterns from individual samples and the calibrated TCE pattern. [e] nd: not detected.

CHAPTER V

Microfabricated Gas Chromatograph for On-Site Determinations of trichloroethylene in Indoor Air Arising from Vapor Intrusion Part II: Spatial/Temporal Monitoring

5.1 Introduction

Concern over indoor air contamination by vapor intrusion (VI) of volatile organic compounds (VOCs) into occupied buildings from underlying contaminated soil and groundwater has increased in recent years.[1] Trichloroethylene (TCE), a prevalent groundwater contaminant in the U. S., is a 'compound of concern' (COC) for VI above shallow groundwater plumes due to its mobility, persistence in the environment, and relatively high Henry's Law constant.[2,3] Risk-based guidelines for controlling indoor air concentrations of TCE (and other COCs) arising from VI are in the low- or sub-parts-per-billion (ppb, by volume) range.[1,4] Determining whether mitigation actions are warranted is therefore complicated by the presence of numerous common indoor VOCs at similar concentrations.[4]

Conventional indoor air monitoring methods (e.g., EPA Methods TO-15, TO-17) [5,6] entail field sample collection followed by laboratory analysis by gas chromatography with mass spectrometric detection (GC-MS). Recognized shortcomings of this approach include the logistical difficulty of placing and retrieving samples, the long averaging

times typically employed (e.g., 24 hr), the delay in obtaining results, and the high costs of analysis. These factors inhibit the ability to locate VI entry points, differentiate indoor sources from VI, and track the variations in contamination levels in response to climatic factors, subsurface phenomena, or mitigation interventions. Continuous, short-term measurements of selected VOCs at the low concentrations required for VI investigations can be provided by some portable GC-MS instruments,[7,8] but high capital cost, maintenance requirements, and need for on-board carrier gas supplies may limit the use of such instruments for routine or extended on-site monitoring.

Microfabricated gas chromatographs (μGC) represent a promising, cost-effective, alternative for near-real time, on-site analysis of indoor VOCs. Although relatively few operational μGC systems have been reported,[9-17] and none have been used for field determinations of VI COCs, on-going research continues to yield significant advances in several aspects of this technology.[18-22]

We recently reported on the development and laboratory characterization of a field-deployable μGC prototype adapted specifically for the selective determination of TCE at low- or sub-ppb levels.[16,23,24] In the companion to this article (i.e., Part I),[25] we reported the results of inaugural field tests in a house with active TCE VI. In that study, we assessed the accuracy, selectivity, and stability of two prototypes by comparison with air samples collected with canisters and analyzed for TCE by GC-MS according to EPA Method TO-15. The utility of microsensor array detection was highlighted.

Another aspect of that study was to test the capability of the μGC prototypes to monitor spatial and temporal variations in indoor TCE vapor concentrations. Toward that end, data were collected in two houses, one with active TCE VI and the other in which a

(non-VI) source of TCE was intentionally placed. Comparisons of prototype measurements of TCE with those from side-by-side canister samples analyzed by GC-MS and a portable GC-MS were used to verify the observed trends. In this article we present the results of this aspect of the study.

5.2 Experimental Methods

5.2.1 Prototype Features and Functions

Detailed descriptions of the design, operation, and laboratory characterization of the μGC prototypes (Proto 1 and Proto 2) can be found elsewhere.[16, 23,24] Each prototype measures 44 (w) × 25.5 (d) × 14.5 cm (h), weighs 4.5 kg, uses AC power, and contains the following key analytical components: an adsorbent-packed pretrap, an adsorbent-packed high-volume sampler; a microfabricated Si/glass focuser (μF); a pair of 3-m long, spiral, Si/glass, microfabricated columns (μcolumn); and an array of four chemiresistor microsensors (μarray) employing different thiolate-monolayer protected gold nanoparticles (MPN) as the sorptive interface layers.[26] Figure 5-1a shows the microanalytical system components mounted on printed-circuit-boards (PCB) within Proto 2. Additional components include a set of 6 latching mini-valves mounted on a stainless steel manifold and two diaphragm mini-pumps for directing air flow. Two sets of adsorbent scrubbers are used to purify and dehumidify the ambient-air carrier gas.

Each μGC prototype is controlled by a laptop computer running a program written in LabView (Ver. 8.5, National Instruments, Austin, TX) that provides real-time data display and permits continued unattended operation. Figure 5-1b shows Proto 1 with its laptop controller following a measurement. A complete analytical cycle comprises a

sequence of four operating modes; sampling, focusing, stabilization, and analysis. The cycle time varies with the sample volume collected, which can range from 0.5-20 L. For the performance testing in this study, typical volumes ranged from 4-10 L, and the associated cycle times ranged from 13 to 23 min. The pre-trap removes interfering VOCs with vapor pressures below ~3 Torr and can be manually or automatically regenerated thermally with backflushing. The high-volume sampler selectively traps VOCs with vapor pressures ranging from ~3-100 Torr (including TCE). Collected VOC samples are then thermally desorbed from the sampler adsorbent and transferred to the μF. Subsequent rapid thermal desorption of the μF injects the VOC sample into the dual-μcolumn ensemble for separation and detection by the integrated μarray.

During the 3-week study period, the prototypes were periodically blank-tested and were calibrated and regularly checked for proper response by analyzing standard samples collected from a certified compressed gas cylinder containing 9.6 ppb of TCE in N_2 (Air Liquide, Plumesteadville, PA). Corrections were applied to the data on the basis of these periodic standardization checks as described in Part I. The indoor temperature remained at ~ 25°C and the relative humidity ranged from 20–60%.

Responses from the sensors in the CR array were stored as a text file and then imported into GRAMS/32 AI (Ver. 6.0, Thermo Scientific, Waltham, MA) for off-line data analysis. TCE concentrations were determined from the average of the peak height values following Fourier self-deconvolution, by comparison to the calibrated values. Response patterns derived from the array of CR sensors were used to identify the presence of significant interferences that were not chromatographically resolved from TCE (note: although this feature of the prototypes was implemented,[16] it was not used for

correcting the TCE concentrations for this study). Statistical analyses were performed with the statistics toolbox in MATLAB; ver. 2010a, Mathworks, Natick, MA). Contour maps for estimating the spatial variability of TCE concentrations were generated by a kriging estimator in Surfer (Ver. 8.0, Golden Software Inc., Golden, CO).

5.2.2 Field Demonstration Sites

Testing was performed in two different houses. House 1 is a 2-story structure (1200 sq. ft) with central air conditioning and an attached garage in Layton, UT, located over a shallow TCE groundwater plume originating from Hill AFB. The house is owned and operated by Arizona State University for a Strategic Environmental Research and Development (SERDP) project examining VI processes.[27] The primary VI entry point is located in a crawl space in the basement where there is a gap between the concrete foundation wall and the poured-concrete floor. The house has wall-to-wall carpeting on the second floor and was partially furnished during the study. Obvious sources of background VOCs (e.g., gasoline tanks, paints, solvents, etc.) were removed and the small quantities of liquid TCE and other solvents brought by the study team were stored in a refrigerator located in the garage.

House 2 is a 2-story, 1800 sq. ft., split-level residence also located in Layton, UT, several miles from House 1 in an area without groundwater contamination (i.e., there is no active TCE VI). It has central air conditioning and was fully furnished and used as a primary residence during the study period. No special preparations were made prior to testing.

5.2.3 Reference Measurements

To verify the TCE air concentrations, periodic concurrent Summa canister samples (6 L) were collected within ~30 cm of the prototype inlet(s). A flow restrictor was installed on each canister inlet to span as much of the prototype sampling interval as possible. All canister samples were sent to Columbia Analytical Services (CAS, Simi Valley, CA) within two days for TCE analysis by GC-MS according to EPA Method TO-15.[5]

Measurements were also collected every two hours with a portable GC-MS (Hapsite, Inficon, East Syracuse, NY) located in the hallway adjacent to the primary VI entry location. Selected ion monitoring (SIM) mode was used, with TCE detected on the basis of peaks at 95, 130, and 132 m/z. The peak at 130 m/z was used for quantification and the TCE detection limit was < 0.2 ppb for the 0.1-L preconcentrated air samples. Calibration and quality control procedures followed documented protocols for EPA Method TO-17. μGC prototype samples were collected within about 30 cm of the portable GC-MS inlet port.

5.2.4 Temporal Variations

Temporal variations in TCE concentrations were measured in House 1 on several days within the study period. The prototypes were placed on a table in the main basement room, and short sections of stainless-steel tubing (1.6-mm i.d.) were affixed to the inlets and extended either to the primary VI entry point in the basement crawl space or to the center of the hallway adjacent to the crawl space near the portable GC-MS inlet (Figure

5-1c). To obtain side-by-side reference samples in the crawl-space near the main VI entry point, canisters were also fitted with short sections of stainless steel tubing.

In order to vary the TCE concentrations for the μGC performance assessments, the extent of TCE VI was increased over scheduled time intervals in House 1 by temporarily reducing the indoor air pressure.[28] This was achieved with a three-speed, box-style, exhaust fan placed in the window of one of the bedrooms on the second floor. The pressure differential between the hallway adjacent to the VI entry point and the sub-slab headspace was monitored using a logging pressure sensor (Omniguard 4, Omnitec Design, Inc., Lynnwood, WA), and subsequently downloaded to a laptop computer. Prior to collecting air samples each day, and following a defined sample collection period, the exhaust fan was turned on and several windows opened to draw outside air through the house to reduce any accumulated TCE. The fan was then turned off and windows closed. Note that, as discussed in Part I,[24] on the basis of a small set of canister samples collected during the study period and analyzed for compounds on the CAS target list for indoor air contaminants (n = 8), it was found that up to 52 compounds (including TCE) were detected at least once, and up to 37 compounds were detected in a single sample.

5.2.5 Spatial Variations

Spatial TCE concentration variations in House 1 were assessed by collecting a succession of measurements with Proto 1 at each of several locations on second floors and in the basement. The exhaust fan was operated continuously (low setting) for this series of measurements. In House 2, an aerosol can of a cleaning product known to contain TCE was hidden within the house at a location that was not disclosed to the

prototype operator. Measurements were then collected systematically in several rooms throughout the house in an attempt to map the concentration gradients and locate the source. For convenience, the prototype and laptop were placed on a folding chair (Figure 5-1d) during the measurements. Since each measurement required ~23 min and 19 total samples were collected, this segment of the study spanned two days. The house was ventilated the next morning prior to continuing the measurements.

5.3 Results and Discussion

5.3.1 Temporal Monitoring

Figure 5-2a presents the results of monitoring continuously for 12 hr from the crawl space of House 1 with Proto 1 and Proto 2. A total of 22 measurements were collected with each prototype (note: several data points overlap in Figure 5-2a). Five reference canister samples were collected during this time period. As shown, over the first 90 min, prior to the first induced pressure differential, the concentration of TCE was stable and low, averaging 0.56 ppb and 0.26 ppb for Proto 1 and 2, respectively and 0.14 ppb for the single canister/TO-15 sample. The exhaust fan was then turned on, stepped through low, medium, and high settings over ~ 1 hr, and then maintained at the high setting for 110 min. The net indoor pressure reduction was 0.013″ of H_2O. During the transition, the increase in the TCE coincided with the decrease in differential pressure for both prototype measurements and the canister/TO-15 value. Once the pressure stabilized over this first induced-VI interval, the average TCE concentrations (n = 6) measured with Proto 1 and 2 were 6.6 and 6.3 ppb, respectively. The two canister samples collected during this interval gave an average of 13 ppb of TCE, while the concurrently collected

individual measurements from the prototypes gave averages of 9.3 and 8.9 ppb of TCE, for Proto 1 and 2, respectively (average error = -27%).

Upon stepping the fan speed down to the low setting, the differential pressure decreased and the TCE concentration quickly decreased to a level similar to that prior to the pressure reduction. At this point, several windows were opened in the basement and left open for 2 hr. They were then closed for another 2 hr. Over this 4 hr interval, the average TCE concentrations (n = 6) measured by Proto 1 and 2 were 0.44 ppb and 0.56 ppb, respectively. The single canister sample collected during this interval gave a TCE concentration of 0.12 ppb, while the concurrent single prototype values were 0.25 ppb and 0.28 ppb for Proto 1 and 2, respectively (average error = +117%). Note that the large positive errors in the prototype values observed at the lower concentrations (i.e., < 2.3 ppb, which is the mitigation action level for this site)[24] are attributable to interferences that could not be resolved either chromatographically or by pattern recognition methods, as noted in Part I.[24]

At t = 8.5 hr the fan was again stepped up to full speed over ~ 3 hr and the TCE values again increased to values similar to those observed during the first induced-VI interval. The TCE concentration measured with Proto 2 was within 6% of the canister/TO-15 value of 12 ppb, while Proto 1 measured only 7.9 ppb, which may be due to a concentration gradient in the crawl space area. Regardless, the two prototype measurements continued to track the TCE concentration changes well and are in reasonably good agreement with the each other and with the reference value.

Figure 5-2b shows a series of measurements collected in a manner similar to those depicted in Figure 5-2a, with similar scheduled changes in differential pressure. In this

case, however, Proto 1 and canister samples were collected from the crawl space and Proto 2 and portable GC-MS samples were collected from the adjacent hallway. Again, a total of 22 measurements were collected with each prototype. Five concurrent canister samples were also collected. Six measurements were collected with the portable GC-MS over the entire period, but they were not synchronized with the prototype measurements.

Over the first 1.5 hrs, TCE concentrations were low and stable. As the fan was stepped up to its highest setting over the next 2 hr and subsequently back down to its low setting over ~1.5 hr (see Figure 5-2b), the TCE concentrations measured with the prototypes increased and decreased accordingly. However, the concentration in the crawl space (Proto 1) was consistently higher than that in hallway (Proto 2), and in the interval corresponding to the largest pressure differential (-0.015″ H_20) the concentration ratio was about 2.2 (i.e., 12 ppb vs. 5.6 ppb for Proto 1 and 2, respectively). The most closely time-matched GC-MS and Proto 2 values, taken during the transition periods, agreed to within 9% and the three concurrent canister/TO-15 and Proto 1 values tracked each other and agreed to within 22% on average.

Curiously, during the second reduced-pressure excursion the TCE concentration did not increase nearly as much as during the first excursion. Both prototypes and both reference methods gave low TCE values and there was no significant concentration gradient evident between the crawl space and the hallway. We speculate that the soil immediately beneath the house was temporarily depleted of TCE. Regardless, the prototype measurements remained consistent with each other (i.e., 2.2 and 1.6 ppb, n = 11) and with the reference measurements (average = 2.7 ppb).

Figure 5-1c shows a third series of measurements during which the fan was not operated. The pressure differential naturally drifted downward slightly (-0.03″ H_2O) over the time period. There was no detectable difference in TCE concentrations between the crawl space and the hallway. However, there was a slight increase in TCE concentration commensurate with the gradual indoor pressure reduction: during the first 4-hr interval, the average TCE concentrations measured by the prototypes were 0.36 ppb and 0.24 ppb in the crawl space and hallway, respectively; and during the second 4-hr they increased to 1.5 ppb for both areas. Prototype values were in good agreement with those from the reference methods. This result demonstrates the capability for the prototypes to detect small changes in TCE concentrations arising apparently from minor shifts in atmospheric pressure.

For the measurements described above, the prototypes were operated manually; that is, they were started and stopped manually for each measurement collected, and they were allowed to remain in standby mode between successive. To verify the capability for unattended, automated monitoring, both prototypes were operated continuously for 48 hr; 10-L samples were analyzed every 50 min (46% duty cycle, n= 58). As above, Proto 1 and canister samples were taken from the crawl space and Proto 2 and Hapsite samples from the hallway. Two intervals of reduced pressure were created to induce VI.

As shown in Figure 5-3, the Proto 1 and canister/TO-15 measurements from the crawl space were similar, except for the pair of measurements collected during the pressure transition at t = 5.5 hr (6.8 ppb and 3.9 ppb from the canister/TO-15 and Proto 1, respectively). Otherwise, the Proto 1 average was 46% higher than that of the canister/TO-15 average (n=6), reflecting the aforementioned positive bias at low

concentrations by the prototypes. Proto 2 results were compared to the closest-matched portable GC-MS values (the largest sampling time difference was ~25 min, and most were within 10-15 min).. The temporal trends in TCE concentration from the Proto 2 and Hapsite GC-MS measurements were consistent, but the Proto 2 average of 3.4 ppb is 54% higher than that of the portable GC-MS (2.2 ppb) (n = 23).

During the two reduced indoor-air pressure intervals a concentration gradient from the crawl space to the hallway was evident, reflecting the enhanced TCE VI in the crawl space observed previously. At other times, and particularly from t = 30-48 hr, the gradient was from the hallway to the crawl space, suggesting that the crawl space (i.e., VI) was not the dominant source of TCE. As it turns out, at t = 10 hr on the first day, the garage door was closed, and it remained closed for the remaining 38 hr spanned by this survey. Subsequent probing with the portable GC-MS confirmed that the TCE stored in the refrigerator in the garage was an unexpected non-VI source of contamination in the house that only became significant when the garage door was closed. Between the first and second reduced-pressure intervals, this source apparently contributed only slightly to the TCE concentration measured in the hallway, leading to similar levels in the crawl space and hallway. During the second pressure-reduction interval, the levels in the hallway were higher than expected, and from t = 10-48 hr the peak in TCE concentration in the hallway (Proto 2) reflects a more significant contribution from the TCE source in the garage.

5.3.2 Spatial Monitoring

For the initial spatial concentration mapping survey, 15 measurements were collected with Proto 1 over a single day from multiple locations in House 1. Results are shown in Figure 5-4. Concentrations (from Proto 1) ranged from 0.51 to 3.8 ppb with a mean value of 1.3 ppb. The average TCE concentration in the basement was higher than that on the second floor (i.e., 2.2 ppb vs. 0.86 ppb, respectively) and the highest concentration was observed in the crawl space, consistent with TCE VI. The TCE concentration contours shown in Figure 5-4b convey the shallow gradients. Four of the five pairs of concurrently collected Proto 1 and canister/TO-15 values agreed to within 30%.

Testing in House 2 was then conducted to demonstrate that a non-VI source could be detected and located by means of the spatial distribution of TCE concentrations determined with a μGC prototype. After venting the house for about 2 hr and placing the hidden TCE source, four measurements were collected on the second level, one in the stairwell, and four in the basement. Since this took most of the day, sampling had to be suspended. On the second day, after venting the house in the morning, measurements were resumed, with two being collected from the second floor and eight from the basement.

Results are shown in Figure 5-5. Measurements from similar locations on different days were quite consistent. For the five Proto 1 measurements with concurrently collected canister samples, the Proto 1 values were ~2-fold higher on average (excluding one sub-ppb-level outlier with a 9-fold difference). On average, the TCE concentrations on the second floor (1.6 ppb, n = 6) were lower than those in the basement (2.9 ppb, n =

7), excluding the measurements from the basement bedroom in which the source was ultimate found. Interestingly, the second-floor measurement near the cabinet in which the TCE source had been stored prior to this study gave the highest value found on the second floor (i.e., 3.9 ppb), suggesting residual TCE in the cabinet. The corner room in the basement showed much higher TCE concentrations (Figure 5-5), with an average of 21 ppb (n = 5), and in the closet of this room where the source was located the TCE concentration was determined to be 56 ppb by Proto 1 and confirmed by canister/TO-15 as 66 ppb.

5.4. Conclusions

In summary, this study stands as the first of its kind, where μGC instrumentation was shown capable of sustained, reliable, automated measurements of a trace-level component of a complex VOC mixture under field conditions. As shown here for TCE, selective measurements were obtained in the presence of up to ~50 background interferences at concentrations in low-/sub-ppb concentration range. The temporal resolution of the measurements was sufficiently high to detect transient fluctuations in concentration resulting from short-term changes in variables affecting the extent of VI, and the sensitivity, selectivity, and accuracy were sufficient to evaluate the degree to which such factors affect VI. The capability to differentiate VI from non-VI sources of contamination was also illustrated (intentionally and unintentionally) via fixed-location and portable measurements obtained from the two μGC prototypes. Although a consistent and significant positive bias was observed in the prototype data at lower TCE concentrations, due to unresolved interferences, it did not impede the assessment-related

decision making process to a significant extent. Together with the results described in Part I of this study,[24] it is clear that μGC technology holds great promise informing efforts to assess and mitigate VI in affected homes, as well as for other environmental monitoring problems where speciated VOC measurements are required. Although not implemented in the present study, the prototypes could be remotely controlled and interrogated via a wireless internet connection, permitting long-term monitoring without an operator being present on-site. Future work will be directed at further reducing the size of the instrument, implementing hardware and software refinements to reduce the number of interferences and their influence on the accuracy of target-VOC determinations, and expanding the range of VOCs for which such measurements can be obtained.

5.5 References

1. U.S. EPA, OSWER Draft Guidance for Evaluating the Vapor Intrusion to Indoor Air Pathway from Groundwater and Soils (Subsurface Vapor Intrusion Guidance); EPA530-D-02-004; U.S. Environmental Protection Agency, 2002.
2. Pankow, J.F.; Feenstra, S.; Cherry, J.A.; Ryan, M.C. Dense Chlorinated Solvents in Groundwater: Background and History of the Problem. In *Dense Chlorinated Solvents and Other DNAPLs in Groundwater*; Pankow, J.F.; Cherry, J.A., Ed.; Waterloo Press, Guelph, Ontario, 1996.
3. ATSDR, Toxicological Profile for Trichloroethylene (TCE), U.S. Department of Health and Human Services, September, 1997. Available at http://www.atsdr.cdc.gov/toxprofiles/tp.asp?id=173&tid=30 , accessed August 2011.
4. McHugh, T.E.; Connor, J.A.; Ahmand, F. An empirical analysis of the groundwater-to-indoor-air exposure pathway: The role of background concentrations to indoor air *Environ. Forensics* **2004**, 5, 33-44.
5. U. S. Environmental Protection Agency (EPA), Compendium Method TO-15 Second Edition, Determination Of Volatile Organic Compounds (VOCs) In Air Collected In Specially-Prepared Canisters And Analyzed By Gas Chromatography/Mass Spectrometry (GC-MS), available at http://www.epa.gov/ttnamti1/files/ambient/airtox/to-15r.pdf
6. U. S. Environmental Protection Agency (EPA), Compendium Method TO-17 Second Edition, Determination of Volatile Organic Compounds in Ambient Air Using Active Sampling Onto Sorbent Tubes, http://www.epa.gov/ttnamti1/files/ambient/airtox/to-17r.pdf
7. http://www.inficon.com
8. Gorder, K. A.; Dettenmaier, E. M. Portable GC/MS Methods to Evaluate Sources of cVOC Contamination in Indoor Air *Ground Water Monitoring and Remediation* **2011**, 31, 113-119.
9. Lu, C.-J.; Tian, W.-C.; Steinecker, W. H.; Guyon, A.; Agah, M.; Oborny, M. C.; Sacks, R.; Wise, K. D.; Pang, S. W.; Zellers, E. T. Functionally integrated MEMS micro gas chromatograph subsystem *7th lnternational Conference on Miniaturized Chemical and Biochemical Analysts Systems, uTAS '03*: Squaw Valley, CA, October 5-9 2003, pp 415-419.
10. Zellers, E. T.; Steinecker, W. H.; Lambertus, G.; Agah, M.; Lu, C.-J.; Chan, H. K. L.; Potkay, J. A.; Oborny, M. C.; Nichols, J. M.; Astle, A.; Kim, H. S.; Rowe, M.; Kim, J.; da Silva, L. W.; Zheng, J.; Whiting, J. J.; Sacks, R. D.; Pang, S. W.; Kaviany, M.; Bergstrom, P. L.; Matzger, A. J.; Kurdak, C.; Bernal, L. P.; Najafi, K.; Wise, K. D. A versatile MEMS gas chromatograph for determinations of environmental vapor mixtures *Solid-State Sens., Actuator and Microsyst. Workshop*: Hilton Head, SC, June 6-10 2004, pp 61-66.
11. Lu, C.-J.; Steinecker, W. H.; Tian, W.-C.; Oborny, M. C.; Nichols, J. M.; Agah, M.; Potkay, J. A.; Chan, H. K. L.; Driscoll, J.; Sacks, R. D.; Wise, K. D.; Pang, S. W.; Zellers, E. T. First-generation hybrid MEMS gas chromatograph *Lab Chip* **2005**, 5, 1123-1131.
12. Lewis, P. R.; Manginell, R. P.; Adkins, D. R.; Kottenstette, R. J.; Wheeler, D.; Sokolowski, S. S.; Trudell, D.; Byrnes, J. E.; Okandan, M.; Bauer, J. M.; Manley, R.

G.; Frye-Mason, C. Recent advancements in the gas-phase MicroChemLab *IEEE Sens. J.* **2006**, 6, 784-795.
13. Kim, H.; Steinecker, W. H.; Reidy, S.; Lambertus, G. R.; Najafi, A. A. A. K.; Zellers, E. T.; Bernal, L. P.; Washabaugh, P. D.; Wise, K. D. A micropump-driven high-speed MEMS gas chromatography system *Proc. Transducers '07,* Lyon, France, June 10-14 2007, pp 1505-1508.
14. Zellers, E. T.; Reidy, S.; Veeneman, R. A.; Gordenker, R.; Steinecker, W. H.; Lambertus, G. R.; Kim, H.; Potkay, J. A.; Rowe, M. P.; Zhong, Q.; Avery, C.; Chan, H. K. L.; Sacks, R. D.; Najafi, K.; Wise, K. D. An integrated micro-analytical system for complex vapor mixtures *Proc. Transducers '07,* Lyon, France, June 10-14 2007, pp 1491-1494.
15. Zampolli, S.; Elmi, I.; Mancarella, F.; Betti, P.; Dalcanale, E.; Cardinali, G. C.; Severi, M. Real-time monitoring of sub-ppb concentrations of aromatic volatiles with a MEMS-enabled miniaturized gas-chromatograph *Sens. Actuators. B* **2009**, 141, 322-328.
16. Kim, S. K.; Chang, H.; Zellers, E. T. Microfabricated gas chromatograph for the selective determination of trichloroethylene vapor at sub-parts-per-billion concentrations in complex mixtures *Anal. Chem.* **2011**, 83, 7198-7206.
17. Defiant technology, Canary-Canary™, available at http://www.defiant-tech.com/products.php
18. Manginell, R. P.; Bauer, J. M.; Moorman, M. W.; Snachez, L. J.; Anderson, J. M.; Whiting, J. J.; Porter, D. A.; Copic, D.; Achyuthan, K. E. A monolithically-integrated μGC chemical sensor system *Sensors* **2011**, 11, 6517-6532.
19. Kim, S.-J.; Serrano G.; Wise K. D.; Kurabayashi K.; Zellers E. T. Evaluation of a microfabricated thermal modulator for comprehensive two-dimensional microscale gas chromatography *Anal. Chem.* **2011**, 83, 5556-5562.
20. Li, M.; Myers, E.B.; Tang, H.X.; Aldridge, S.J.; McCaig, H.C.; Whiting, J.J.; Simonson, R.J.; Lewis, N.S.; Roukes, M.L. Nanoelectromechanical resonator arrays for ultrafast, gas-phase chromatographic chemical analysis *Nano Lett.* **2010**, 10, 3899-3903.
21. Jian, R.-S.; Huan, R.-X.; Lu C.-J. A micro GC detector array based on chemiresistors employing various surface functionalized monolayer-protected gold nanoparticles *Talanta* **2011**, DOI: 10.1016/j.talanta.2011.10.025.
22. Seo, J. H.; Kim, S. K.; Zellers, E. T.; Kurabayashi, K. Microfabricated passive vapor preconcentrator/injector designed for microscale gas chromatography *Lab Chip* **2011**, in press.
23. Chang, H.; Kim, S. K.; Sukaew, T.; Bohrer, F.; Zellers, E. T. Microfabricated gas chromatograph for sub-ppb determinations of TCE in vapor intrusion investigations *Procedia Engineering* **2010**, 5, 973-976.
24. Sukaew, T.; Chang, H.; Serrano, G.; Zellers, E. T. Multi-stage preconcentrator/focuser module designed to enable trace level determinations of trichloroethylene in indoor air with a microfabricated gas chromatograph *Analyst* **2011**, 136, 1664-1674.
25. Kim, S. K.; Chang, H.; Bryant, J. G.; Burris, D. R.; Zellers, E. T. Microfabricated gas chromatograph for TCE determination in indoor air vapor intrusion studies. Part I: Field evaluation *Environ. Sci. Technol.,* submitted.

26. Rowe, M. P.; Plass, K. E.; Kim, K.; Kurdak, Ç.; Zellers, E. T.; Matzger, A. Single-phase synthesis of functionalized gold nanoparticles *Chem. Mater.* **2004**, 16, 3513-3517.
27. http://estcp.org/Program-Areas/Environmental-Restoration/Contaminated-Groundwater/Emerging-Issues/ER-1686
28. McHugh, T.; Gorder. K. Methods to distinguish between vapor intrusion and indoor sources of VOCs at residences near Hill AFB, Utah, USA In Vapor Emission to Outdoor Air and Enclosed Spaces for Human Health Risk Assessment: Site Characterization, Monitoring, and Modeling, eds. S. Saponaro, E. Sezenna, L. Bonomo. Hauppauge, New York: Nova Science Publishers, Inc., 2010.

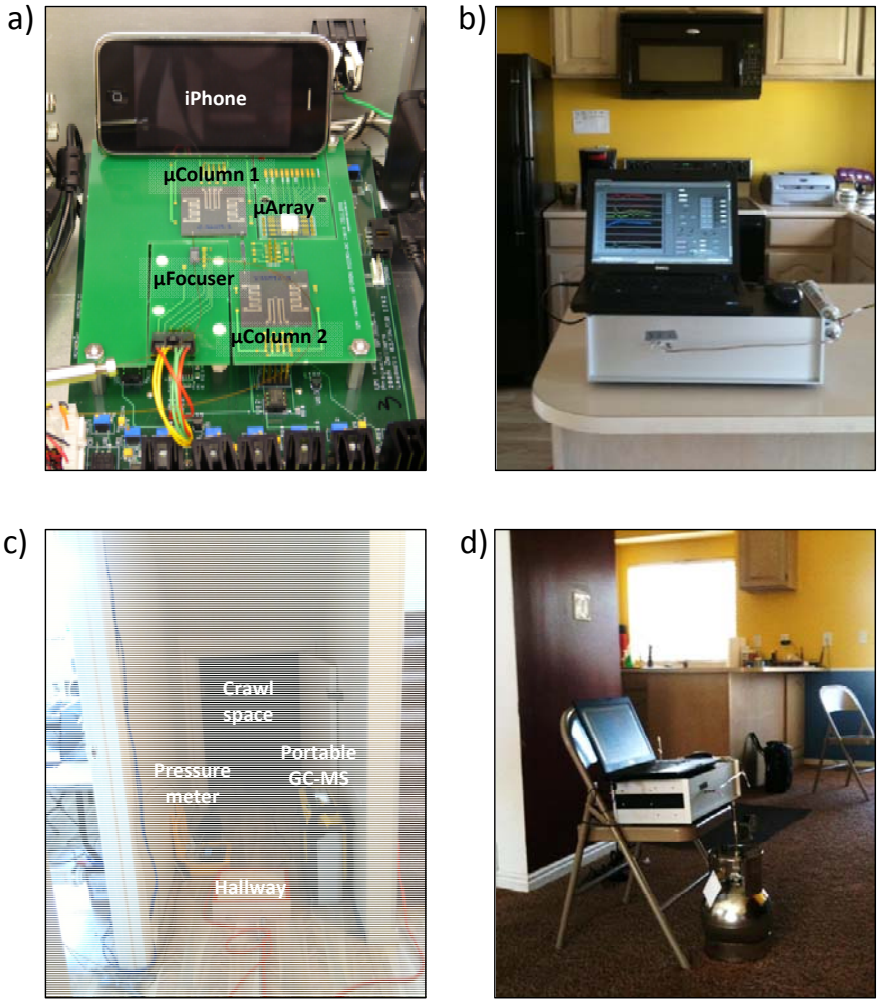

Figure 5-1. Photographs of (a) PCB-mounted microfabricated components of the prototype µGC (iPhone is shown for scale); (b) laptop and prototype in the kitchen of House 1; (c) crawl space and hallway in the basement of House 1, with the Hapsite GC-MS and pressure sensor readout unit (prototypes are situated on the table in the room to the left); and (d) prototype and Summa canister during measurement of spatial TCE distribution in House 1.

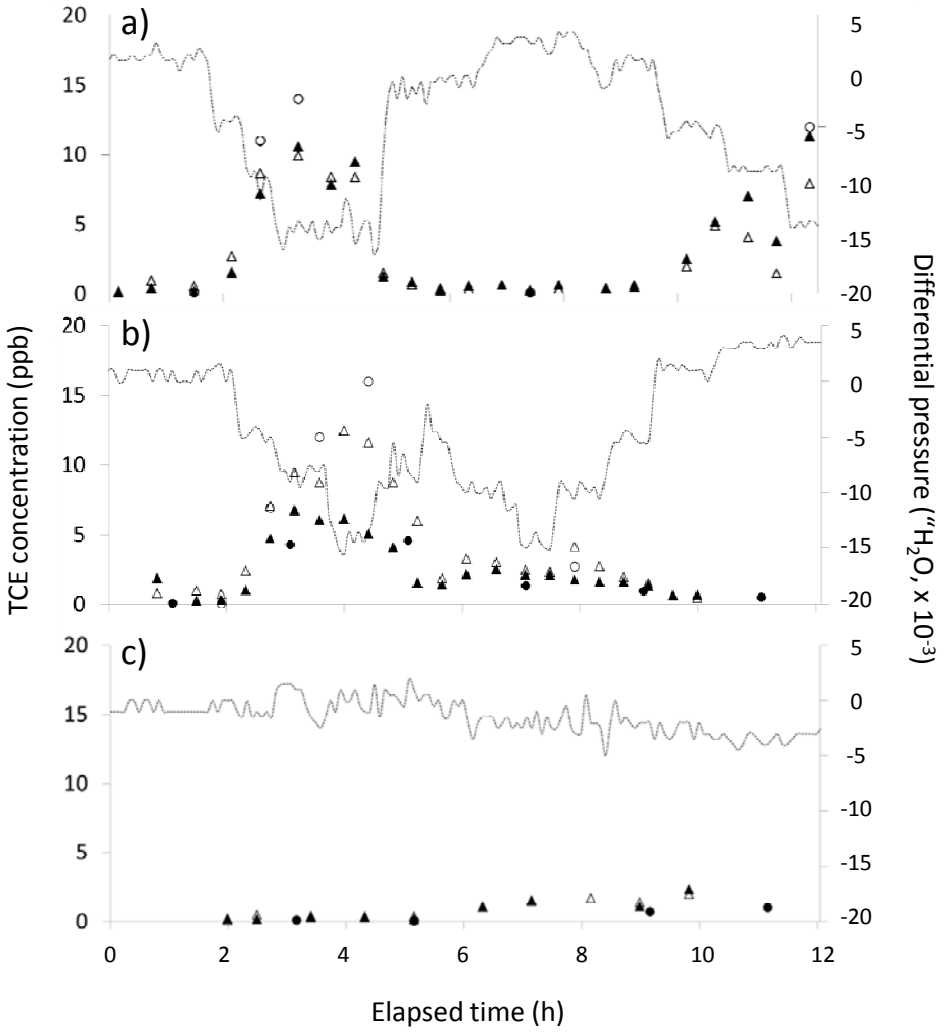

Figure 5-2. Temporal variations in the TCE concentration (left-hand ordinate) determined by Proto 1 (open triangles), Proto 2 (filled triangles), canister/TO-15 (open circles), and Hapsite GC-MS (filled circles) as a function of the differential pressure (dashed lines) between the sub-slab headspace and the basement hallway of House 1 (right-hand ordinate): (a) measurements collected from the crawl space near the primary VI entry location with and without pressure changes induced by an exhaust fan located on the second floor; (b) measurements collected from the crawl space (Proto 1 and canister/TO-15) and from the hallway adjacent to the crawl space (Proto 2 and Hapsite GC-MS) with induced pressure changes; and (c) measurements collected from same locations as in (b) without induced pressure changes.

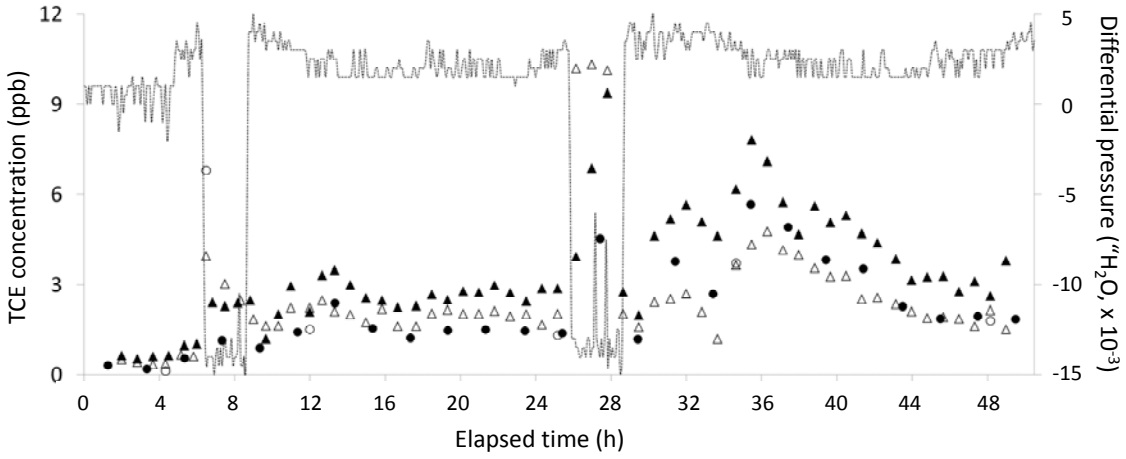

Figure 5-3. Results of 48 hr of continuous, automated (unattended) TCE concentration measurements (left-hand ordinate) with Proto 1 (open triangles, crawl space) and Proto 2 (filled triangles, hallway), along with discrete reference measurements by canister/TO-15 (open circles, crawl space) and Hapsite GC-MS (filled circles, hallway) as a function of the differential pressure between the sub-slab headspace and the basement hallway of House 1 (dashed line, right-hand ordinate).

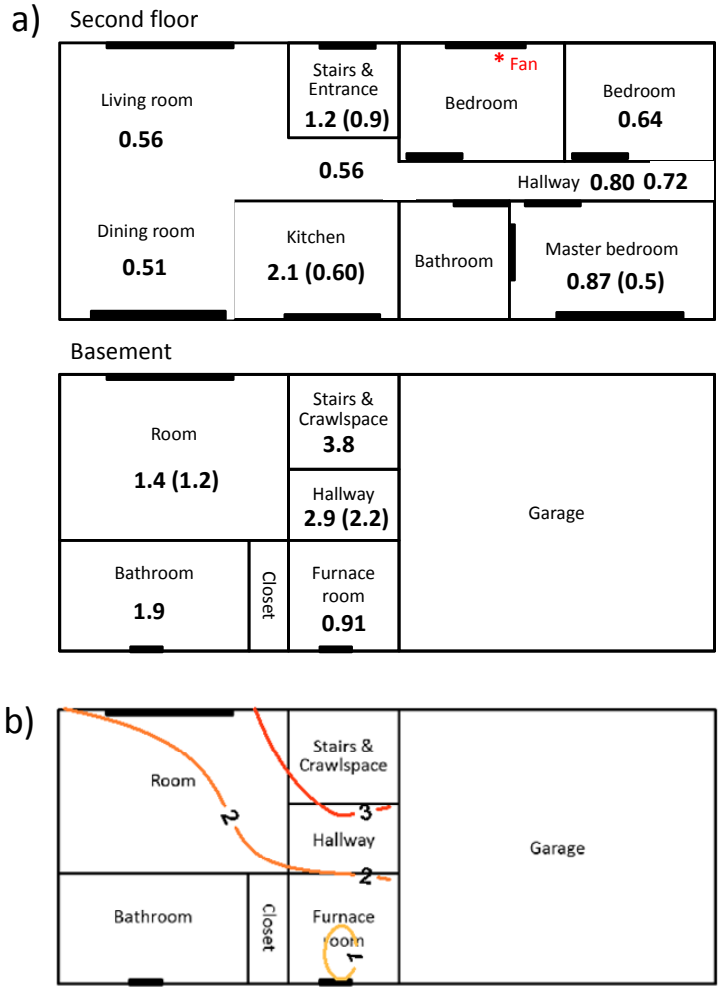

Figure 5-4. Floor plan of House 1 showing the spatial distribution of TCE vapor concentrations: (a) sampling locations and corresponding TCE concentrations (ppb) determined by Proto 1 and by canister/TO-15 (in parentheses); and (b) kriged contour map of TCE concentrations (ppb) in the basement showing the gradient with distance from the primary VI entry location in the crawl space.

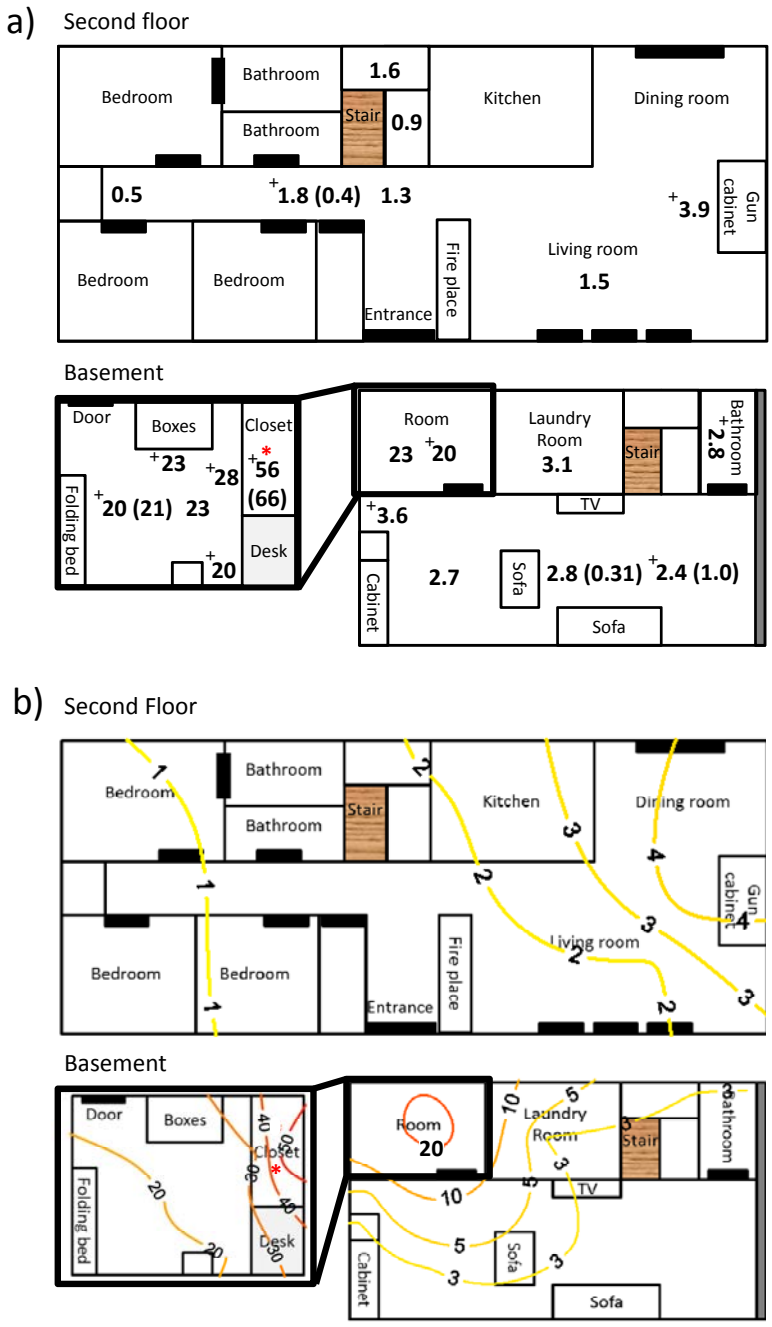

Figure 5-5. Spatial distributions of TCE in House 2 in which a non-VI source of TCE was placed: (a) Sampling locations and their corresponding TCE concentrations (ppb) determined by Proto 1 and by canister/TO-15 (in parentheses); samples with "+" were collected on the second day and b) corresponding contour map of TCE concentrations (ppb) derived from the Proto 1 data. Lower left-most image shows an enlarged view of the bedroom in the basement and the closet in which the TCE source was hidden (indicated by "*").

CHAPTER VI

Multivariate Curve Resolution of Co-Eluting Peaks Measured with Microsensor Array Detectors in Micro- and Meso-Scale Gas Chromatographs

6.1 Introduction

Various types of microfabricated vapor sensor arrays that employ sorptive interface layers have been widely studied.[1-14] Even though individual sensors in the array are generally responsive to the vapors of wide range of volatile organic compounds (VOC), they are still partially selective. A stand-alone array can often differentiate individual components from a population of 20 or more possible vapors by use of pattern recognition methods, but it is necessary to have an upstream chromatographic separation stage in order to determine the components of mixtures of three or more VOCs due to inherent limitations on the degree of selectivity afforded by such arrays.[9-14]

By coupling an upstream separation column with a microsensor array, the problem of identifying and quantifying the components of a complex VOC mixture can be reduced into a time-resolved series of more manageable problems concerned with small subsets of that mixture. Defining retention time windows in which only specific VOCs would be found further simplifies the problem.[15] Even if co-elution of vapors is likely with a GC-microsensor array system, especially in a μGC which is often focused on rapid

determination, a high performance with a minimum of calibration and computation complexity should be achieved with this approach.

A handful of studies that have been reported about the implementation of GC-microsensor array instrumentation[14-24] or on the chemometric analysis using data obtained from such systems.[9-15, 18-20] Extended disjoint principal component regression (EDPCR) models has been mainly used in our group for assigning identities to chromatographically resolved single vapors and to the components of unresolved or partially resolved simple mixtures on the basis of the response patterns combined with Monte Carlo simulations,[9-15,18,19] while a study has compared EDPCR and a non-negative least squares (NNLS) method for their sensor array.[20] Among those studies, only one study, which is a previous work performed in our group, employed a multivatiate curve resolution (MCR) method to deconvolute overlapping peak.[14]

MCR methods are often used to determine the components of mixtures with overlapping spectra in case spectrometric signals can be obtained such as in vibrational spectroscopy and gas and liquid chromatography with a spectrometric detector (e.g., GC-MS, HPLC-diode array, etc.).[25-33] MCR methods can determine the number of components in overlapped chromatographic peak composites and then can extract and recover the elution profile and spectrum of each component of the composite peak without prior knowledge of the mixture composition. Following MCR, the reconstituted spectra can then be matched to those in a library in order to determine the identities and concentrations of the individual analytes. As the reason, various MCR algorithms have been introduced and applied, such as AutoBTEM[34] for FT-IR, Raman, and IR imaging data, PARAFAC[35, 36] for GC×GC and GC×GC-TOFMS, alternating least square (ALS)[37-

[39] for multiple applications, evolving factor analysis (EFA) with ALS[14] for microsensor array as mentioned above, etc.

EFA is the most common MCR method applied to chromatography.[27-29] EFA performs factor analysis on a composite peak profile in sequential time segments. If the detector can differentiate components making up the composite peak, the rank of the corresponding data matrix will be equal to the number of components in the composite peak. EFA is also used to find the location of the start and end of the peak profile of each component in the composite peak by performing in both the forward and backward directions. Another MCR algorithm, ALS, is an iterative process of least squares algorithm to approximate the elution profile and the spectrum of each component of composite peak to the true profile and spectrum, starting with given initial estimate of elution profile or spectrum.[30-32] More details about EFA and ALS methods can be found elsewhere.[14, 27-32, 37-39] EFA can be used to locate selective elution regions and to estimate the rank of the composite data matrix (i.e., number of components in a composite peak), and then ALS can be used to improve the accuracy of recovery for elution profile and/or spectrum. Once information (peak profile and spectrum) of each component of composite peak is extracted, pattern recognition is required to match the recovered peak belongs to what compound in the library by comparing response patterns. Accurate recovery would be assumed to lead directly to accurate vapor recognition.

Adaptation of such MCR method to chromatographic data obtained from microsensor arrays has been successfully performed and reported,[14] but it used a set of simulated sensor responses based on calibrated responses. Until now, there has been no

study reported about application of any MCR method for peak deconvolution with experimental data set of binary or ternary mixtures derived from such systems.

In this study, the application of EFA-ALS to experimental data generated from an array of microsensors used as the detector in a GC is explored as the follow-up study of our previous work mentioned above.[14] The main purpose of this study is to demonstrate the applicability of this hybrid MCR method to experimental data to recover each component qualitatively (i.e., vapor recognition) in partially time-resolved binary mixtures. The quantitative information (i.e., vapor concentration) derived from the accurate recovery of the elution profile is addressed only in passing. Experimental data generation using CR arrays with a portable and μGC is explored first, followed by the use of EFA to determine the number of components in a composite peak, as well as fidelity test and simple pattern recognition of recovered CR array pattern of each component. The influence of pattern similarity, resolution and relative response ratio on the performance of EFA-ALS is then briefly assessed.

6.2 Experimental Methods

6.2.1 Materials

All chemicals were purchased from Sigma-Aldrich/Fluka (Milwaulkee, WI) or Acros/Fisher (Pittsburgh, PA) in high purity (>95% and most > 99%) and were used as received. As the adsorbents in the instruments, graphitized carbons, Carbopack B (C-B, specific surface area = 100 m^2/g, for pre-trap) and Carbopack X (C-X, 250 m^2/g, for sampler and the μF) obtained from Supelco (Bellefonte, PA) were used. 60/80 mesh C-B and C-X were sieved and the fractions with nominal diameters in 212-250 μm range were

used for packing the appropriate devices. MPNs thiolated with n-octanethiol (C8), 6-phenoxyhexane-1-thiol (OPH), 4-(phenylethynyl)-benzenethiol (DPA), and methyl-6-mercaptohexanoate (HME) were taken from existing supplies that were synthesized by the method reported[40] and used for sensor coating. The MPNs had core diameters in the range of 3.4-4.7 nm.[41,42]

6.2.2 Instrument Description, Experimental Setup and Vapor Selection

To test the compatibility of the MCR method, two different miniaturized GCs (portable[15,19,21,22] and micro-scale[18,23,43-49]) using the same type of CR sensor array as the detector[41,42] were used for generating experimental data sets of selected binary mixtures. Figure 6-1 shows the schematic diagrams of both instruments. Briefly, both instruments contain a preconcentration/focusing module for sampling and injection (portable GC: stainless steel tubing preconcentration/focuser (PCF); μGC: stainless steel tubing high volume sampler and microfabricated focuser (μF)), two at-column temperature programmable columns in series as the separation module coated with polydimethylsiloxane (portable GC: low thermal mass column (Agilent Technologies, Santa Clara, CA); μGC: microfabricated columns), and the same CR array as the detector that uses MPN films as the interface layer. More detail about these instruments can be found elsewhere.[21,23] Sequential steps of analysis (sampling, focusing, and analysis) are controlled by routines written in LabView (Ver. 7.1 and 8.5, National Instruments, Austin, TX).

Experimental setup to generate data is presented in Appendix 2, which includes an upstream external six-port valve. Prior to sampling by portable or μGC, an aliquot of

test atmosphere in a Tedlar bag was drawn into a sample loop connected to the six-port valve by suction flow generated by a pump. Then, the six-port valve was actuated to load the sample to the preconcentration module of portable or μGC on a background of clean, dry N_2 from a compressed cylinder. Sample was then analyzed (separated and detected) by the instrument. Voltage drop across individual sensors as the CR sensor resistance changes were recorded into a text file by the DAQ card at 20 Hz after amplification of the signal difference between baseline and measured values. Each data stored in a text file was then imported into Grams 32 software (Thermogalactics, Inc., Salem, NH) to be converted to chromatograms and analyzed.

To generate experimental data sets of binary mixtures which can be tested with the MCR method (EFA-ALS), two different vapor pairs were selected based on response pattern similarity (correlation coefficient, ρ), one as "similar" and the other as "dis-similar". Vapors for a binary mixture should have similar chromatographic characteristics and should overlap together. In our previous field study of the μGC discussed in Chapters 4 and 5, it was found that trichloroethylene (TCE) and n-heptane (HEP) have similar retention time and co-eluted with each other with the ρ value ~0.80 which can be considered as the "similar" pair. As the other pair which should have the response pattern similarity low enough to be considered as "dis-similar", preliminary test result showed that cyclohexane (CHX) and n-butanol (BOH) had different CR array responses due to their chemical property difference, probably because of polarity difference. Table 6-1 shows the chemical properties of those selected vapors.

6.2.3 Calibration and Data Set Generation

As mentioned above, because of the use of two different instruments, two CR arrays were used for the experiments. Each CR array coated with same MPNs (C8, DPA, OPH, and HME) was installed into an instrument and calibrated prior to use. Portable GC and μGC were applied for the pair of CHX and BOH, and TCE and HEP, respectively. For the calibrations, test atmospheres at certain concentrations (CHX: 100 ppm, BOH: 100 ppm, TCE: 100 ppm, and HEP: 300 ppm) were generated in a Tedlar bag by injecting certain amount of liquid vapors. Samples were left for an enough time to be fully stabilized (i.e., fully evaporated) before use. Calibrations were performed by samples using various volumes of external sample loops (100-2000 μL for CHX and BOH, and 25-500 μL for TCE/HEP), resulting the calibration range from 2.5-50 ppb-L for TCE and 7.5-150 ppb-L for HEP, and 10-200 ppb-L for CHX and BOH.

Experimental data sets of pure components and their binary mixtures were generated with multiple scenarios by adjusting chromatographic resolution (R) varied by changing the retention time difference (Δt_r) of the component-peak maxima and relative response ratio (RRR) of the two components in order to evaluate the influences on the curve resolution. Figure 6-2 shows the example chromatograms with various R (0.1-1.0), where $R = 0.59\Delta t/W_{1/2}$ and $W_{1/2}$ is the peak width at half maximum[50] and RRR (1:10-10:1) tested in this study. To adjust R over desired range, temperature program of the columns was controlled. RRR range was also controlled by loading different amount of samples using different volumes of sample loop. Signal-to-noise (S/N) ratio (i.e., ratio between signal and average baseline) was also controlled to be always ≥ 10 on the least

sensitive sensor. Table 6-2 summarizes the conditions used for binary mixture data generation.

6.2.4 Multivariate Curve Resolution (EFA-ALS)

A matrix (***X***) that includes sensor responses can be decomposed to a concentration profile matrix (***C***) at each value of retention time assuming a Gaussian elution profile, and the spectra matrix (***S***) for each sensor with a random error matrix (***E***). It is created as shown in Eq. 1,

$$\boldsymbol{X}=\boldsymbol{C}\cdot\boldsymbol{S}+\boldsymbol{E} \qquad (1)$$

To deconvolute pure components from the matrix ***X***, an estimate of the concentration profile matrix ***C*** should be obtained within the selective elution region of each component using the EFA algorithm. In this study, an algorithm developed by Maeder *et al.* was used as the EFA method.[28,29] The estimate of ***C*** is then refined to minimize the random error (***E***) by iterative ALS calculations using the following two equations:

$$\boldsymbol{S}_{est} = (\boldsymbol{C}'\cdot\boldsymbol{C})^{-1}\boldsymbol{C}'\cdot\boldsymbol{X} \qquad (2)$$

$$\boldsymbol{X}_{est} = \boldsymbol{C}\cdot\boldsymbol{S}_{est} \qquad (3)$$

$$\boldsymbol{C}_{est} = \boldsymbol{X}_{est}\cdot\boldsymbol{S}_{est}(\boldsymbol{S}_{est}'\cdot\boldsymbol{S}_{est})\cdot\boldsymbol{S}_{est}^{-1} \qquad (4)$$

Eq. 2 solves the equation $\boldsymbol{X} = \boldsymbol{CS}$ with respect to ***S*** with given ***X*** and estimates ***C*** by EFA, and Eq. 3 estimates a new ***X*** matrix. Given the new $\boldsymbol{X}_{est}$ and $\boldsymbol{S}_{est}$, Eq. 4 calculates a new $\boldsymbol{C}_{est}$, and another estimate of ***X*** is calculated. By iterating Eq. 2 to 4, starting from an initial estimate of ***C***, one approaches an optimized solution for ***X***. The

ALS algorithm stops iteration by a convergence denoted by the point at which further iteration changes the sum of squares of the residual error matrix $\boldsymbol{E}$ by $< 10^{-6}$.

The EFA-ALS method was successfully tested with simulated sensor data set in a previous study,[14] and was employed in this study again with another ALS algorithm which was proposed by Lin.[51] According to his article, the new method of ALS using projected gradients would give stronger optimization result than the popular multiplicative update method of ALS. As in our previous study, the constraint that both $\boldsymbol{C}$ and $\boldsymbol{S}$ both must be non-negative has been applied for ALS algorithm. Matlab code for the new ALS method can obtained from either the same article or his webpage.[52]

6.2.5 Fidelity, Confusion and Recognition of Recovered Pattern

The primary focus of this study is placed on assessing the quality of curve resolution in terms of the fidelity of the array response pattern recovered from the EFA-ALS analysis to its true response pattern. The correlation coefficient, *r,* between estimated and actual (pure component or library) response patterns is used as the metric. As another way to determine the quality of recovery, the degree of confusion which is the correlation coefficient, r_c, between estimated pattern of one compound and actual pattern of the other compound was used.

Recognition of recovered pattern is also one of the main purposes of performing MCR analysis. To assign recovered array pattern as a certain compound in the library, correlation coefficients, r_m, between the recovered array pattern and those of compounds in the library were calculated, and then the recovered pattern was assigned as a compound that had the highest correlation coefficient among compounds in the library.

6.2.6 Software and Calculations

The routines used for the multivariate analyses were written in-house in Matlab 2010a (Mathworks, Natick, MA), including the EFA-ALS and pattern recognition algorithms. The function for singular value decomposition in Matlab was used for extracting principal components from the CR response data matrix $\boldsymbol{X}$.

6.3 Results and Discussion

6.3.1 Calibration, Response Pattern, and Parameter Adjustment

CR array detector responses were calibrated over the following ranges of injected masses (integrated volumes): 2.5-50 ppb-L (13-270 ng) for TCE, 7.5-150 ppb-L (31-615 ng) for HEP, and 10-200 ppb-L for both CHX and BOH (34-688 ng and 30-606 ng for CHX and BOH, respectively). Calibration curves of injected mass vs. peak height gave forced-zero linear regression r^2 values ≥ 0.98 for all sensors for all compounds in both CR arrays (shown in Appendix 2). The normalized CR array response pattern for each vapor was derived from the slopes of the calibration curves and are presented in Figure 6-3. The pair of TCE and HEP had the pattern similarity, ρ value, ~0.80 and the other pair (CHX and BOH) had the value ~0.20.

The limit of detection (LOD) of each sensor for each vapor was determined as 3 times the baseline noise divided by the slope sensitivity obtained from calibration. In order to insure responses from all four sensors, the minimum injection mass must be greater than the LOD for the least sensitive sensor in the array for a given analyte. In the array used for the TCE+HEP pair, the HME-coated sensor had the lowest LOD for TCE (1.7 ppb) and HEP (8.9 ppb). In the array used for CHX and BOH, the OPH-coated

sensor was the LSS (40 ppb for CHX and 12 ppb for BOH). Random baseline noise was converted to a concentration calculated by using the LSS, and 10 times of the concentration was used as the minimum concentration for all experiments in order to keep the S/N ratio ≥ 10. The LSS was also used to adjust the *RRR*. The ratio of peak areas for vapors of the tested pair obtained from the LSS was calculated. For the "similar" pair, the LSS (HME) had ~4:1 of TCE and HEP ratio with vapor samples at same concentration. For the "dis-similar" pair, the ratio of CHX and BOH peaks from OPH sensor was ~1:7 at same concentration level. As a convenient way to adjust the *RRR*, samples for experiments were generated having opposite ratio in terms of concentration (e.g. TCE sample of 660 ppm and HEP sample of 2600 ppm would give *RRR* of 1:1), and the sample volume loaded into the instruments were controlled accordingly. For example, in case of TCE/HEP pair, to achieve S/N ratio=10, the concentration of TCE sample was made to be 6.6 ppb-L (660 ppm × 10 μL) and that of HEP was made to be 34 ppb-L (2600 ppm × 10 μL). *RRR* was adjusted only from 1:10 (10 μL of 660 ppm TCE sample: 100 μL of 2600 ppm HEP sample) to 10:1 (100 μL of 660 ppm TCE sample: 10 μL of 2600 ppm HEP sample) due to limited dynamic range of sensor response.

As mentioned in the previous section, *R* was controlled ranging (0.1-1.0) by changing retention times of two composite peaks of a mixture using temperature control of separation columns. For the TCE+HEP pair, temperatures of the columns were maintained (isothermal) at 30, 55, and 70 °C to obtain *R* value of 1.0, 0.5, and 0.1, respectively. For the CHX/BOH pair, heating rate of the columns was controlled to reach at 150 °C from room temperature at 0.068, 0.18, and 0.27 °C/s for *R* value of 0.1, 0.5, and 1.0, respectively

6.3.2 Number of Components in the Composite Peak

In cases where $R \leq 0.5$ or where $R > 0.5$ but the *RRR* is large, it may not be obvious to determine the number of components in a peak of binary mixture from visual inspection of the chromatogram. The first step to solve the problem is using EFA. In the previous study which was conducted with a set of simulated data,[14] it was shown that the performance of EFA method to determine the number of components was generally good when the *S/N* of 10:1, $R > 0.1$ and that there was some decline in performance as the *RRR* increases, but up to an *RRR* of 5:1 most pair components could be detected.

In this study, *S/N* ratio is always ≥ 1:10 and the maximum *S/N* ratio on the LSS is 1:100 in case of the *RRR* is 1:10, while the other three sensors should have higher *S/N* ratio. This fact should have led the result of EFA to determine the number of components to better than that of the previous study. Table 6-2 shows the result to determine the number of components in binary mixtures under various conditions, and two components were detected by EFA analysis with all conditions. Overall, the ρ values for both pairs are sufficient for the determination of number of compounds, and the capability of the EFA method to detect the presence of both components in these mixtures is quite good.

6.3.3 Fidelity, Confusion, and Pattern Recognition

The next step is to recover the elution profiles and sensitivities (response patterns) of the two pure components from the composite peak. Figure 6-4 shows an example of EFA-ALS analysis with TCE and HEP with the condition of *S/N* ≥10, *R*=0.5, *RRR*=1:1. As shown, *fidelity* (correlation coefficient, *r*, between the recovered pattern and those stored in the library), of recovered array pattern was used as the metric to determine the

quality of pattern recovery. The *r* value should be ≥ the pattern similarity value (ρ) of the pair, but in some cases of CHX/BOH pair (R=0.1 or RRR ≥ 1:10), the *r* values are not sufficiently high enough, making it is difficult to determine the quality of recovery. For such cases, another way to determine the quality of recovery is applied, which is *confusion* (correlation coefficient, r_c, between recovered pattern of one compound and those stored in the library) of recovered array pattern. The r_c value should be ≤ the pattern similarity value (ρ) of the pair. After recovering patterns using EFA-ALS algorithm, recovered patterns were compared with those in the library by calculating correlation coefficient (r_m) between the recovered pattern and individual patterns in the library, assuming that only patterns for the two compounds of binary mixture tested were in the library. The recovered pattern was then assigned as the compound in the library which had the highest r_m value.

Table 6-3 summarizes all the results of EFA-ALS analysis for data sets of both "similar" and "dis-similar" pairs. In case of TCE+HEP pair, recovered patterns show their *r* values ≥ 0.94 which is remarkably high, while all r_c values are ≤ 0.80 which is the ρ value of the pair. (Note: the value for HEP in the case 19 is also < 0.80, which is 0.795.) With high *r* values and low enough r_c values, all the recovered patterns were correctly assigned after being compared with the patterns in the library. In case of CHX+BOH pair, in general, *r* values are somewhat lower than expected regarding their pattern dis-similarity. In detail, cases 1, 10, and 19 were expected to have low *r* values, due to low *R* = 0.1 (case #1 and 10, Note: case #1 and 10 are same data) or high *RRR* = 1:10 (case #19), based on the result of previous study.[14] The result for BOH in the case #17 (R = 0.5 and RRR = 2.5:1) is difficult to explain, which should be much higher than its current value

(0.22). In terms of confusion, r_c values are all lower than the ρ value of the pair (0.20), except one data point for BOH with R = 0.1 and RRR = 1:1, which would be expected, because of the low R. In the exceptional case, however, the r value is > ρ value which would allow the pattern recognition possible. As for TCE/HEP pair, patterns recovered from the binary mixtures of CHX/BOH are all correctly assigned as they are supposed.

Overall, the ability to correctly recover the patterns of individual components and to recognize them as correct compounds in the library shows that the EFA-ALS algorithm would be appropriate to be used for experimental data derived from microsensor array. Ideally, however, the pair for CHX/BOH (dis-similar) should have higher fidelity and lower confusion than the TCE/HEP pair, because of the lower correlation coefficient between their response patterns. However, this study showed an opposite result that the TCE/HEP pair was recovered better. Figure 6-S3 in Appendix 2 would explain a possible reason. As seen in Figure 6-S3, OPH-coated sensor shows a long tailing for both CHX and BOH which distort the response pattern for BOH. The response pattern of BOH changes, as the peak elutes due to the tailing of OPH-coated sensor. This response pattern change would lower the recovery rate. In addition, the portable GC used for CHX/BOH shows a baseline decrease (i.e. overshooting) after a high concentration peak elutes, which also distort sensor responses. This would be another reason for the low recovery rate of BOH in the cases that CHX concentration is at high concentration. For the TCE/HEP pair analyzed with the microGC, these problems were not found. This would be the reason to have been able to obtain better MCR result for the similar pair.

6.3.4 Influence of Chromatographic Resolution and Relative Response Ratio

Figure 6-5 illustrates the effect of a) *R* on the quality of the recovered individual-component response patterns for both pairs, b) *RRR* for "similar" pair, and c) *RRR* for "dis-similar" pair. To evaluate the influence of chromatographic resolution, the *RRR* was fixed to 1:1 and *R* between two components in a mixture was adjusted at 0.1, 0.5, and 1.0 by controlling the temperature of separation columns (explained in "Experimental Methods" section). As shown in Figure 6-5a and as expected, there is a trend that the quality of recovery decreases as *R* decreases. The effect is more for a polar compound (BOH) which has *r* value from 0.91 at *R*=1.0 to 0.49 at *R*=0.1, while it is less for the others. Usually polar compounds have more tailing on their peaks, resulting the peak shapes are distorted. It would be possible that the distorted peak shape of a polar compound reduces the performance of EFA-ALS.

The effect of *RRR* on the quality of the recovered response patterns for both pairs was evaluated. For the test, *RRR* was adjusted to be 1:10, 1:5, 1:2.5, 1:1, 2.5:1, 5:1 and 10:1 with $S/N \geq 10:1$ and $R = 0.5$. Figures 6-5b and c present the results of the test. In the previous study,[14] it showed that the r value would decrease from 1.0 to < 0.91, as the fraction of one component decrease from 100% to 60% in case of $\rho = 0.81$. In cases of $\rho = 0.56$ and 0.023, the fraction decreased to 20% and 9%, respectively. In this study, there is no obvious trend in quality of recovery found, as the fraction (i.e. *RRR*) change for both pairs. However, BOH shows decrease in *r* value, when the fraction of BOH decreases, while the others do not. As mentioned in the previous section, the third last data point (RRR=2.5:1) for BOH is somewhat lower than expected. If it could be considered as an outlier, it would be possible that BOH has an effect of *RRR* due to the

chemical property difference. The *RRR* could not be adjusted higher than 1:10 or 10:1 ratio, because of the dynamic range limitation that instruments can measure. Overall, the effect of variables such as chromatographic resolution and relative response ratio was not significantly high as expected, even though some effect was observed for a polar compound.

6.4 Conclusions

This is the first report on the use of MCR to analyze experimental data from a microsensor array used as the detector for a gas chromatograph. The MCR method which is EFA combined with ALS was successfully adapted to such data. The microsensor array used in this study gives relatively less information (i.e. low dimension) than conventional spectrometric GC detectors. Results shown here, however, including recovery of response patterns, estimation of the number of components in binary composite peaks with multiple conditions, fidelity and confusion of recovered patterns, pattern recognition of recovered patterns, and effect of variables on the quality of recovery, proved the capability of the hybrid method to be used for the type of array. That also proves such an array would be a useful detector for GC systems.

Calibrations and data generation using microsensor arrays were systemically performed prior to the MCR analysis. With the data, response patterns recovered by the algorithm had high fidelity and low confusion in terms of correlation coefficient. Pattern recognition and assignment of recovered patterns were all tolerable (successful) for various conditions tested in this study, pattern similarity (“similar” with correlation coefficient of 0.80 and “dis-similar” with that of 0.20), chromatographic resolution of

0.1-1.0 and relative response ratio (*RRR*) of 10:1-1:10, even though a decline in performance was observed with a polar compound (n-butanol) at low resolution (*R*=0.1). It would be stated as one of conclusions that distortion of peak shape due to the chemical property could be a cause of decline in the performance. The effect of *RRR* was not as high as that was expected. However, the range of *RRR* tested would not be wide enough to evaluate more detail of the *RRR* effect, because of the limited dynamic range instrument can measure. This should be re-evaluated after modifying the instrument in near future.

As the diversity of response patterns from the CR-array is typical of that in other microsensor arrays using sorptive interface layers, the results shown here can be considered as the representative for other other microsensor arrays used as GC detectors. Despite successful results shown here, it is important to mention that the results would not reflect the full extent of the MCR performance, because of the limited data set. As the next step, the issues of defining the retention time window and determining the number and nature of vapors in the window to which recovered patterns are compared must also be considered. Quantification of recovered components is another issue to address.

As a conclusion, this study showed an improved way to identify unknown components in any partially co-eluted peak from GC-microsensor array combination, which was relied on only pattern recognition without any degree of separation in previous studies. Thus, it should be a valuable addition to develop a GC system combined with a microsensor array as the detector.

6.5 References

1. Röck, F.; Barsan, N.; Weimar, U. *Chem. Rev*. **2008**, 108, 705-725.
2. Grate, J. W. *Chem. Reviews* **2000**, 100, 2627–2648.
3. Patel, S. V.; Jenkins, M. W.; Hughes, R. C.; Yelton, W. G.; Ricco, A. J. *Anal. Chem*. **2000**, 72, 1532-1542.
4. Severin, E. J.; Doleman, B. J.; Lewis, N. S. *Anal. Chem*. **2000**, 72, 658-668.
5. Lange, D.; Hagleitner, C.; Hierlemann, A.; Brand, O.; Baltes, H. *Anal. Chem*. **2002**, 74, 3084-3095.
6. Abbas, M. N.; Moustafa, G. A.; Mitrovics, J.; Gopel, W. *Anal. Chim. Acta* **1999**, 393, 67-76.
7. Chapman, P. J.; Vogt, F.; Dutta, P.; Datskos, P. G.; Devault, G. L.; Sepaniak, M. J. *Anal. Chem*. **2007**, 79, 364-370.
8. Hana, L.; Shi, X.; Wu, W.; Kirk, L.; Jin, L.; Wang, L.; Mott, D.; Cousineau, L.; Zhong, C.J. *Sens. Actuators B* **2002**, 106, 431-441.
9. Park, J.; Groves, W. A.; Zellers, E. T. *Anal. Chem*. **1999**, 71, 3877-3886.
10. Zellers, E. T.; Batterman, S. A.; Han, M.; Patrash, S. J. *Anal. Chem.* **1995**, 67, 1092-1106.
11. Hsieh, M. D.; Zellers, E. T. *Anal. Chem*. **2004**, 76, 1885-1895.
12. Jin, C.; Kurzawski, P.; Hierlemann, A.; Zellers, E. T. *Anal. Chem*. **2008**, 80, 227-236.
13. Jin, C.; Zellers, E. T. *Anal. Chem.* **2008**, 80, 7283–7293.
14. Jin, C.; Zellers, E. T. *Sens. Actuators. B* **2009**, 139, 548-556.
15. Lu, C. J.; Whiting, J. R.; Sacks, D.; Zellers, E. T. *Anal. Chem.* **2003**, 75, 1400-1409.
16. Frye-Mason, G.; Kottenstette, R.; Mowry, C.; Morgan, C.; Manginell, R.; Lewis, P.; Matzke, C.; Dulleck, G.; Anderson, L.; Adkins, D. in Proceedings Micro Total Analysis Systems Workshop, ed. J. M. Ramsey and A. van den Berg, Kluwer, Dordrecht, The Netherlands, May 2001, pp. 658–660.
17. Cai, Q. Y.; Zellers, E. T. *Anal. Chem.* **2002**, 74, 3533-3539.
18. Lu, C.-J; Steinecker, W. H.; Tian, W.-C.; Agah, M.; Potkay, J. A., Oborny, M. C.; Nichols, J.; Chan, H. K. L.; Driscoll, J.; Sacks, R. D.; Pang, S. W.; Wise, K. D.; Zellers, E. T. *Lab Chip* **2005**, 5, 1123-1131.
19. Lu, C.-J ; Jin, C. ; Zellers, E. T. *J. Environ. Monit.* **2006**, 8, 270-278.
20. Woodka, M. D. ; Brunschwig, B. S. ; Lewis, N. S. *Langmuir* **2007**, 23, 13232-13241.
21. Lewis, P. R.; Manginell, R. P.; Adkins, D. R.; Kottenstette, R. J.; Wheeler, D. R.; Sokolowski, S. S.; Trudell, D. E. *IEEE Sensors Journal* **2006**, 6, 784-795.
22. Zhong, Q.; Steinecker, W. H.; Zellers, E. T. *Analyst* **2009**, 134, 283-293.
23. Zhong, Q.; Veeneman, R.; Steinecker, W.; Jia, C.; Batterman, S.; Zellers, E. T. *J. Environ. Monit.* **2007**, 9, 440-448.
24. Kim, S. K.; Chang, H.; Zellers, E. T. *Anal. Chem.* **2011**, 83, 7198-7206.
25. Jaumot, J.; Tauler, R. *Chemom. Intell. Lab. Syst.* **2010**, 103, 96-107.
26. De Juan, A.; Tauler, R. *J. Chromatog. A* **2007**, 1158, 184–195**.**
27. Manne, R. *Chemom. Intell. Lab. Syst.* **1995**, 27, 89-93.
28. Maeder, M. *Anal. Chem*. **1987**, 59, 527–530.
29. Gampp, H.; Maeder, M.; Meyer, C. J.; Zuberbuehier, A. D. *Talanta* **1985**, 32, 1133-1139.

30. Amrhein, M.; Srinivasan, B.; Bonvin, D.; Schumacher, M.M. *Chemom. Intell. Lab. Syst*.**1996**, 33, 17– 33.
31. Tauler, R.; Smilde, A.K.; Kowalski, B. J. *J. Chemom.***1995**, 9, 31– 58.
32. Tauler, R. *Chemom. Intell. Lab. Syst*. **1995**, 30, 133– 146.
33. Kowalski, B. R.; Sharaf, M. A. *Anal. Chem*. **1982**, 54, 1291-1296.
34. Xu, W.; Chen, K.; Liang, D.; Chew, W. *Anal. Biochem.* **2009**, 387, 42–53.
35. Hoggard, J. C.; Wahl, J. H.; Synovec, R. E.; Mong, G. M.; Fraga, C. G. *Anal. Chem.* **2010**, 82, 689–698.
36. Hoggard, J. C.; Siegler, W. C.; Synovec, R. E. *J. Chem.* **2009**, 23, 421–431.
37. Loszano, V. A.; Tauler, R.; Ibanez, G. A.; Olivieri, A. C. *Talanta* **2009**, 77, 1715–1723.
38. Szymanska, E.; Makuszewski, M. J.; Vander Heyden, Y.; Kaliszan, R. *Electrophoresis* **2009**, 30, 3573–3581.
39. Carneiro, R. L.; Braga, J. W. B.; Poppi, R. J.; Tauler, R. *Analyst* **2008**, 133, 774–783.
40. Rowe, M. P.; Plass, K. E.; Kim, K.; Kurdak, Ç.; Zellers, E. T.; Matzger, A. *Chem. Mater*. **2004**, 16, 3513-3517.
41. Bohrer, F. I.; Covington, E.; Kurdak, Ç.; Zellers, E. T. *Anal. Chem.* **2011**, 83, 3687-3695.
42. Steinecker, W. H.; Rowe, M. P.; Zellers, E. T. *Anal. Chem.* **2007**, 79, 4977-4986.
43. Kim, S. K.; Chang, H.; Bryant, J. G.; Burris, D. R.; Zellers, E. T. *Proc. Transducers '11*, Beijing, China, June 5-9 2011, pp. 799-802.
44. Chang, H.; Kim, S. K.; Sukaew, T.; Bohrer, F.; Zellers, E. T. *Procedia Engineering* **2010**, 5, 973-976.
45. Chang, H.; Kim, S. K.; Sukaew, T.; Bohrer, F.; Zellers, E. T. *Solid-State Sens., Actuator and Microsyst. Workshop*: Hilton Head, SC, June 6-10 2010, pp 278-281.
46. Zellers, E. T.; Reidy, S.; Veeneman, R. A.; Gordenker, R.; Steinecker, W. H.; Lambertus, G. R.; Kim, H.; Potkay, J. A.; Rowe, M. P.; Zhong, Q.; Avery, C.; Chan, H. K. L.; Sacks, R. D.; Najafi, K.; Wise, K. D. *Proc. Transducers '07*, Lyon, France, June 10-14 2007, pp 1491-1494.
47. Kim, H.; Steinecker, W. H.; Reidy, S.; Lambertus, G. R.; Najafi, A. A. A. K.; Zellers, E. T.; Bernal, L. P.; Washabaugh, P. D.; Wise, K. D. *Proc. Transducers '07*, Lyon, France, June 10-14 2007, pp 1505-1508.
48. Lu, C.-J.; Tian, W.-C.; Steinecker, W. H.; Guyon, A.; Agah, M.; Oborny, M. C.; Sacks, R.; Wise, K. D.; Pang, S. W.; Zellers, E. T. *7th lnternational Conference on Miniaturized Chemical and Biochemical Analysts Systems, uTAS '03*: Squaw Valley, CA, October 5-9 2003, pp 415-419.
49. Zellers, E. T.; Steinecker, W. H.; Lambertus, G.; Agah, M.; Lu, C.-J.; Chan, H. K. L.; Potkay, J. A.; Oborny, M. C.; Nichols, J. M.; Astle, A.; Kim, H. S.; Rowe, M.; Kim, J.; da Silva, L. W.; Zheng, J.; Whiting, J. *Solid-State Sens., Actuator and Microsyst. Workshop*: Hilton Head, SC, June 6-10 2004, pp 61-66.
50. Grob, R. L.; Barry, E. F. *Modern Practice of Gas Chromatography*; 4th ed., Wiley: NY, 2004.
51. Lin, C.-J. *Neural Computation* **2007**, 19, 2756-2779.
52. http://www.csie.ntu.edu.tw/~cjlin/

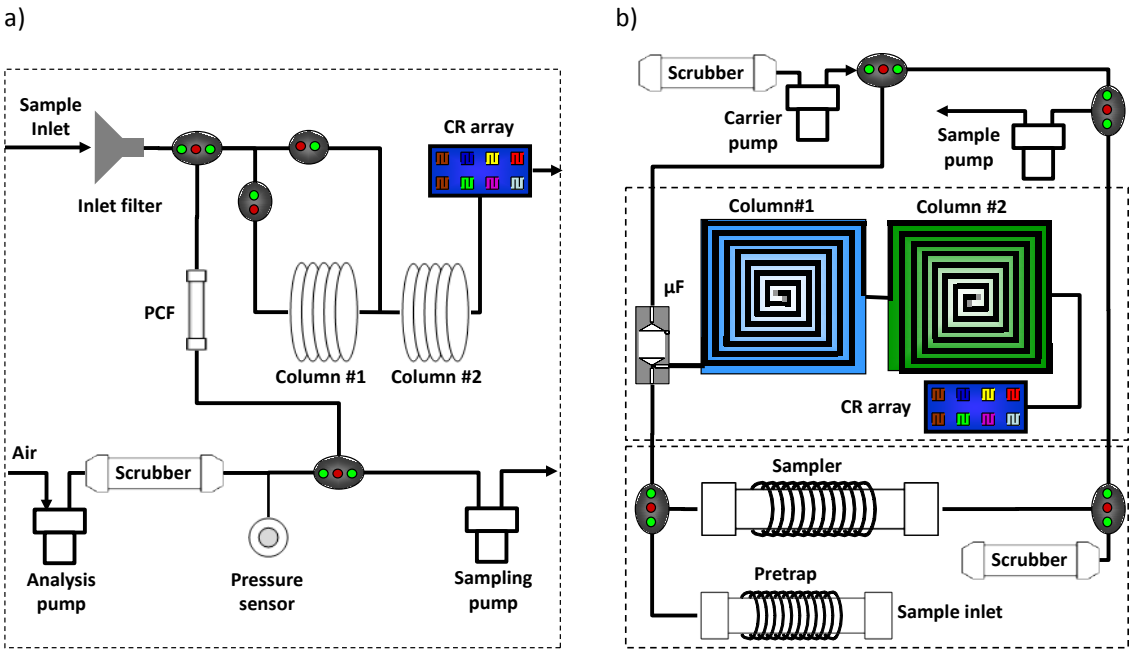

Figure 6-1. Schematic diagrams of a) portable and b) micro-scale GCs.

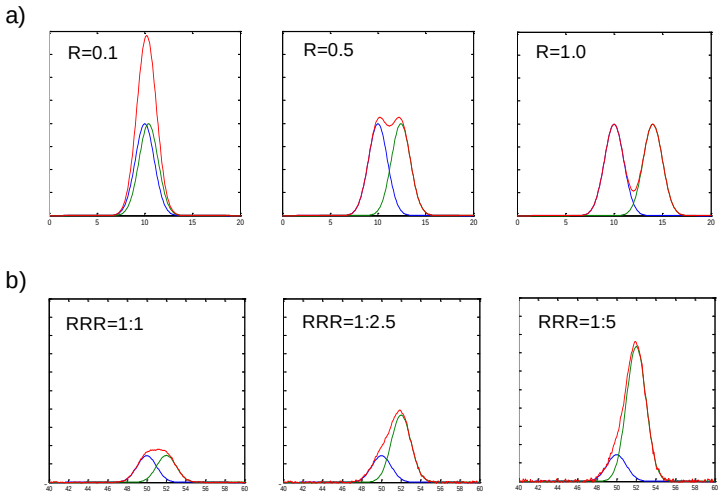

Figure 6-2. Example chromatograms of pure and binary mixture with various a) *R* with *RRR*=1:1 and b) *RRR* with *R*=0.5. Blue and green lines are chromatograms of pure components. Red lines are chromatograms of binary mixtures

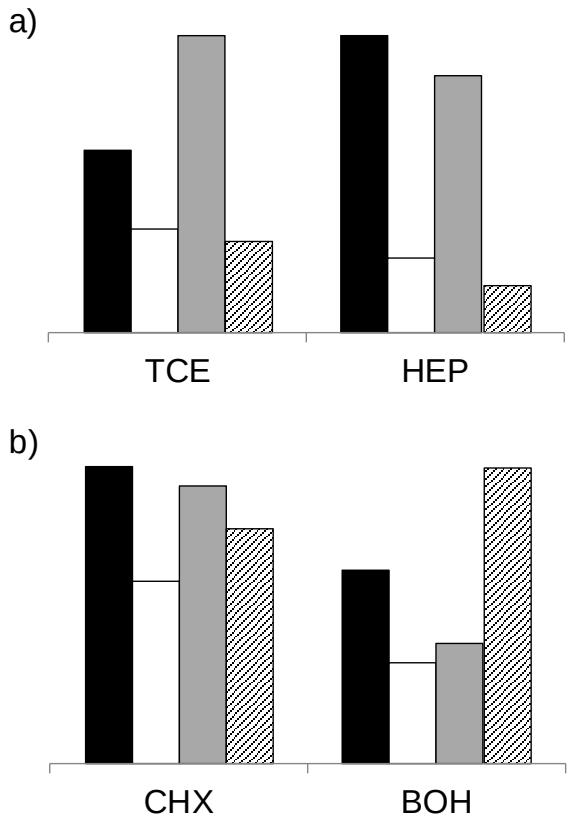

Figure 6-3. CR array response patterns to selected vapors, a) TCE (trichloroethylene) and HEP (n-heptane) with $\rho = 0.80$, and b) CHX (cyclohexane) and BOH (n-butanol) with $\rho = 0.20$. Bars are in the order of C8, DPA, OPH, and HME from the left hand side.

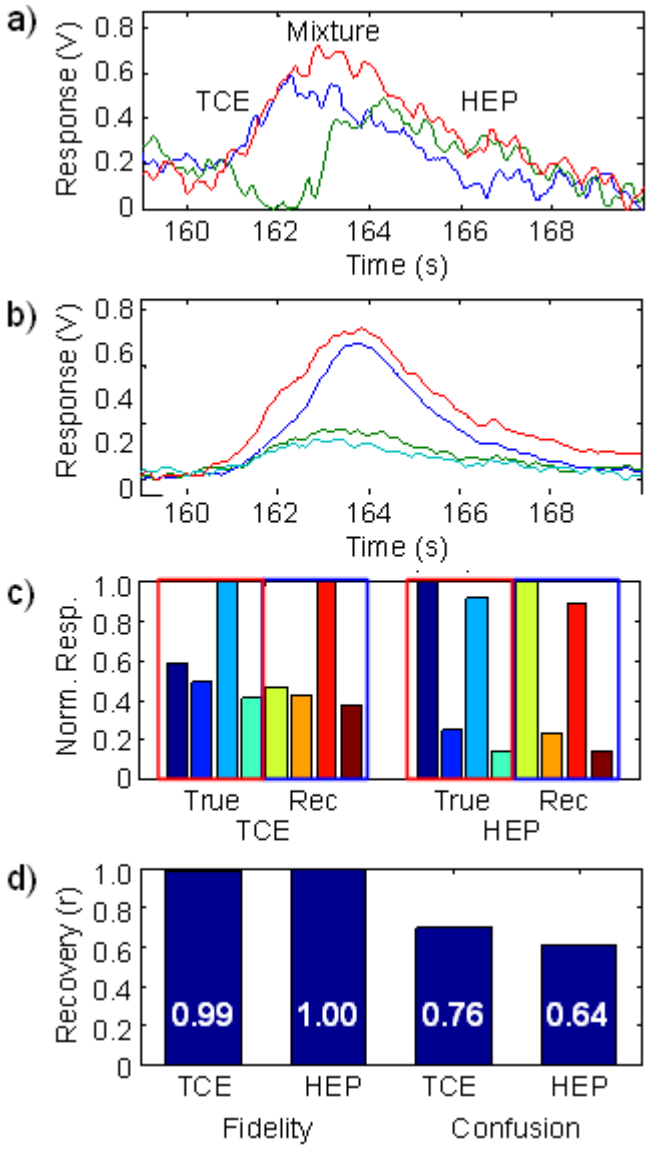

Figure 6-4. Example of EFA-ALS analysis (*S/N ratio*=10, *R*=0.5, *RRR*=1:1). a) Chromatograms of TCE (trichloroethylene), HEP (n-heptane), and mixture from the least sensitive sensor (HME); b) chromatograms of mixture from four different sensors; c) normalized response patterns of true and recovered CR array responses to TCE and HEP; d) fidelity (correlation coefficient between true and recovered patterns) of recovered patterns of TCE and HEP and confusion (correlation coefficient between true pattern of one compound and recovered pattern of the other compound). Numbers on the bars in d) are correlation coefficients.

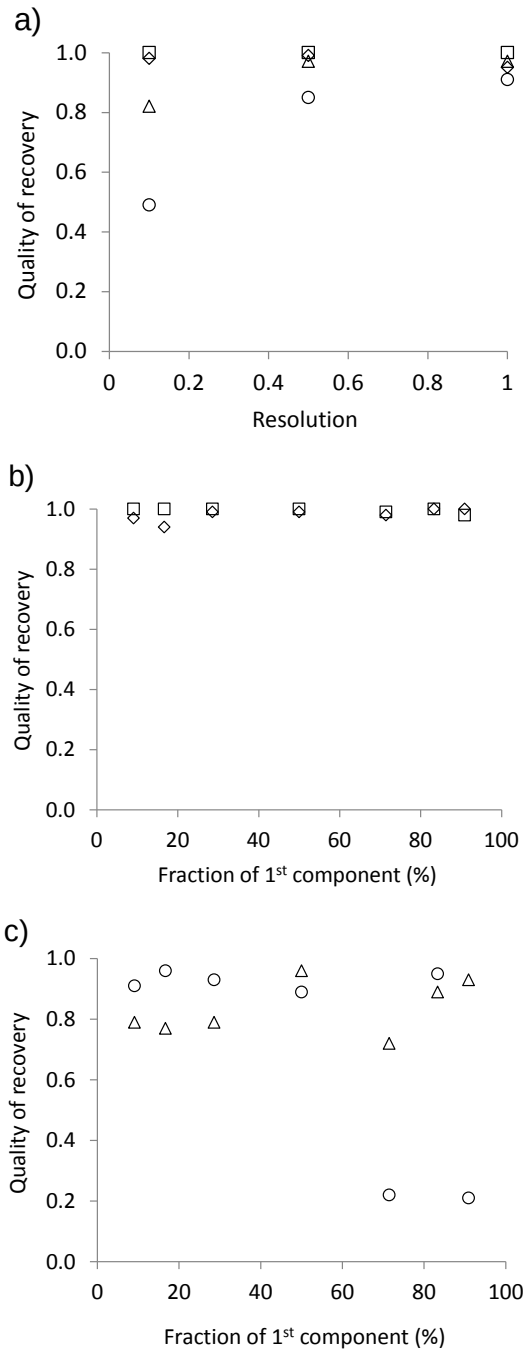

Figure 6-5. Influence of variables on the quality of recovery. a) chromatographic resolution b) relative response ratio of two components in a composite peak for trichloroethylene (TCE) and n-heptane (HEP); TCE is the first component; c) relative response ratio of two components in a composite peak for cyclohexane (CHX) and n-butanol (BOH); CHX is the first component. Symbols: diamonds (TCE), squares (HEP), triangles (CHX), circles (BOH).

Table 6-1. Chemical properties of selected vapors.

Compound	MW[a]	p_v[b]	BP[c]
TCE	131	69	87
HEP	100	46	98
CHX	84	98	81
BOH	74	7.2	118

[a] Molecular weight; [b] Vapor pressure (Torr); [c] Boiling point;
Abbreviations: TCE (trichloroethylene), HEP (n-heptane), CHX (cyclohexane), BOH (n-butanol)

Table 6-2. Conditions for binary mixture data generation and number of components determined by EFA analysis.

ID	S/N ratio[a]	*R*[b]	*RRR*[c]	Number of components	
				Similar[d]	Dis-similar[e]
1	10	0.1	1:1	2	2
2		0.5	1:1	2	2
3			1:2.5	2	2
4			1:5	2	2
5			1:10	2	2
6		1.0	1:1	2	2
7			1:2.5	2	2
8			1:5	2	2
9			1:10	2	2
10	10	0.1	1:1	2	2
11		0.5	1:1	2	2
12		1.0	1:1	2	2
13	10	0.5	1:10	2	2
14			1:5	2	2
15			1:2.5	2	2
16			1:1	2	2
17			2.5:1	2	2
18			5:1	2	2
19			10:1	2	2

[a] Signal-to-noise ratio; [b] Resolution between two components; [c] Relative response ratio based on the least sensitive sensor; [d] Pair of vapors having similar CR array patterns (trichloroethylene and n-heptane); [e] Pair of vapors having dis-similar CR array patterns (cyclohexane and n-butanol)

Table 6-3. MCR analysis results for binary mixtures having different pattern similarities under various conditions of S/N ratio, resolution, and relative response ratio.

ID	*S/N*[a]	*R*[b]	*RRR*[c]	*Fidelity*[d]				*Confusion*[e]				*Recognition*[f]			
				TCE	HEP	CHX	BOH	TCE	HEP	CHX	BOH	TCE	HEP	CHX	BOH
1	10	0.1	1:1	0.98	1.00	0.82	0.49	0.72	0.59	-0.27	0.31	'TCE'	'HEP'	'CHX'	'BOH'
2		0.5	1:1	0.99	1.00	0.97	0.85	0.70	0.61	-0.10	-0.11	'TCE'	'HEP'	'CHX'	'BOH'
3			1:2.5	0.99	1.00	0.79	0.91	0.76	0.64	-0.37	-0.41	'TCE'	'HEP'	'CHX'	'BOH'
4			1:5	0.94	1.00	0.77	0.96	0.72	0.52	-0.20	-0.31	'TCE'	'HEP'	'CHX'	'BOH'
5			1:10	0.97	1.00	0.79	0.91	0.67	0.53	-0.07	-0.11	'TCE'	'HEP'	'CHX'	'BOH'
6		1.0	1:1	0.95	1.00	0.97	0.91	0.61	0.38	0.03	0.07	'TCE'	'HEP'	'CHX'	'BOH'
7			1:2.5	0.99	1.00	0.87	0.97	0.61	0.55	0.07	-0.09	'TCE'	'HEP'	'CHX'	'BOH'
8			1:5	0.95	1.00	0.87	0.99	0.69	0.59	-0.04	-0.31	'TCE'	'HEP'	'CHX'	'BOH'
9			1:10	0.98	1.00	0.91	0.97	0.59	0.47	0.05	-0.03	'TCE'	'HEP'	'CHX'	'BOH'
10	10	0.1	1:1	0.98	1.00	0.82	0.49	0.72	0.59	-0.27	0.31	'TCE'	'HEP'	'CHX'	'BOH'
11		0.5		0.99	1.00	0.97	0.85	0.70	0.61	-0.10	-0.11	'TCE'	'HEP'	'CHX'	'BOH'
12		1.0		0.95	1.00	0.97	0.91	0.61	0.38	0.03	0.07	'TCE'	'HEP'	'CHX'	'BOH'
13	10	0.5	1:10	0.97	1.00	0.79	0.91	0.67	0.53	-0.07	-0.11	'TCE'	'HEP'	'CHX'	'BOH'
14			1:5	0.94	1.00	0.77	0.96	0.72	0.52	-0.20	-0.31	'TCE'	'HEP'	'CHX'	'BOH'
15			1:2.5	0.99	1.00	0.79	0.93	0.76	0.64	-0.28	-0.30	'TCE'	'HEP'	'CHX'	'BOH'
16			1:1	0.99	1.00	0.96	0.89	0.70	0.61	-0.14	-0.19	'TCE'	'HEP'	'CHX'	'BOH'
17			2.5:1	0.98	0.99	0.72	0.22	0.71	0.67	-0.32	-0.15	'TCE'	'HEP'	'CHX'	'BOH'
18			5:1	1.00	1.00	0.89	0.95	0.76	0.79	-0.42	-0.15	'TCE'	'HEP'	'CHX'	'BOH'
19			10:1	1.00	0.98	0.93	0.21	0.68	0.80	-0.47	0.07	'TCE'	'HEP'	'CHX'	'BOH'

[a] Signal-to-noise ratio ; [b] Resolution; [c] Relative response ratio; [d] correlation coefficient between the recovered pattern and those stored in the library; [e] correlation coefficient between recovered pattern of one compound and those stored in the library; [f] Vapor recognition after pattern matching of recovered pattern with patterns in the library. Abbreviations: TCE (trichloroethylene), HEP (n-heptane), CHX (cyclohexane), BOH (n-butanol)

Chapter VII

Summary and Conclusions

This dissertation describes the development and field application of a complete microfabricated gas chromatograph (μGC) that has been tailored to selectively and accurately determine trichloroethylene (TCE) vapors in the presence of complex volatile organic compound (VOC) mixtures, concerning the problem of indoor air contamination by TCE vapor intrusion (VI), as well as the application of an existing multivariate curve resolution (MCR) method, evolving factor analysis combined with alternating least squares (EFA-ALS), to experimental data sets of binary mixtures obtained from microsensor arrays. The broad goals were 1) to demonstrate automated and near-real-time analysis of TCE vapors with up to 45 interferences at sub-parts-per-billion (ppb) concentrations, targeting 0.06 ppb, 2) to prove its use in short- and long-term on-site analysis of indoor air in support of VI assessments, and 3) to evaluate the capability of EFA-ALS method to extract pure components from partially co-eluting binary mixtures. The instrument is a complete fully automated μGC with a microfabricated focuser, dual microfabricated separation columns, and a microsensor array interfaced to a non-microfabricated front-end pre-trap and high-volume sampler module to reduce

analysis time and limits of detection (LOD). Fast analysis of TCE vapors in complex mixtures in a short period of time becomes achievable with this development. The process of developing the instrument included a preliminary test with an extant meso-scale GC (Chapter 2), development and characterization of the μGC (Chapter 3), its field evaluation and application (Chapter 4-5), and MCR application (Chapter 6).

The strategy to develop the μGC entailed initial tests with an extant meso-GC to obtain basic knowledge (Chapter 2). A key challenge of this task was addressing a new concept of using an upstream high volume sampler for lowering the LOD while reducing the sampling time, and showing the possibility of using it for quantitative determination of TCE vapors at trace part-per-trillion levels in moderately complex VOC backgrounds. Another purpose of the study was to determine the LODs of CR sensors for TCE vapors in terms of mass, which would guide the design of the μGC, especially required sampling volume. 200 mg of commercial adsorbents (Carbopack X) was used to pack the high volume sampler. Comparison result with U.S. EPA TO-15 method showed that the instrument can accurately determine TCE vapors at ppt level with the detection limit of ~7.5 ng. To select interferences for the separation test, a total of previously measured 12 field sample data sets for 75 compounds including TCE were received from another research group (Kyle Gorder, U. S. Air Force, UT). The samples were collected from VI-impacted residences near the site where field tests of the μGC were ultimately conducted. From these data sets, the 10 most common interferences were selected based on the frequency measured among 12 sets and on the vapor pressure to cover wide range of vapor pressure. TCE at 0.4 ppb level was successfully detected with a 6-L sample, and separated from the interferences without any overlapping in ~80 sec.

The results from Chapter 2, including LODs were transferred to the design process of the μGC (Chapter 3), and used as the first criterion combined with the target LOD of 0.06 ppb to determine the required sample volume (~20 L). The second criterion for the μGC design was vapor pressure (p_v) range of VOCs to collect. The compounds used as potential interferences are a subset of the 63 VOCs found (by GC-MS) in a series of the 12 samples (mentioned above). These ranged in p_v values from 0.085 to > 5,000 torr. Since most of the 27 detected compounds with p_v values > 100 torr are (by design) not captured efficiently by the adsorbent (Carbopack X) in the sampler, all but a few of them were eliminated from the test set. Adding some moderate- and low-volatility compounds often found as contaminants in indoor air, a set of 45 co-contaminants, which was considered sufficient to demonstrate selective TCE determinations, was selected as the interferences. To eliminate low volatility compounds having p_v < 3 Torr entering into the system, a pre-trap was employed. Carbopack B (C-B, specific surface area = 100 m^2/g) was used in the pre-trap and Carbopack X (C-X, 250 m^2/g) was used in the sampler and the μF. The mass for each device was optimized for the selective and quantitative sampling (performed by another student in Prof. Zellers group). The third criterion was the entire operation time, including sampling, focusing, and analysis. The initial target cycling time was ~ 30 min per cycle. Operation time for focusing and analysis would be less flexible than sampling time which could be reduced by using a higher flow rate, even though there is a tradeoff between sampling flow rate and the sampler capacity. The sampling flow rate was also related to the adsorbent mass in the pre-trap and sampler. Not to have any breakthrough of TCE on the sampler for 20 min, the flow rate was determined to be ~ 1 L/min. Another key parameter was the column length. From the Golay plot test, the

minimum required column length (6-m) was determined to have no co-elution of TCE with the nearest eluting interference. As mentioned above, the μGC was designed based on these critical criteria to consist of a single stage microfabricated focuser, dual microfabricated separation columns, and a microsensor array, interfaced to a non-microfabricated front-end pre-trap and high-volume sampler module.

After integration of all the devices into an instrument, the μGC was characterized, including calibration, LODs, accuracy, stability of the system (i.e. reproducibility) and short- and long-term stability of the CR array, chromatographic resolution of TCE from moderately and very complex mixtures, and response patterns from the CR array. With the calibration range of captured TCE masses from 9-390 ng and integrated vapor volumes of 1.7-72 ppb-L, the projected LOD for TCE was 40 ppt (4.2 ng captured, 20-L sample). The accuracy test, using 0.12 ppb and 11 ppb samples confirmed by TO-15, showed the average value of 0.12 ± 0.033 ppb and 11 ± 0.40 ppb, respectively. This degree of accuracy would be sufficient for any practical purpose. The stability tests performed with replicate samples for short-term (same day, n=10) and medium-term (1 month, n=15) proved the μGC would have high stability in terms of sensor responses. Mixtures of 12 compounds and 46 compounds including TCE were challenged to the system to characterize its chromatographic separation capability. In both cases, TCE was separated from all other interferences, having same retention time, ~50 sec. Response pattern for each compound could be obtained. Entire cycle time was ~ 36 min due to an unexpected pressure drop in the manifold. The sensitivity, selectivity, accuracy, stability, and analytical cycle time demonstrated here, coupled with the capability for automated operation, indicate that this type of instrument would be effective in guiding efforts to monitor and mitigate TCE vapor

intrusion in affected residences.

In Chapters 4 and 5, the field evaluation and application results of the μGC prototype were presented. For the field deployment, two prototypes were tested in houses in Layton, UT near Hill AFB. Prior to the application, those prototypes were evaluated in the field including field calibration, LODs, inter-prototype comparison, and comparison with a reference method (Chapter 4). Field-generated calibration curves were linear for injected TCE masses of 26–410 ng (4.8–77 ppb·L; $r^2 > 0.98$) and the projected single-sensor detection limit was 0.052 ppb for an 8-L air sample collected and analyzed in 20 min. Two prototypes showed good agreement for concurrent samples (forced zero r^2=0.88 and slope=1.12, n=23). In case of comparison with a reference method (TO-15), generally good agreement with the reference method was observed (force-zero $r^2 = 0.87$, Slope = 0.90, n=60, range: 0.047 to 16 ppb). In detail, above the mitigation action level (MAL) of 2.3 ppb for the field-test site, μGC TCE determinations fell within ±25% of those from the reference method for 21 of 26 measurements, in the presence of up to 43 documented background VOCs. Below the MAL, positive biases were consistently observed, which are attributable to background VOCs that were unresolvable chromatographically or by analysis of the sensor-array response patterns. This result suggests that the need of better separation or a MCR method to deconvolute overlapping peaks. Regardless, again, these results demonstrate that this type of μGC instrument could serve the need for routine TCE determinations in VI-related assessment and mitigation efforts.

Field application results in Chapter 5 included the use of two prototype μGC for the continuous (temporal variations) and short-term (spatial variations) measurements of

indoor trichloroethylene (TCE) vapor concentrations in houses. Temporal variations in TCE air concentrations (range: 0.23-26.6 ppb) were monitored continuously for up to 48 hrs near the primary VI entry location under different levels of induced differential pressure (relative to the sub-slab) in the first house, in which TCE VI was previously documented over three week period. Concentration trends agreed closely with those determined from concurrent reference samples collected/analyzed by TO-15 method or measured on-site with a portable GC-MS. Spatial variations in TCE air concentrations within the same house showed a decreasing concentration gradient with increasing distance from the primary VI entry location. An unintentional source of TCE stored in the attached garage was reflected in the prototype (and reference) data. In the second house, with no TCE VI, the μGC prototype was used to locate an intentionally hidden source of TCE within a closet, demonstrating the capability for locating non-VI sources (range: 0.51-56 ppb, n=19), and with good agreement with reference method values. This field demonstration of μGC technology for automated, near-real-time, selective VOC monitoring at low- or sub-ppb levels augurs well for its use in short- and long-term on-site analysis of indoor air in support of VI assessments.

As mentioned, the need of MCR to improve the performance of a μGC is apparent. In Chapter 6, application of the MCR method, EFA-ALS, to partially co-eluting analyte vapors measured with CR arrays used as the detector in a μGC and a portable GC was presented. Two pairs of vapors having different array response pattern similarities (ρ) were selected for testing: trichloroethylene (TCE) and n-heptane (HEP) as similar patterns (ρ=0.80), and cyclohexane (CHX) and n-butanol (BOH) as dis-similar patterns (ρ=0.20). After establishing calibration curves and a response pattern library for individual vapors,

binary mixtures were analyzed at values of chromatographic resolution ranging from 0.1 to 1.0, and relative concentrations leading to relative response ratios ranging from 1:10 to 10:1 for the least sensitive sensor in the array. EFA-ALS analysis permitted recovery of the original response patterns with high fidelity ($r > 0.95$ in all cases for TCE+HEP and >0.9 in most cases with CHX-BOH). Subsequent pattern matching with calibrated patterns was successful in all cases. Polar compound (BOH) was found to have decline in performance, perhaps due to the chemical property resulting peak shape distortion (tailing). Overall, despite the low dimensionality of the array data, EFA-ALS could provide an effective means to extract individual components from composite peaks in (μ)GC-microsensor array systems, thereby improving the capability for identifying analytes in complex mixtures.

There are some tasks not included in this dissertation that can be performed in the near future to either improve the performance or validate the value of the current project. One task is another evaluation of the μGC, especially the accuracy test in the presence of more challenging co-contaminants such as C7 isomers or some other compounds eluting very closely or co-eluting with TCE peak. Second, further modifications can be made on the μGC to improve the performance, such as thermostating of the CR array for obtaining better sensitivity and stability, and employing more sensitive sensors. Third, quantification of extracted components from binary mixtures by the MCR method should be performed to improve its usability. In addition, pattern matching method to recognize and assign response patterns of extracted components should be tested with more complex library than the library with only two compounds.

In conclusion, to our knowledge, the research in this dissertation reports the first field deployable μGC employing microsensor array detection for trace-level determinations of targeted environmental VOC air contaminants, and the first field application result of such instrument. The instrument relies on selective high-volume preconcentration; microfocuser injection; rapid, temperature-programmed, dual-microcolumn separation; and microsensor-array recognition and quantification. Since all of the analytical components of this μGC were microfabricated using standard processing methods and materials, which affords several inherent advantages, including: simple, high-yield, modular (interchangeable) components; small fluidic path dimensions and low dead volumes; rapid, low-power heating (for the μF and microcolumns); and low-profile multi-dimensional (spectrometric) detection, it appears feasible to extend the use of the μGC prototype to many other applications for the simultaneous analysis of other VOCs at sub-ppb concentrations, such as benzene, toluene, ethylbenzene, and xylene. Regarding this aspect, a project concerning an occupational health problem (exporsure assessment) has been proposed and will be started in near future.

APPENDICES

Appendix I. Supporting Information for Chapter 3

The information provided below includes the rationale for using 6 m of total microcolumn length, the table of 46 test VOCs, a representative μF heating profile, Golay plots and a representative chromatogram from the dual 3-m microcolumn ensemble, descriptions of the printed circuit boards and DAQ boards used for instrument control, a summary of power dissipation for the prototype, and methods used for data analysis and chemometrics.

Rationale for Two 3-m Microcolumns. The use of two microcolumns in series, each 3 m in length, can be rationalized on the basis of the required number of theoretical plates, N_{req}, which is defined as follows for the peaks of a critical pair of compounds, 1 and 2: [S1]

$$N_{req} = 16R_s^2\left(\frac{\alpha}{\alpha-1}\right)^2\left(\frac{k_2}{k_2-1}\right)^2 \quad \text{(eq. S1)}$$

where R_s is the resolution, α is the separation factor, k_2 is the retention factor of the later eluting compound (TCE in this case), and each of these variables is defined as follows:

$$R_s = 1.18\frac{(t_{R2}-t_{R1})}{(fwhm_1 + fwhm_2)} \quad \text{(eq. S2)}$$

where t_{Ri} is the retention time of compound i, $fwhm_i$ is the full width at half maximum the peak;

$$\alpha = \frac{k_2}{k_1} \quad \text{(eq. S3)}$$

and

$$k = \frac{t_R^{'}}{t_M} \quad \text{(eq. S4)}$$

where t_R' is the adjusted retention time and t_M is the hold-up time (evaluated as the retention time of methane).

For TCE, a *k* value of 3.3 and a *fwhm* value of 2.0 s were assumed on the basis of experimental data,[S2] and values of α =1.1 and R_s = 1.5 (i.e., baseline separation) were imposed. This yields an N_{req} value of 7,400 plates. For operation at 1.2 mL/min, it is estimated that each microcolumn generates ~1,400 plates per meter (derived by extrapolation of the Golay plot presented in Figure 3-S1; see below). Therefore, a total microcolumn length $\geq$ 5.3 meters would be required.

Microcolumn Characterization. In order to compare the chromatographic efficiency of the current microcolumn design, with chamfered corners, to that of the previous design, with right-angle corners, the relationship between the linear velocity and the plate height was determined using n-octane as the test compound. For these experiments two series coupled 3-m microcolumns of a given design were connected between the injector and FID of a conventional GC (7890, Agilent Technologies, Pal Alto, CA) and mounted in the GC oven held at 30 °C.

Serial injections (1000:1 split) of methane and n-octane (headspace above liquid, k = 3.7) were performed over a range of N_2 carrier gas inlet pressures that produced a range of average linear velocities, u, estimated from the methane hold-up times. Retention times and peak widths were used to calculate the number of theoretical plates, N, from which the theoretical plate height, H, was determined (i.e., H = N/L, where L is the microcolumn length; $N = 5.54(t_R'/fwhm)^2$, where t_R' is the adjusted retention time and *fwhm* is the full-width at half maximum of the peak).

These data were used to create the Golay plots for n-octane shown in Figure S2. The value of the optimal velocity, u_{opt}, was ~ 10 cm/s (0.22 mL·min^{-1}) for both types of microcolumns, but those with the chamfered corners yielded a minimum value of H = 0.022 cm, which was 20% smaller than those with sharp corners (minimum H = 0.027 cm). This results in a commensurate increase in N produced by the dual 3-m microcolumn ensemble from 22,000 to 27,300 plates (i.e., 4,550 plates·m^{-1}).

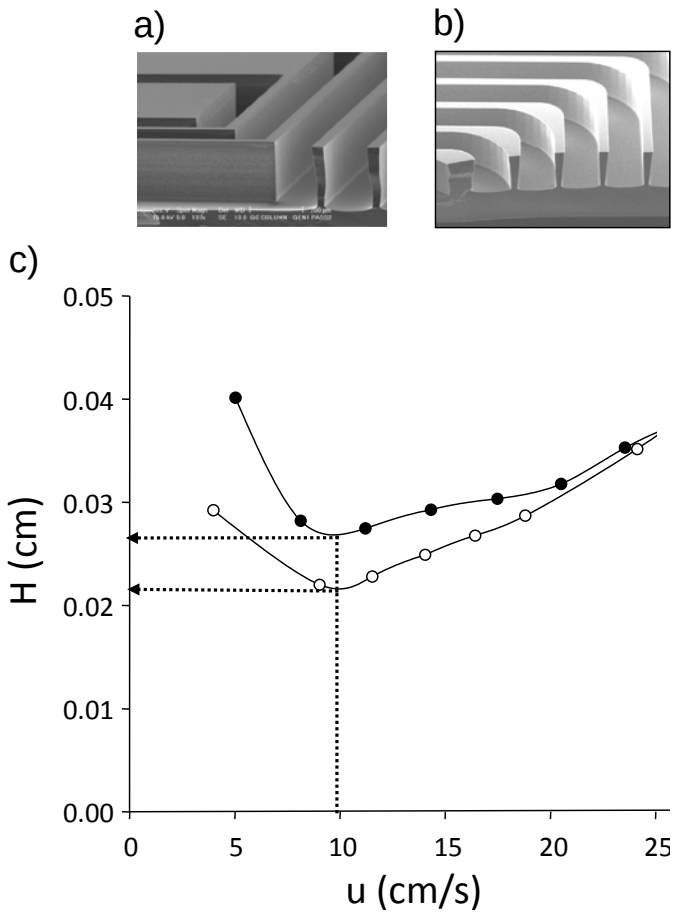

Figure 3-S1. SEM images of sub-sections of the etched-Si channels used in the 3-m-long microcolumns of the μGC prototype prior to sealing and coating with PDMS stationary phase: a) previous design with right-angle corners; b) current design with chamfered corners. The Golay plots in c) were generated with n-octane (1000:1 split, k = 3.7) using N_2 as the carrier gas by connecting the dual 3-m microcolumn ensemble between the injector and FID of a bench-scale GC: previous design (filled symbols) and current design (unfilled symbols).

The chromatogram in Figure 3-S2 shows the 2.2-min separation of a 10-component mixture, including TCE, using the dual 3-m microcolumns of the current design, configured as described above for generating the data in Figure 3-S1. The separation conditions, including the temperature program used with the integrated microcolumn heaters, are given in the caption of Figure 3-S2. All compounds were baseline separated, TCE eluted in about 45 s, and the entire mixture eluted in < 2.2 min. The *fwhm* values ranged from 0.6 to 1.9 s. On the basis of 6 replicate injections, the retention time variations ranged from 0.35 to 0.89% of the average values.

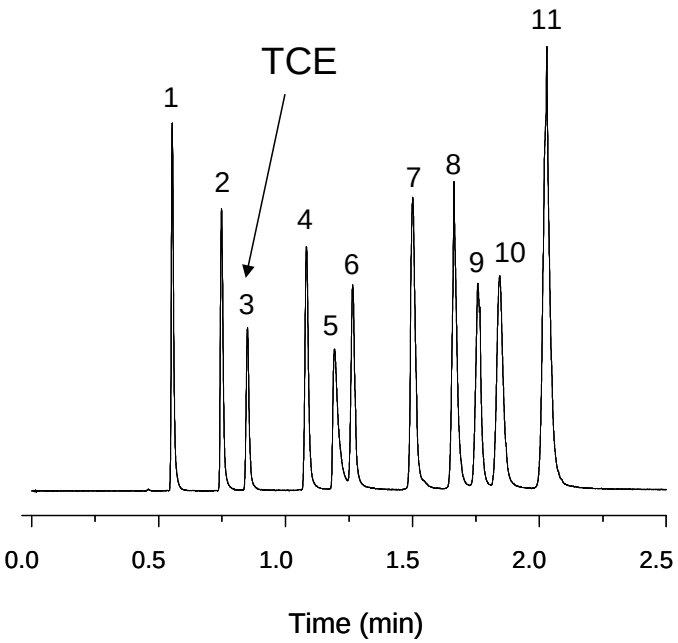

Figure 3-S2. TCE separation from 10 VOC interferences using a conventional (bench scale) GC inlet/injection port and FID, and the dual 3-m microcolumns of the current design. (0.1 μL injection of the neat mixture; inlet pressure: 4 psi; inlet temperature: 250°C; split ratio: 100:1; Temperature program of 1st microcolumn: hold at 25 °C for 60 s, heat to 60 °C at 70 °C/min, heat to 100 °C at 80 °C/min, hold at 100 °C for 30 s. Temperature program of 2nd microcolumn: hold at 25 °C for 60 s, heat to 60 °C at 70 °C/min, heat to 120 °C at 120 °C/min, hold at 120 °C for 30 s. Compounds: 1, n-hexane; 2, benzene; 3, TCE; 4, toluene; 5. 2-hexanone; 6, PCE; 7, ethylbenzene; 8, o-xylene; 9, nonane; 10, cumene; 11, n-propylbenzene.

Microcolumn Temperature Programming. For applied dc biases of 5-25 V (0.6-15 W), the corresponding steady-state microcolumn temperature ranged from 40 - 200 °C, respectively. The maximum heating rate, taken from the initial stages of the 15-W curve is 7.6 $°C \cdot s^{-1}$. Higher heating rates may be possible but were not explored.

Actuation and Control Circuitry. A custom pneumatic control circuit board and associated digital I/O card (USB-6501, National Instruments, Austin, TX) for actuating the valves, pumps, and the heaters on the pre-trap and sampler, were located beneath the manifold on the chassis floor. A second printed circuit board and associated 16-bit multi-functional DAQ card (USB-6218, National Instrument, Austin, TX) for monitoring and controlling the devices in the analytical subsystem (i.e., the μF and microcolumn heaters and temperature sensors, and the sensors in the CR array) were located beneath the analytical subsystem components. A USB hub permitted connections to a laptop computer running a control program written in LabView (Ver. 8.5, National Instruments, Austin, TX).

Power Dissipation. The average operating power varies with the sample volume:

for the maximum sample volume of 20 L (i.e., 36 min cycle), the average power per analysis is 30 W; whereas, for a sample volume of, say, 4 L (i.e., 15 min cycle) the average power increases to about 39 W. The corresponding energy required per analysis is ~63 kJ for a 36-min cycle to ~35 kJ for a 15-min cycle time. The single largest power drain is the sampler heater (55 W for 3 min, 9.9 kJ, ~16 % of the total energy for a 36-min cycle). The energy required to operate the microfabricated components is ~5.9 kJ (9 % of the total energy).

Data Analysis and Chemometrics. Peak heights and peak areas were determined after importing the raw response data into GRAMS AI/32 (Ver. 6.00, Thermo Scientific Inc., West Palm Beach, FL), and linear regressions of calibration data were performed using Excel. The performance of the CR array in differentiating among TCE and several potential interfering VOCs eluting nearby was assessed using Monte Carlo simulations coupled with extended disjoint principal components regression (EDPCR) classification models. Details of this approach to array assessment have been published elsewhere (see, for example, refs 4d, 4g, and 4h in the main article) and are summarized in the following paragraph.

Using the experimental sensitivity values, synthetic MPN-CR responses to each vapor were generated by randomly selecting a vapor concentration within the range of 5-10×LOD, where the LOD was dictated by the least sensitive sensor in the array to ensure that all sensors contributed to the response patterns. The response was calculated from the calibration-curve regression equation for each sensor. Then, error was introduced by adding to the response a value obtained by multiplying that response value by a factor derived from randomly sampling a Gaussian distribution with a mean of zero and a standard deviation corresponding to the random sensitivity errors derived from the calibration data (Figure 3-4, main body) for each sensor for TCE (i.e., C8, 8.1%; DPA, 2.7%; OPH, 2.2%; HME, 9.5%). The error enhanced responses from all sensors were combined and the location of the resulting response vector was projected onto the principal component corresponding to the original calibrations for each vapor via EDPCR. The identity of the vapor assigned to this synthetic response vector was determined by the shortest Euclidean distance. This procedure was performed iteratively (i.e., 500 samples) to yield a statistical estimate of recognition rate (RR) for each vapor.

References

S1. Jennings, W.; Mittlefehldt, E.; Stremple, P. *Analytical Gas Chromatography*, 2nd Ed., Academic Press, 1997.

S2. Chang, H.; Kim, S. K.; Sukaew, T.; Bohrer, F.; Zellers, E. T. *Procedia Engineering* **2010**, 5, 973-976.

S3. Department of Chemistry at the University of Akron, The Chemical Database, available at http://ull.chemistry.uakron.edu/erd/

Appendix II. Supporting Information for Chapter 6

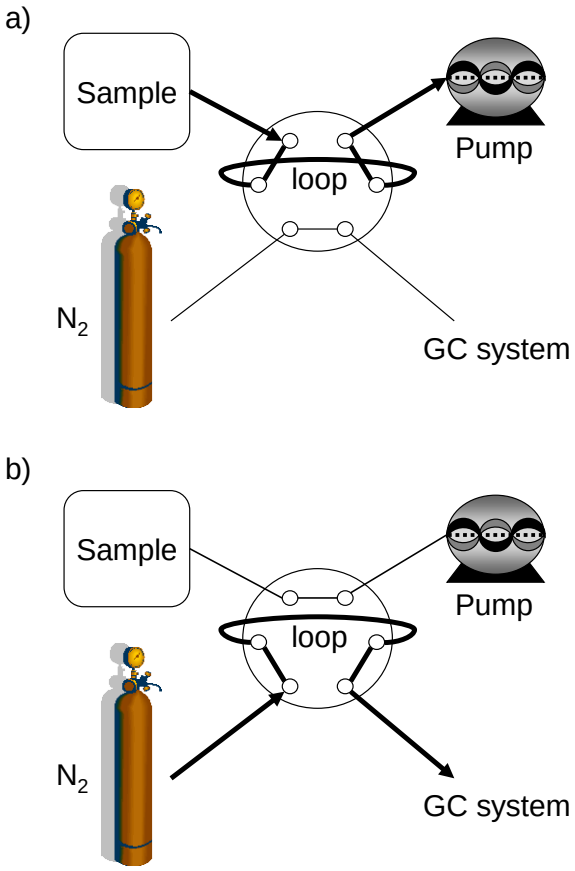

Figure 6-S1. Experimental setup to generate data sets of binary mixtures. a) setup for sample loading to sample loop in an external six-port valve and b) setup for sample loading from sample loop to a GC system.

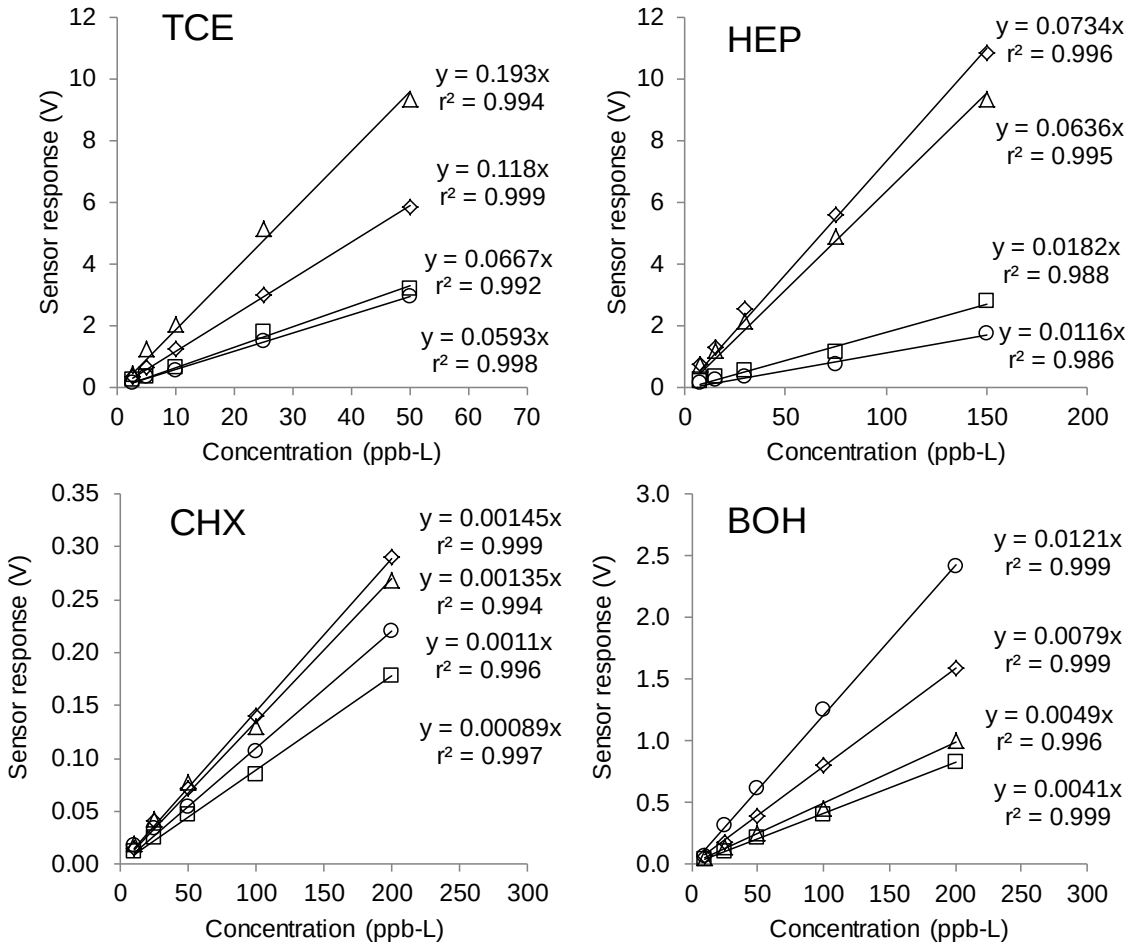

Figure 6-S2. Calibration result of two CR arrays for selected vapors. One CR array in the portable GC was calibrated for TCE and HEP, and the other array was calibrated for CHX and BOH, showing all sensors with $r^2 > 0.98$ (forced-zero). Symbols: unfilled diamonds (C8), unfilled squares (DPA), unfilled triangles (OPH), and unfilled circles (HME).

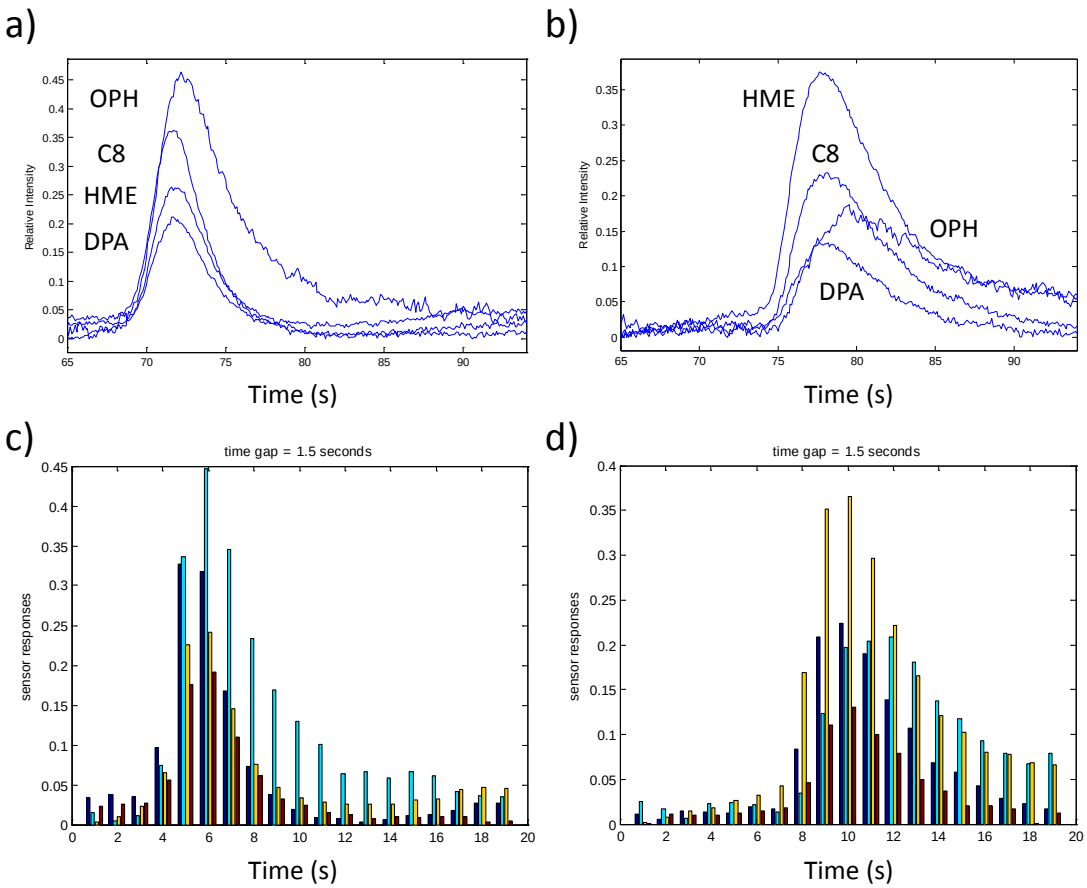

Figure 6-S3. Sensor responses for (a) cyclohexane and (b) n-butanol, and changes in the response pattern of every 1.5 s in peaks for (c) cyclohexane and (d) n-butanol.